A finite element investigation on the mechanical effect of ply drops in blended laminates

Evgenios Skitsas

Faculty of Aerospace Engineering · Delft University of Technology
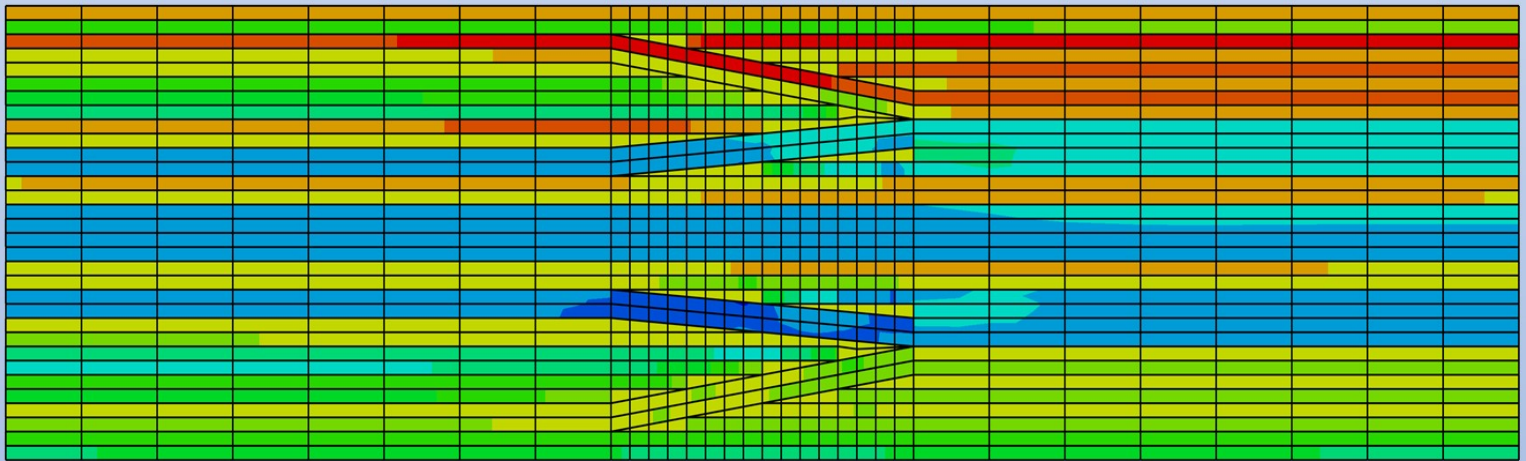
TUDelft
Delft
University of
Technology

A finite element investigation on the mechanical effect of ply drops in blended laminates

MASTER OF SCIENCE THESIS

For obtaining the degree of Master of Science in Aerospace Engineering
at Delft University of Technology

Evgenios Skitsas

28-08-2020

Faculty of Aerospace Engineering · Delft University of Technology

TUDelft

Delft
University of
Technology

DELFT UNIVERSITY OF TECHNOLOGY
FACULTY OF AEROSPACE ENGINEERING
DEPARTMENT OF AEROSPACE STRUCTURES AND MATERIALS

GRADUATION COMMITTEE

Dated: <u>28-08-2020</u>

Chair holder:

_____

Dr. I. Fernandez Villegas

Committee members:

_____

Dr.ir. J.M.J.F. van Campen

_____

Dr.ir. O.K. Bergsma

_____

Dr.ir. D.M.J. Peeters

Abstract

This thesis project begins with an introduction on blended laminates and a summary of the most popular laminate blending techniques. The particular laminate blending technique used in this project is the relaxed generalized blending by Van Campen et al.. This method allows for more blending possibilities which can lead to lighter structures. Van den Oord developed a blending algorithm that allows many different sections of a laminate to be blended together using the relaxed generalized blending technique. Later, Gomaa manufactured a blended laminate using the same algorithm, achieving 80% more buckling load compared to a conventional laminate of the same weight. Due to the stiffness mismatch between the different sections of the blended laminate, it had severe imperfections caused during the cooling down in the autoclave cycle.

The purpose of this research project is to investigate the effects the ply drops have in the stress and the out of plane displacement in blended laminates under buckling loading. In particular, FEM analysis is used to investigate the stress field and the out of plane displacement of blended laminates, taking into account the geometry of the ply drops. For the stress analysis, a global-local modelling technique is used, where the global model is built using 2D elements and the local ply drop section models are built using 3D elements. For the out of plane displacement analysis, an algorithm is used to calculate the stiffness properties of the ply drop sections utilizing a methodology similar to Representative Volume Element techniques. Then, using an algorithm, the calculated ply drop section stiffnesses are transferred back to the global model with the purpose of more accurately predicting the global stiffness of a blended laminate. The stress and out of plane displacement results are then compared to the results from a simple global FEM model which does not take into account the geometry of the ply drops, similar to the one used by Gomaa. Finally, a thermal FEM model of the blended laminate is built to simulate the saddle type imperfections. This FEM model uses 2D coupled temperature-displacement elements and simulates the out of plane displacement due to thermal stresses caused by the stiffness missmatch of the different sections of the blended laminate. The results from this FEM model are compared to real data of saddle type imperfections taken from Gomaa's thesis, in order to find out the accuracy of the FEM model. This or similar FEM models can be used in future projects to help diminish the saddle type imperfections by directly showing the effects different solution methods have on the laminate.

Table of Contents

Nomenclature

Abbreviations

CA Cellular Automaton

CLT Classical Laminate Theory

GA Genetic Algorithm

NC Neighbour count

PDS Ply Drop sequence Tables

RVE Representative Volume Element

SST Stacking Sequence Tables

FEM Finite Element Method

Greek Symbols

β Penalty parameter for fitness function

ϵ_i Components of the strains

γ_{ij} Components of the shear strains

κ_{ij} Curvatures components

σ_i Components of the normal stress

τ_{ij} Components of the shear stresses

Θ Fiber orientation angle

θ Fitness value

ε Bonus parameter for fitness function

Latin Symbols

$\Delta 1$ Length difference 1

$\Delta 2$ Length difference 2

ΔH Length height

ΔL Length difference

ΔT Temperature difference

ΔW Length width

A_{ij} Components of the in-plane stiffness matrix

a_{ij} Components of the inverse in-plane stiffness matrix

a_{ij} Expansion coefficient components

B_{ij} Components of the bending extension coupling stiffness matrix

b_{ij} Components of the inverse bending extension coupling stiffness matrix

D_{ij} Components of the bending stiffness matrix

d_{ij} Components of the inverse bending stiffness matrix

E_{ij} Stiffness components

G_{ij} Shear stiffness components

g_{min} Buckling constraint

H Height

k_{ij} Thermal conductivity components

L Length

l_{ij} Direction cosine components

M_{ij} Moment components

N_0 Maximum buckling load a section can achieve

N_x Buckling load the section is supposed to carry

N_{ij} In plane load components

Q_{ij} Ply stiffness components

S_{ij} Compliance tensor components

t_{ply} Ply thickness

U_i Boundary condition components

V_i^A In-plane lamination parameters

V_i^B Coupling lamination parameters

V_i^D Flexural lamination parameters

v_{ij} Poisson ratio components

W Weight

W Width

Z_i Through-the-thickness coordinate

Acknowledgments

The idea of doing my thesis on the subject of composite laminate blending came after a discussion I had with Dr.ir. J.M.J.F. van Campen . I immediately got interested in the subject since it's a relatively new area of composite materials, a lot of research is currently going on and it has promising capabilities on weight reduction. I would like to thank my supervisor Dr.ir. J.M.J.F. van Campen for the guidance he provided me during my thesis and of course my parents without whom it would not have been possible to study at Delft University in the first place.

Delft, University of Technology   Evgenios Skitsas
28-08-2020

Chapter 1

Introduction

Aircraft, cars, rockets and many other vehicles have one word in common when it comes to optimal design: weight. Weight is the one thing that engineers want to get rid of their vehicles when designing them, since less weight means less need for power, lower emissions and lower fuel consumption, among other things. Composite materials is the new trend in designing lightweight structures with high specific properties and this can be verified in new aircraft like Boeing 787 and Airbus A350, in which composite materials already make 50% of their structure [12]. Despite the fact that composite materials already offer great specific properties, they can offer even greater specific properties by utilizing composite laminate blending.

The common practise for engineers when it comes to designing a laminate, is to dictate the whole thickness and stacking sequence of the laminate by the area of the laminate with the highest load. However, that means all the other areas of the laminate except the area with the highest load, are over designed, meaning more weight than is actually needed. One way to surpass this problem, is to divide the laminate in small areas and dictate a specific thickness and stacking sequence for each separate area. This however, has bad implications on manufacturing and structural integrity of the laminate making it impossible to manufacture it. In order to solve this problem, laminate blending comes into play.

The local optimization of a composite panel by dividing it into multiple sections but at the same time taking into acount continuity and manufacturability guidelines, is known as Composite laminate blending. The loads in these sections are assumed to be constant but different [13]. As stated previously, composite laminate blending takes into account manufacturability, which means that there must be continuity between the different sections of the laminate despite the different stacking sequence and thickness of the areas that the laminate is divided into.

The goal of this thesis project is to investigate the effects that ply drop sections have in blended laminates by using a newly designed blended laminate panel with 25 different sections. This blended panel was manufactured by Gomaa and the different sections of the panel

were blended together using an algorithm proposed by Van den Oord, making use of the generalized blending method of Van Campen et al. [7, 29, 31]. This investigation is carried out using FEM software and is focused mainly on the stress field and the out plane displacement of the blended panel under buckling loading. Along with the ply drop investigation that is done, an investigation is also taking place on the thermal response of the laminate in conditions simulating the autoclave cycle. A FEM model is created to simulate the imperfections created during the autoclave cycle on the manufactured panel due to the different expansion coefficients in each section.

Chapter 2

Background

2.1 Fiber-reinforced composite laminates

In general, composite material is any material that consists of at least two constituents. In this particular thesis project though, composite material will refer to a mixture of fibers and matrix. In terms of fibers, there can be carbon fibers, E and S glass fibers, quartz, graphite, Kevlar, Boron or silicon fibers. From the matrix perspective, the options can include epoxy, polyester, phenolics, polymides and bismaleimids [12].

A composite material can be built using many different methods. In this project, the method that is used is by stacking plies together which results in the laminate. These plies consists of fibers pre-impregnated with resin, typically called pre-pregs. The most typical kind of plies used are unidirectional or fabric. In the later, fibres are oriented in directions with 90 degrees difference, in other words perpendicular to each other. A laminate can be described by its stacking sequence or layup. This can be shown below:

$$[\theta 1/\theta 2/\theta 3...]$$

Where $\theta 1, \theta 2$ etc, are the angles of the plies from top to bottom of the laminate [12]. A sketch of a laminate as well as The laminate axes and the definition of positive θ angle can be seen in figure 2.1 [12].
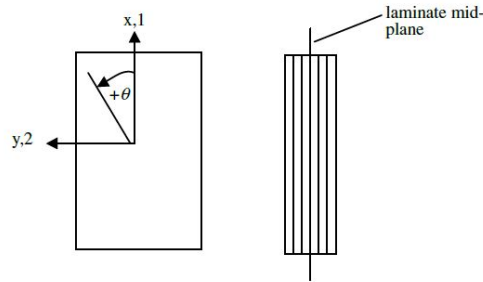
Figure 2.1: Laminate axes and definition of positive θ angle [12].

There are many different types of laminate stacking sequences. The most common are [12]:

- Symmetric: "these are laminates that have a symmetric stacking sequence in respect to midplane".

- Balanced: "these are laminates in which for each $+\theta$ ply there is a $-\theta$ in the stacking sequence".

- Cross ply and angle ply: "For the cross ply, the laminate consists of only 0° and 90° plies, whereas for the angle ply, the laminate does not contain any 0° or 90° plies".

- Quasi-isotropic: "these laminates have the same stiffness in any direction in their plane".

- The most commonly used type of laminate is the balanced and symmetric laminate in order to eliminate the coupling effects caused by a non zero B matrix, as will be explained later. An example of a balanced and symmetric laminate is $[45/-45/30/-30/60/-60]_s$.

2.1.1   Review of the classical laminate theory

The assumptions for CLT are:

- The laminate consists of perfectly bonded layers

- Each ply is considered to be a homogeneous layer

- Each ply is in a state of plane stress

- The individual ply can be isotropic, orthotropic or transversely isotropic

- The normals to the mid-plane remain straight and normal to the midplane even after deformation

- The normals to the mid-plane do not change their lengths

Composite materials are originally anisotropic, which is translated into having 3 normal stresses $[\sigma_x, \sigma_y, \sigma_z]$ and strains $[\varepsilon_x, \varepsilon_y, \varepsilon_z]$ as well as 3 shear stresses $[\tau_{yz}, \tau_{xz}, \tau_{xy}]$ and strains $[\gamma_{yz}, \gamma_{xz}, \gamma_{xy}]$ [12].

Stresses and strains are related through the generalized stress-strains relations or Hooke's law. This relation can be seen in equation 2.1.

$$
\begin{bmatrix} \sigma_x \\ \sigma_y \\ \sigma_z \\ \tau_{yz} \\ \tau_{xz} \\ \tau_{xy} \end{bmatrix} = \begin{bmatrix} E_{11} & E_{12} & E_{13} & E_{14} & E_{15} & E_{16} \\ E_{21} & E_{22} & E_{23} & E_{24} & E_{25} & E_{26} \\ E_{31} & E_{32} & E_{33} & E_{34} & E_{35} & E_{36} \\ E_{41} & E_{42} & E_{43} & E_{44} & E_{45} & E_{46} \\ E_{51} & E_{52} & E_{53} & E_{54} & E_{55} & E_{56} \\ E_{61} & E_{62} & E_{63} & E_{64} & E_{65} & E_{66} \end{bmatrix} \begin{bmatrix} \varepsilon_x \\ \varepsilon_y \\ \varepsilon_z \\ \gamma_{yz} \\ \gamma_{xz} \\ \gamma_{xy} \end{bmatrix}
\tag{2.1}
$$

Where E_{ij} is the stiffness component.

In most cases with composite laminates though, the material is orthotropic. That means it has two planes of symmetry. In that case:

$$
E_{14} = E_{15} = E_{16} = E_{24} = E_{25} = E_{26} = E_{34} = E_{35} = E_{36} = 0
$$

In the case of orthotropic material, equation 2.1 becomes:

$$
\begin{bmatrix} \sigma_x \\ \sigma_y \\ \sigma_z \\ \tau_{yz} \\ \tau_{xz} \\ \tau_{xy} \end{bmatrix} = \begin{bmatrix} E_{11} & E_{12} & E_{13} & 0 & 0 & 0 \\ E_{21} & E_{22} & E_{23} & 0 & 0 & 0 \\ E_{31} & E_{32} & E_{33} & 0 & 0 & 0 \\ 0 & 0 & 0 & E_{44} & 0 & 0 \\ 0 & 0 & 0 & 0 & E_{55} & 0 \\ 0 & 0 & 0 & 0 & 0 & E_{66} \end{bmatrix} \begin{bmatrix} \varepsilon_x \\ \varepsilon_y \\ \varepsilon_z \\ \gamma_{yz} \\ \gamma_{xz} \\ \gamma_{xy} \end{bmatrix}
\tag{2.2}
$$

In case the express of strains in terms of stresses is needed, the inverse of equation 2.2 is used:

$$
\begin{bmatrix} \varepsilon_x \\ \varepsilon_y \\ \varepsilon_z \\ \gamma_{yz} \\ \gamma_{xz} \\ \gamma_{xy} \end{bmatrix} = \begin{bmatrix} S_{11} & S_{12} & S_{13} & S_{14} & S_{15} & S_{16} \\ S_{21} & S_{22} & S_{23} & S_{24} & S_{25} & S_{26} \\ S_{31} & S_{32} & S_{33} & S_{34} & S_{35} & S_{36} \\ S_{41} & S_{42} & S_{43} & S_{44} & S_{45} & S_{46} \\ S_{51} & S_{52} & S_{53} & S_{54} & S_{55} & S_{56} \\ S_{61} & S_{62} & S_{63} & S_{64} & S_{65} & S_{66} \end{bmatrix} \begin{bmatrix} \sigma_x \\ \sigma_y \\ \sigma_z \\ \tau_{yz} \\ \tau_{xz} \\ \tau_{xy} \end{bmatrix}
\tag{2.3}
$$

Equation 2.3 is called compliance matrix and S_{ij} is called the compliance tensor.

Since most of the times the laminates used are very thin, it can be assumed that the laminate is in a plane stress state. This is due to the fact that the thickness to length ratio of the laminate is very small. This leads to the eliminations of the out of plane stresses which are:

$$
\sigma_z = \tau_{yz} = \tau_{xz} = 0
$$

The equation for plane stress can be rewritten as:

$$\begin{bmatrix} \sigma_x \\ \sigma_y \\ \tau_{xy} \end{bmatrix} = \begin{bmatrix} Q_{xx} & Q_{xy} & 0 \\ Q_{xy} & Q_{yy} & 0 \\ 0 & 0 & Q_{ss} \end{bmatrix} \begin{bmatrix} \varepsilon_x \\ \varepsilon_y \\ \gamma_{xy} \end{bmatrix} \tag{2.4}$$

In order to obtain the stress-strains relations of equation 2.4 but for any ply rotated by an angle θ, the equation becomes:

$$\begin{bmatrix} \sigma_1 \\ \sigma_2 \\ \tau_{12} \end{bmatrix} = \begin{bmatrix} Q_{11} & Q_{12} & Q_{16} \\ Q_{12} & Q_{22} & Q_{26} \\ Q_{16} & Q_{26} & Q_{66} \end{bmatrix} \begin{bmatrix} \varepsilon_1 \\ \varepsilon_2 \\ \gamma_{12} \end{bmatrix} \tag{2.5}$$

The Q_{ij} terms are calculated using standard transformation equations:

$$S_{mnpq} = l_{mi}l_{nj}l_{pk}l_{qr}S_{ijkr}$$

Where l_{ij} is the direction cosine between axes i and j.

ABD matrix

The stiffness of the laminate is defined by integrating through the thickness. The stiffness matrix or ABD matrix is composed of 3 parts, the A matrix which contains the in plane stiffness properties, the D matrix which contains the out of plane stiffness properties and the B matrix which contains the coupled stiffness properties. Force resultants and laminate strain relations are obtained by using equation 2.5. The result is shown below:

$$\begin{bmatrix} N_{xx} \\ N_{yy} \\ N_{xy} \\ M_{xx} \\ M_{yy} \\ M_{xy} \end{bmatrix} = \begin{bmatrix} A_{11} & A_{12} & A_{16} & B_{11} & B_{12} & B_{16} \\ A_{12} & A_{22} & A_{26} & B_{12} & B_{22} & B_{26} \\ A_{16} & A_{26} & A_{66} & B_{16} & B_{26} & B_{66} \\ B_{11} & B_{12} & B_{16} & D_{11} & D_{12} & D_{16} \\ B_{12} & B_{22} & B_{26} & D_{12} & D_{22} & D_{26} \\ B_{16} & B_{26} & B_{66} & D_{16} & D_{26} & D_{66} \end{bmatrix} \begin{bmatrix} \varepsilon_{xo} \\ \varepsilon_{yo} \\ \varepsilon_{xyo} \\ \kappa_x \\ \kappa_y \\ \kappa_{xy} \end{bmatrix} \tag{2.6}$$

Where $\varepsilon_{xo}, \varepsilon_{yo}, \varepsilon_{xyo}$ are the midplane strains and $\kappa_x, \kappa_y, \kappa_{xy}$ are the curvatures. If the in plane strains need to be found, equations below have to be used:

$$\varepsilon_x = \varepsilon_{xo} + zk_x, \varepsilon_y = \varepsilon_{yo} + zk_y, \gamma_{xy} = \varepsilon_{xyo} + zk_{xy}$$

The terms A,B and D are calculated from:

$$A_{ij} = \sum_{k=1}^{N} Q_{ij}(Z_k - Z_{k-1})$$

$$B_{ij} = \frac{1}{2}\sum_{k=1}^{N} Q_{ij}(Z_k^2 - Z_{k-1}^2)$$

$$D_{ij} = \frac{1}{3} \sum_{k=1}^{N} Q_{ij}(Z_k^3 - Z_{k-1}^3)$$

and Z_k, Z_{k-1} are the upper and lower Z coordinates of the Kth ply, as shown in figure 2.2.
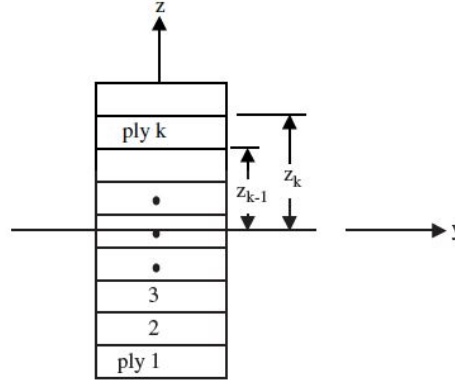
Figure 2.2: Ply numbering system [12]

If midplane strains need to be found, the inverse of equation 2.6 can be used:

$$
\begin{bmatrix} \varepsilon_{xx}^o \\ \varepsilon_{yy}^o \\ \varepsilon_{xy}^o \\ \kappa_{xx} \\ \kappa_{yy} \\ \kappa_{xy} \end{bmatrix} =
\begin{bmatrix}
a_{11} & a_{12} & a_{16} & b_{11} & b_{12} & b_{16} \\
a_{12} & a_{22} & a_{26} & b_{12} & b_{22} & b_{26} \\
a_{16} & a_{26} & a_{66} & b_{16} & b_{26} & b_{66} \\
b_{11} & b_{12} & b_{16} & d_{11} & d_{12} & d_{16} \\
b_{12} & b_{22} & b_{26} & d_{12} & d_{22} & d_{26} \\
b_{16} & b_{26} & b_{66} & d_{16} & d_{26} & d_{66}
\end{bmatrix}
\begin{bmatrix} N_{xx} \\ N_{yy} \\ N_{xy} \\ M_{xx} \\ M_{yy} \\ M_{xy} \end{bmatrix}
\tag{2.7}
$$

2.1.2 Equivalent laminate properties

In case the stiffness properties of a laminate need to be calculated, the following equations can be used:

$$E_{1m} = \frac{1}{ha_{11}} \quad E_{1b} = \frac{12}{h^3 d_{11}}$$

$$E_{2m} = \frac{1}{ha_{11}} \quad E_{2b} = \frac{12}{h^3 d_{22}}$$

$$G_{12m} = \frac{1}{ha_{66}} \quad G_{12b} = \frac{12}{h^3 d_{66}}$$

$$v_{12m} = -\frac{a_{12}}{a_{22}} \quad v_{12b} = -\frac{d_{12}}{d_{22}}$$

$$v_{21m} = -\frac{a_{12}}{a_{11}} \quad v_{21b} = -\frac{d_{21}}{d_{11}}$$

Where m and b refers to membrane and bending stiffness respectively.

2.1.3 Lamination parameters

The lamination parameters is a way of describing the stiffness of a laminate using 12 continuous variables terms. These terms are very suitable in describing and optimizing the stiffness properties of a laminate without knowing its original stacking sequence [27, 28]. If the laminate is balanced and symmetric, variables are diminished to 4, since $V_2^A, V_4^A, V_1^B, V_3^B, V_4^B, V_2^D, V_4^D$ can be assumed negligible. The main disadvantage of calculating the stiffness of the laminate using laminating parameters is that post processing is needed to acquire the stacking sequence of the laminate. The lamination parameters can be seen in equation 2.8.

$$(V_1^A, V_2^A, V_3^A, V_4^A) = \int_{-\frac{1}{2}}^{\frac{1}{2}} (cos2\theta, sin2\theta, cos4\theta, sin4\theta)d\bar{z}$$

$$(V_1^B, V_2^B, V_3^B, V_4^B) = 4 \int_{-\frac{1}{2}}^{\frac{1}{2}} \bar{z}(cos2\theta, sin2\theta, cos4\theta, sin4\theta)d\bar{z} \qquad (2.8)$$

$$(V_1^D, V_2^D, V_3^D, V_4^D) = 12 \int_{-\frac{1}{2}}^{\frac{1}{2}} \bar{z}^2(cos2\theta, sin2\theta, cos4\theta, sin4\theta)d\bar{z}$$

where, $V_i^{A,B,D}$, i=1,2,3,4 are the lamination parameters and $\bar{z}$ is the normalized through the thickness dimension.

2.2   Review on laminate blending methods

2.2.1   Laminate blending definition

When manufacturing a normal composite laminate, the laminate is over designed since the thickness and the stacking sequence are calculated based on the area of the laminate with the highest load. Composite laminate blending comes to solve this issue by incorporating different thicknesses and stacking sequences at different areas of the laminate but at the same time taking into account continuity and manufacturability guidelines. The term composite laminate blending was introduced by Zabinsky [34]. Laminate blending is the division of a composite laminate into many different regions/panels, where the loads are constant but different in each region/panel [34]. Kristinsdottir et al. used the "less than equal to rule" of Zabinsky and a genetic algorithm [8] to implement their laminate blending method. This laminate blending method is called "Improving Hit and Run"[13]. A Genetic Algorithm is defined as a probabilistic, non deterministic optimization algorithm which uses the Darwinian theory and more particularly, the theory of the survival of the fittest [31]. It is important to consider that a laminate blending design needs to have structural integrity since there might be inconsistency between different layers in different sections. In order to achieve that, continuity, structural and manufacturing constraints need to be applied [34].

More laminate blending techniques are explained in the next paragraphs.

2.2.2   Guidelines for blending a laminated composite plate

The main objective for a blending composite laminate panel is the determination of the stacking sequences of each section of the panel so that the total weight is minimized. In figure 2.3a, a conventional composite laminate is shown, where the stacking sequence is defined by the highest load in the laminate, leading to an overweight design. Figure 2.3b shows the local optima of a laminated composite plate which is divided into 4 sections with constant different loads in each section. This laminate has no structural integrity. Finally figure 2.3c, shows the final blending laminate configuration where blending ensures that plies comply with manufacturing and structural constraints [31]. Ply drops are required in order to have a blended panel design. The absence of ply drops can lead to stress concentrations and failure.
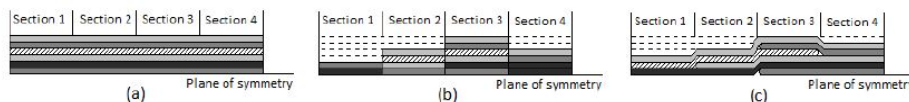
Figure 2.3: (a) Normal composite laminate panel, (b) local optima configuration, (c) Blended configuration [31]

2.2.3   State of the art blending techniques

Introduction of the Laminate Blending terminology

The first introduction on the term of composite laminate blending was done by Zabinsky. The main blending rule used is the less-than-equal-to rule using variables for each ply in each

section of the laminate [34]. Using this blending rule, plies are dropped in consistency, which means that dropped plies can not be added back into the panel. Dropping of the plies starts from the key region, the thickest section of the laminate, which is identified by a star and the "greater-that-or-equal-to" symbols show the direction of permissible ply drops as shown in figure 2.4 [13]. The laminate is divided into sections with varying but constant loads in each one. For the optimization process of blending the different sections together, a random search algorithm called improving Hit and Run is used [34]. Kristinsdottir et al. expanded the work of Zabinsky so that the improving Hit and Run algorithm works for panels with large number of sections and multiple key regions.
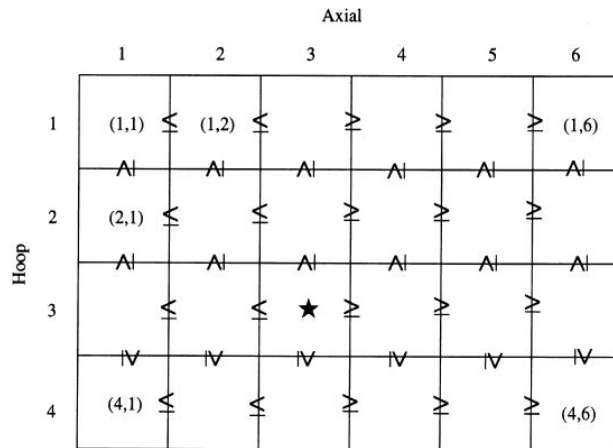
Figure 2.4: Greater-than-or-equal-to blending rule [13]

Classification of laminate blending methods

Before analyzing each laminate blending method separately, two tables are provided with an overview of all the laminate blending methods that are going to be analyzed in the next chapters. Table 2.1 contains all the single-step laminate blending methods whereas table 2.2 contains all the multi-step laminate blending methods. All these methods are further categorized inside each table.

Table 2.1: Single-step blending methods

Single-step blending methods

- Guide-based blending by Adams et al.
- Less than equal rule of Kristinsdottir et al.
- Method using continuity constraints by Liu and Haftka
- Multi-chromosomal guide-based method by Seresta et al.
- Genetic algorithm with migration by Adams et al.

Table 2.2: Multi-step blending methods

Multi-step blending methods

- Two step guide-based method by IJsselmuiden et al.

- Four step guide-based method by Jin et al.

- Two step PDS method by Yang et al.

- Bi-level blending method by Zein and Bruyneel

- Design variable zones method by Soremekun et al.

- New blending constraints method by Macquart et al.

- Two step generalized blending by Van Campen et al.

- Two step SST method by Le Riche and Irisarri

- Global shared layer method by Jing et al.

- Shared layer blending by Liu et al.

- Method with new continuity rules by Fan et al.

Guide-based blending

Guide based laminate blending was first introduced by Adams et al. [3]. This method basically uses stacking sequence of the thickest panel of the laminate as a guide laminate and then defines all the other panels by deleting plies from the guide laminate. The optimization is done by using a genetic algorithm since it is the most efficient way of exploring many different possible designs [3]. The panels are either outwardly or inwardly blended. Outwardly and inwardly blending techniques can be seen in figure 2.5 [3]. The genetic algorithm is used to evaluate a guide laminate design in order to determine the stacking sequence that will later be used to define the local panels [3]. An example of guide based design is shown in figure 2.6 [3]. In this particular example, a laminate divided into 3 panels is used.
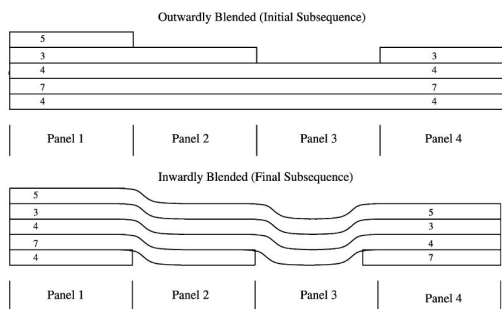
Fig. 1. Outwardly/inwardly blended distinction example.

Figure 2.5: Outwardly/inwardly blending techniques [3]
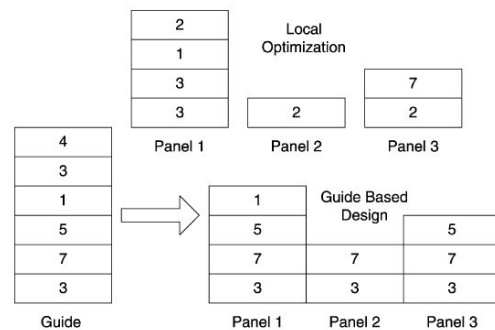
Figure 2.6: Guide based example [3]

A drawback of guide based laminate blending is the use of repetition for the analysis of the

entire structure in order to figure out the most optimal design [9]. IJsselmuiden et al. proposed a milti-step approach for the design of a composite blended panel where in the first step the structure is optimized by finding the optimal thickness and stacking sequence for each panel and on the second step, a genetic algorithm is used to to find the most optimal blended design [9]. Using this multi-step approach method, the computational time is significantly reduced in comparison with the method of Adams et al. [3].

Jin et al. extended the optimization method of IJsselmuiden et al. to a four step optimization process [9, 10]. It uses the lamination parameters of only the guide laminate in contrast to using them for each section of the laminate. Seresta et al. proposed a multi-chromosomal Genetic Algorithm for more efficient blending of a laminate in comparison to the original guide based blending [24]. In more detail, the method of Seresta et al. uses two chromosomes in the Genetic algorithm. The guide laminate stacking sequence is defined by the first chromosome and the second binary chromosome, represents each different panel, where 1 means the corresponding ply from the first chromosome (from the guide laminate) exists and 0 means that it does not exist [24].

All previous methods on laminate blending depend on whether inner or outer layers are retained from a guide laminate. Using these methods though, it is not assured that the most optimal blended design is achieved [29]. Van Campen et al. introduced two new blending definitions which give more freedom in guide based blending [29]. The first definition is called **Generalized blending** where "two adjacent panels are completely blended if all the layers from the thinner panel continue in the thicker one regardless of their position along the thickness of the laminate" [29]. The second definition is called **Relaxed generalized blending** where "two adjacent panels are considered completely blended if there are no dropped edges in physical contact" [29]. These two new blending definitions use the multi-chromosomal Genetic Algorithm of Seresta et al. in combination with the framework of McMahon et al. using a distributed genetic algorithm with migration [29]. Figure 2.7 shows examples of the two new blending definitions [31].
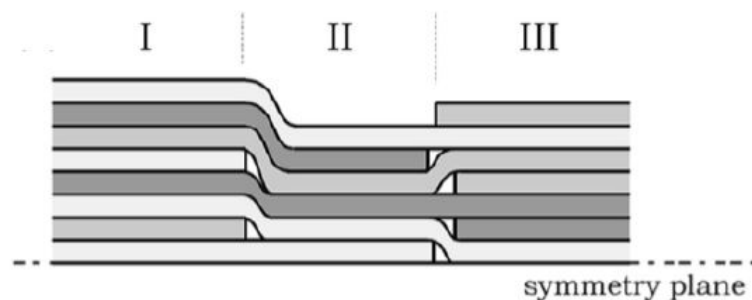
Figure 2.7: Examples of generalized blending (I-II) and relaxed generalized blending (II-III) [31]

Blending based on Stacking Sequence Tables

Blending using Stacking Sequence Tables (SST) was first introduced by Le Riche and Irisarri [14]. This method puts guide based blending a step ahead by handling more design guidelines and as a consequence being able to design a more efficient blended laminate. Basically, the

SST method uses tables to keep additional information concerning the plies composing the structure, giving more information on which plies to drop [14]. An example of SST can be seen in figure 2.8 [31]. Yang et al. proposed a new blending optimization method similar to the one using stacking sequence tables [33]. In this method, ply drop sequence (PDS) tables are used to associate each ply of the guide laminate with a number related to its thickness location. Using ply drop off rules, the stacking sequence of each individual panel is constructed by deleting plies from the guide laminate taking into consideration the values of the PDS tables

Thickness [layers]	Nmin					Nmax
	3	4	5	6	7	8
			0	0	0	0
	+45	+45	+45	+45	+45	+45
					-75	-75
		90	90	90	90	90
				75	75	75
						90
	-45	-45	-45	-45	-45	-45
	0	0	0	0	0	0

Figure 2.8: Example of a Stacking Sequence Table [31]

Jing et al. used a different approach in blending composite laminates. Most papers present blending as a procedure from local to global level [11]. Jing et al. proposed a blending method called global shared layer blending method, which blends the laminate from global level to local level [11]. At global level, the Shared layer blending method of Liu et al. was used in combination with ply continuity rules in order to obtain the global laminate structure [11]. At local level, Stacking sequence tables and design rules were used to define the stacking sequence of each separate panel [11]. Zein and Bruyneel proposed a bilevel approach where the thickness and the stacking sequence are calculated at the same time using a backtracking algorithm [35]. For this optimization method, drop off tables, similar to SST tables, are used, containing the ply angle, stacking sequence and thickness of each region [35].

Other laminate blending methods

Liu et al. proposed the shared layer blending method. In this method, the amount of common layers, with respect to ply angle, between the different panels of the laminate, is used as an optimization tool [16]. Soremekun et al. defined a new two step blending method. Information about the laminate to be blended is gathered and put into two different groups [26]. These groups are the Design variable zones, where information about the similarities of the different separate panels is gathered and the sub-laminates, where information about the differences between the separate panels is gathered [26]. An example of a 4 panel laminate is shown in figures 2.9 and 2.10.
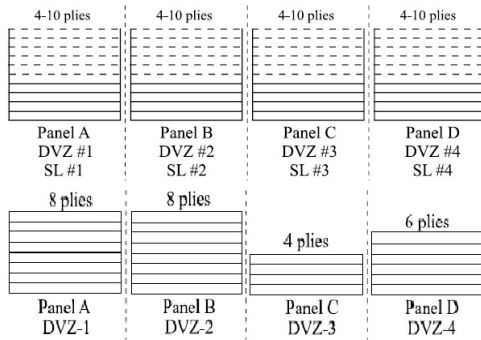
Figure 2.9: Optimization of individual panels [26]
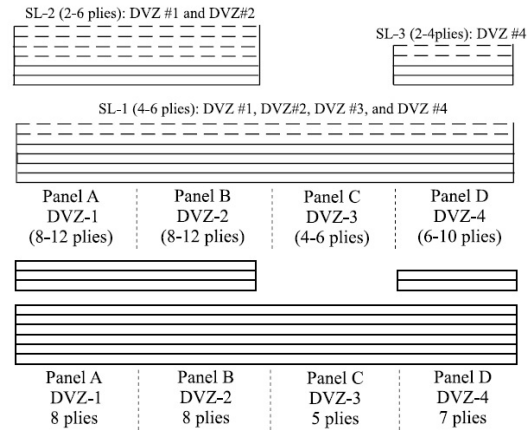
Figure 2.10: Final blended solution [26]

Liu and Haftka came up with a simpler way of optimizing a blended structure. To do that, "measures of continuity" were developed and used for global and local level optimization of the laminate [15]. The first measure of continuity takes into account the common plies between different panels, in respect of material, ply orientation or thickness. The second measure of continuity, takes into account the stacking sequences of different adjacent panels and finds out how many plies can continue between them [15]. Fan et al. altered the genetic algorithm in order to allow more design freedom in the blending between different panels of a laminate. To do that, new blending continuity rules were proposed for laminate optimization as well as new genetic operators [6]. These continuity rules are the ply-composition and ply-ranking chromosomes [6]. Macquart et al. derived new blending constraints in order to reduce the computational effort needed for the procedure of blending all the different panels of a laminate together. These constraints have to do with the coupling of in plane and out of plane lamination parameters [18]. However, this method has not yet been tested in many different blending problems to be verified.

2.2.4 Horseshoe benchmark

Horseshoe benchmark test was first introduced by Soremekun et al. as a representation of a helicopter floor panel to show the effectiveness of his blending method [26]. It was then used by many other authors of composite blending papers as a way to show the effectiveness of their blending methods. It is composed by 18 different panels, each one simply supported with a bi-axial load. The ply orientations are limited between 0 and 90 degrees with increments of ± 15 degrees. The horseshoe configuration can be seen in figure 2.11.
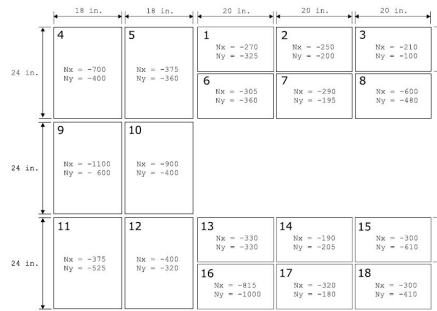
Figure 2.11: The horseshoe panel configuration [26]. All loads are in lb/in

The purpose of this test, is to minimize the weight of each panel individually and then blend all the panels together. The constraint for minimizing weight is the critical buckling load of each panel individually.

Results found in literature

All the results from the state of the art blending methods found in literature are presented in table 2.3. The materials used in all these cases are the graphite-epoxy (IM7/8552), the properties of which can be seen in table 2.4. All the stacking sequences are symmetric but not all of them balanced. In the results of table 2.3, the horseshoe test results using the algorithm of Van den Oord are also presented.

Table 2.3: Results found in literature concerning horseshoe benchmark test

	Soremekun et al.	IJsselmuiden et al.		Jin et al.	Seresta et al.	Le Riche and Irisarri	Fan et al.	Adams et al.	Van den Oord
	Balanced	Balanced	Unbalanced	Balanced	Balanced	Balanced	Balanced	Semi-balanced	Semi-balanced
Section 1	34	34	34	34	34	34	34	34	32
Section 2	30	30	30	28	28	30	28	38	28
Section 3	22	22	22	22	22	22	24	22	22
Section 4	20	18	18	20	20	18	20	18	20
Section 5	16	18	16	16	16	18	16	16	18
Section 6	22	22	22	22	22	22	24	22	22
Section 7	20	20	18	20	20	18	20	18	20
Section 8	24	26	26	26	26	26	26	26	26
Section 9	40	40	38	38	38	38	38	38	38
Section 10	36	36	36	36	36	38	36	36	34
Section 11	32	34	30	30	30	30	30	30	30
Section 12	30	30	30	28	28	30	28	28	28
Section 13	22	22	22	22	22	22	22	22	22
Section 14	20	18	18	20	20	18	20	18	18
Section 15	26	26	26	26	26	26	26	26	24
Section 16	30	34	32	32	30	30	32	38	32
Section 17	20	18	18	20	20	18	20	18	20
Section 18	22	22	22	24	26	22	24	22	22
Total amount of layers	466	470	458	464	464	460	468	460	456
Weight (kg)	29.27	29.46	28.68	28.81	28.82	28.85	28.62	28.63	28.28

Property	Value
Longitudinal modulus E_1 [GPa]	141
Transverse modulus E_2 [GPa]	9.034
In-plane shear modulus G_{12} [GPa]	4.72
Poisson's ration ν_{12}	0.32
Ply thickness t_{ply} [mm]	0.191

Table 2.4: Graphite-epoxy (IM7/8552)

2.3 GA-CA based blending method

2.3.1 Method overview

The algorithm proposed by Van den Oord is a two step optimization method. The first step is the local optimization of each stacking sequence of each section of a panel using a genetic algorithm (GA), whereas the second step is the global optimization of the panel by blending all different sections together leading to a blended design, using a cellular automaton (CA) [31].

2.3.2 Local optimization

As mentioned above, the local optimization is achieved using a genetic algorithm. A genetic algorithm uses the Darwinian theory of survival of the fittest in order to find and select the most appropriate individual between a population [25]. In the case of the blending problem, the population is composed of randomly created stacking sequences (individuals) for the different panels. Within a number of iterations, also called generations, the genetic algorithm will select the most appropriate individual(s) by evaluating the fitness of each one [31]. A flowchart of the genetic algorithm is shown in figure 2.12.
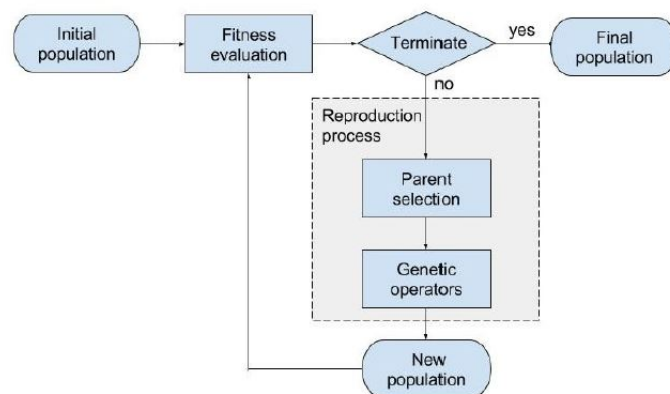
Figure 2.12: Flowchart of a GA [31]

Chromosomes in the GA

Any individual in the genetic algorithm is represented by a chromosome. In our case, the individuals are stacking sequences, which are called genes, meaning that the chromosome consists of numbers referring to ply orientations [31].

Fitness evaluation

Each individual is evaluated according to their design and then ranked taking into consideration the fitness values. The objective of the optimization process of the GA, is the weigh

minimization of the structure, without surpassing a specific constraint or many constraints. In our case, the constraint is the critical buckling load. The equation used to describe the constraint is:

$$g_{min} = \frac{N_o}{N_x} - 1 \tag{2.9}$$

Where, N_o is the maximum buckling load a section can achieve and N_x is the buckling load the section is supposed to carry. Thus, the constraint is:

$$minimize \, W \rightarrow g_{min} \geq 0$$

All the above are combined into a fitness function found in equations 2.10, 2.11:

$$\theta = W + \beta g_{min} \, if \, g_{min} < 0 \tag{2.10}$$
$$\theta = W + \varepsilon g_{min} \, if \, g_{min} < 0 \tag{2.11}$$

Where, W is the normalized weight, β is a penalty parameter and ε is a bonus parameter. The penalty parameter is applied when the maximum buckling load a section can withstand is less than the applied one and the opposite happens for the bonus parameters [31].

Evolution process

The evolution process consists of many iterations that produce new generations of individuals from the initial population. Parents are selected from the individuals, based on their fitness ranking. Then the application of genetic operators is followed in order to create the next generation of individuals. Some of the techniques used are shown below [31]:

- **Crossover**

- **Mutation**

- **Permutation**

- **Swap**

- **Ply addition**

- **Elitist selection**

2.3.3 Local optimization

The local optimization of a blended panel is done after the optimization of the stacking sequence of each cell or section of the panel has finished. To achieve that, a cellular automaton (CA) is used to evolve each cell of the panel based on the state of its neighbours. In other words, the CA translates the blending constraints into local dependencies [31]. A flowchart of the CA procedure is shown in figure 2.13.
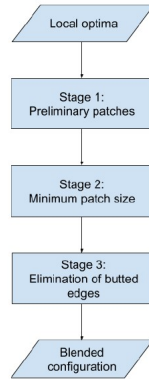
Figure 2.13: Flowchart of the CA algorithm [31]

In order to prevent simultaneous evolution of all cells, which would make it impossible to solve the problem, Van den Oord divided the cells in a chessboard pattern [31].

As shown in figure 2.13, the CA algorithm consists of 3 stages: the assembly of preliminary patches, the minimum patch size and the elimination of butted edges [31]. These are further discussed below:

Assembly of preliminary patches

By using a set of rules, the algorithm forces all plies of a cell to become part of a patch. The assembly of preliminary patches can be done either by using 1 layer or by using multiple layers. Multiple layers increase the design freedom. However, this can increase the complexity of the blended configuration possibly resulting in isolated plies and non-uniform distribution of patches. In order for the algorithm to solve this problem, a genotype is created with the purpose of prioritization of the possible modifications in each ply of a cell. This can be seen in table 2.5, where the ply orientation of the cell and its neighbours are presented as integers [31].

Layer	Cell X	Neighbour			
		1	**2**	**3**	**4**
7	3	6	7	0	7
6	6	6	6	3	6
5	7	3	3	5	1
4	2	2	1	3	4
3	5	5	5	6	6
2	4	3	1	4	1
1	7	2	7	2	2

Table 2.5: Representation of the stacking sequences as integers from the analyzed cell and its neighbours [31]

After the creation of table 2.5, the deviation scheme of the analyzed ply can be created. The deviation scheme is a table showing the necessary orientation steps all the plies in the cell have to make in order to get an orientation similar to their neighbour's. After the creation of the deviation scheme table, it is possible to create the genotype table, which simply is the addition of all the plus and minus orientations in each step and each ply from table 2.6. This new table is called genotype table or NC (neighbour count) table and can be seen in table 2.7 [31].

Cell X	Amount of neighbouring plies per deviation distance											
	Equal	I step		II steps		III steps		IV steps		V steps		VI steps	
		+	-	+	-	+	-	+	-	+	-	+	-
Layer 7						1		2					
Layer 6	3						1						
Layer 5					1				2				1
Layer 4	1	1	1	1									
Layer 3	2	2											
Layer 2	1		1				2						
Layer 1	1										3		

Table 2.6: The deviation scheme of a cell according to its neighbours [31]

Cell X	Neighbour Count per deviation distance						
	Equal	I step	II step	III step	IV step	V step	VI step
Layer 7				+1	+2		
Layer 6	3			-1			
Layer 5			-1		-2		-1
Layer 4	1	0	+1				
Layer 3	2	+2					
Layer 2	1	-1		-2			
Layer 1	1					-3	

Table 2.7: The genotype table [31]

Minimum patch size

The minimum patch size, simply dictates what is the minimum size of the patches created in the previous stage of the algorithm and makes any corrections needed to the patch size. The algorithm procedure for the minimum patch size strategy is divided in 2D and 3D problems [31].

Minimum patch size in 2D problems

In 2d problems, the algorithm is again subdivided in two patch merge options, depending on the amount of layers taken into consideration around the analyzed patch. In other words, when the algorithm tries to merge a non-compliant patch with surrounding patches, it can either look only at the neighbour patches or at the neighbour and the patches just above and below of the neighbour plies that are in the same line with the analyzed ply [31].

Minimum patch size in 3D problems

In 3D problems, the minimum patch size is similar to the minimum cross-sectional length of a patch. Only one layer is allowed to be analyzed for merging non-conventional patches with already existing ones. This is done to avoid fractionation of patches which especially in 3D problems is possible to happen. The strategy of the algorithm is to merge all non-conventional patches in each unique cross section of the laminate with a successive order so that fractionation of patches is avoided as much as possible [31].

Elimination of butted edges

This part of the algorithm tries to get rid of the butted edges from the panel since they produce excessive stresses that can be fatal for the integrity of the panel [31].

Elimination of butted edges in 2D problems

The elimination of butted edges in 2D problems is subdivided in 3 categories. Each category has its own method of elimination of the butted edge and in some cases the elimination of a butted edge can takes more than a single iteration to complete. The 3 different categories of butted edges can be seen in figure 2.14 [31].
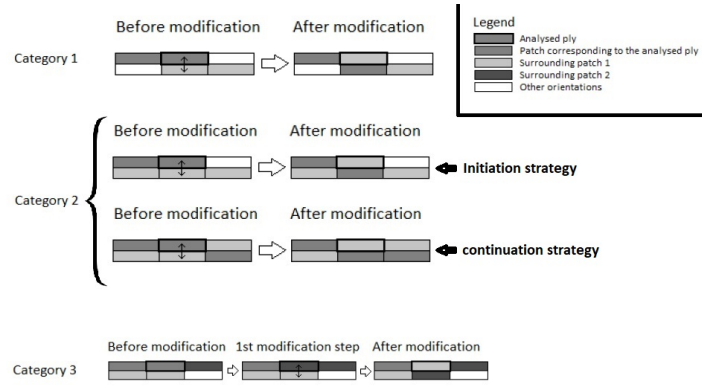
Figure 2.14: Different categories of butted edges [31]

Elimination of butted edges in 3D problems

For the elimination of butted edges in 3D problems, a different approach is followed due to the fact that the amount of surrounding patch scenarios is increased. The proposed method for eliminating the butted edges is by changing the orientation of the analyzed cell to the one which will result in the minimum amount of butted edges afterwards. It has to be noted that the total amount of layers taking into consideration in each iteration is 3. That means the maximum amount of butted edges per analyzed cell can be the amount of neighbours, which is 12 with the exception of the edges of the laminate where the maximum amount can be 8 [31].

2.3.4 Global patch interpretation

The global patch interpretation is the assembly of the final blended laminate design since all previous steps were used to locally blend the laminate. As a consequence, many globally blended designs can be extracted. In order to select the right globally blended design, rules are formulated [31]. These rules include:

- Minimum patch size.

- Butted edges.

- Amount of plies dropped at the same location.

- Decoding of the chromosome.

2.3.5 Horseshoe benchmark case

The horseshoe benchmark case has already been discussed in section 2.2.4. It is a benchmark problem proposed by Soremekun et al. that simulates a helicopter floor panel [26]. Since then, it has been used by almost all authors in composite blending articles, as a proof that their algorithm works fine. Despite the fact that the algorithm proposed by Van den Oord is optimized for laminates with a large number of sections, it is still used in the horseshoe

benchmark case composed of only 18 sections. In table 2.3, the number of plies per section for different composite blending methods is shown, including the proposed method by Van den Oord found at the last column of the table 2.3. The proposed method by Van den Oord responded exceptionally to the horseshoe benchmark case, achieving the lowest weight of all the methods compared in table 2.3.

2.3.6 The proposed benchmark

Van den Oord proposed two benchmark problems, one for 2D and one for 3D problems. However, only the 3D one is relevant to this thesis project and thus only the 3D one is presented [31].

The proposed benchmark problem for 3D problems is a square plate with 21x21 sections and 5 layers under uni-axial compression. The local optima is not provided by a regular GA this time but the genetic algorithm of Van Campen is used based on the limitations parameter distribution [31]. In figure 2.15, the evolution from the local optima up to stage 3 (elimination of butted edges) can be seen. The material properties used in this problem can be seen in figure 2.8.
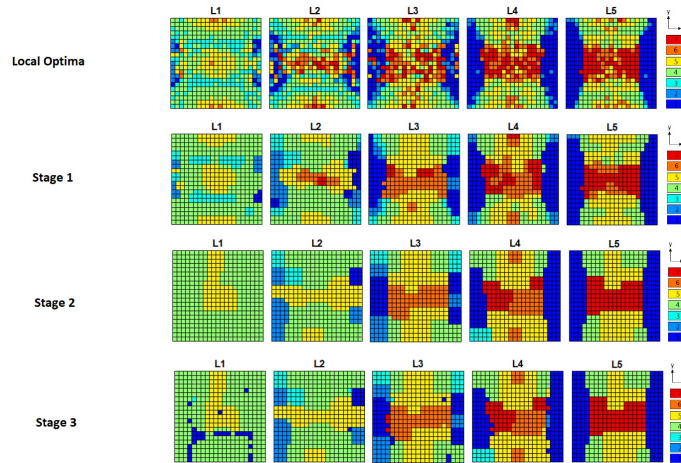
Figure 2.15: A benchmark case of a 21x21 sections 5 layers 3D plate problem [31]

Property	Value
Longitudinal modulus E_1 [GPa]	181
Transverse modulus E_2 [GPa]	10.3
In-plane shear modulus G_{12} [GPa]	7.17
Poisson's ration ν_{12}	0.28

Table 2.8: Material used in 3D benchmark problem

2.3.7 Verification of GA-CA algorithm

Gomaa verified the GA-CA algorithm of Van den Oord by manufacturing a 600x400mm blended laminate [7]. The laminate is composed of 25 different sections each one assigned

with a stacking sequence. All of the sections are symmetric and balanced in order to eliminate any coupling effects during load application. Additionally, the laminate is also symmetric along its plane axes optimised for buckling loading. The local optima of each section was provided by the genetic algorithm of Van Campen and the global optimisation was done by the CA algorithm of Van den Oord [7]. The algorithm is not yet capable of finding a global patch interpretation, so it was manually done by Gomaa [7]. The final global configuration of the patches can be seen in figures 2.18 and 2.19. In figures 2.16 and 2.17, the numbering of the sections of the laminate and the stacking sequence of each section are shown.

I	II	III	II	I
IV	V	VI	V	IV
VII	VIII	IX	VIII	VII
IV	V	VI	V	IV
I	II	III	II	I

Figure 2.16: The different sections of the blended laminate [7]

Guide ID	Stacking sequence
I	$[\pm45/\pm60/\pm45/\pm30/\pm60/0_2/\pm60/0_2]_s$
II	$[\pm45/\pm60_3/0_4/\pm60/0_2]_s$
III	$[\pm45/\pm60/\pm45/\pm30/\pm60/0_2/\pm60/0_2]_s$
IV	$[\pm45/\pm60_7]_s$
V	$[\pm45/\pm60_4/0_2/\pm60_2]_s$
VI	$[\pm45/\pm60_7]_s$
VII	$[\pm45/\pm60_7]_s$
VIII	$[\pm45/\pm60_7]_s$
IX	$[\pm45/\pm60_7]_s$

Figure 2.17: Final blended stacking sequences of each section [7]
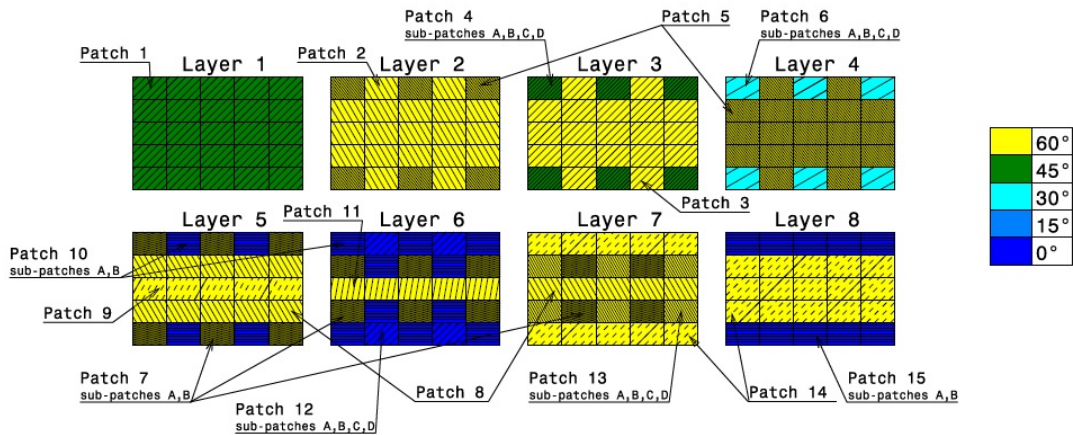
Figure 2.18: The final global patch interpretation by Gomaa [7]
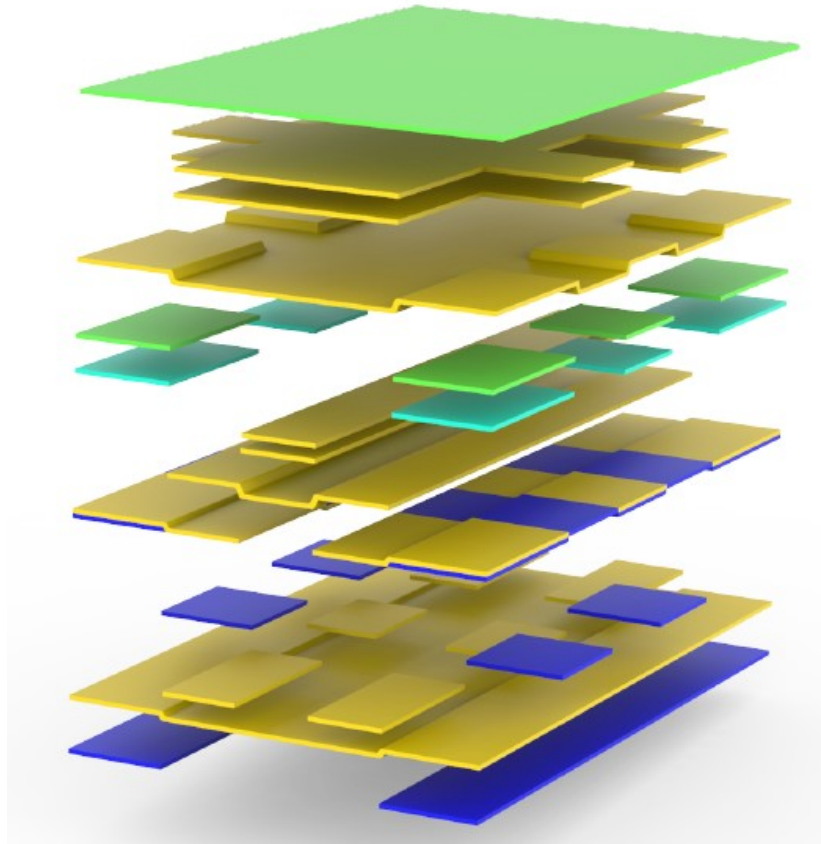
Figure 2.19: The final global patch interpretation in 3D view by Gomaa [7]

3 blended laminates were manufactured and tested in buckling. Also, a conventional laminate of the same weight with an optimized stacking sequence for buckling $[\pm45_8]_s$ was manufactured in order to compare the buckling load it can achieve to the blended one. The blended laminate achieved an 80% higher bucking load with the same weight. The overview of the buckling results is shown in table 2.3 [7].

Laminate [-]	Predicated buckling load [kN]	Average experimental buckling load[kN]	Deviation from predicted buckling load [%]	Experimental Deviation from conventional laminate [%]	Predicted deviation from conventional laminate [%]
Conventional	74.55	71.87	-3.59	-	-
Blended	132.73	130.03	-2.03	80.92	78.04

Table 2.9: The overview of the buckling results [7]

During the cooling down of the autoclave cycle, the laminate possibly experienced thermal pre-stresses due to different thermal expansion coefficients in each section. Despite the fact that each section is symmetric and balanced, due to the different stacking sequence of each section, each section as a whole possibly has a different thermal expansion-contraction coefficient, which leads to thermal pre-stresses. As a consequence, the laminate had severe saddle type imperfection after the processing at the autoclave [7]. These imperfections can be seen in figure 2.20.
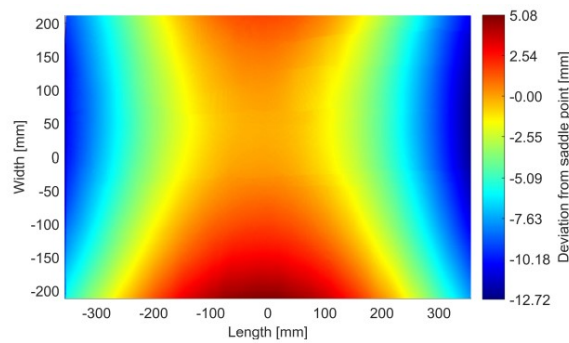
Figure 2.20: The saddle type imperfections of the blended laminate [7]

2.3.8   Conclusions and discussion

This chapter is a summary of the basic principles and equations used in this thesis project. It is the basic knowledge needed for a reader outside the field of composite laminate theory to understand the chapters to follow.

In previous sections concerning laminate blending methods, the state of the art methods for composite blending techniques were analyzed. Despite the fact that all methods have good results in the horseshoe benchmark test, very few of them have been tested using panels with large number of sections. Furthermore, most of the techniques mentioned in the previous sections, use the inner or outer blending as methods for blending different sections together, which is simple and effective but has a lot of restrictions when it comes to blending techniques and possible weight reduction. This leaves open a space for a blending method that is more efficient than the outer or inner blending methods and can be used for a large number of sections. This method is the cellular automaton algorithm developed by Van den Oord. The CA algorithm offers the ability to locally blend laminates with a large number of sections, a feature that is not found in most papers in the field of blended laminates. The algorithm uses rules to progressively blend the sections of the laminate together. Despite the fact that the algorithm is made to work for both 2D and 3D laminates, the 3D blending part of the algorithm sometimes lacks the ability to eliminate butted edges due to fractionation of patches. Future work can include the further development of the algorithm by fixing the part of the code which eliminates butted edges in 3D problems as well as the development of the global patch interpretation part of the algorithm in order to globally blend the laminate.

Chapter 3

Research questions

The main objective of this thesis project is the finite element investigation of the mechanical effects the ply drop sections have in blended laminates and this is done by investigating the blended laminate that Gomaa built, in order to identify what is the difference in the results between FEM models with and without ply drops as well as if a blended laminate FEM model, including the ply drop sections, is necessary in simulating the laminate response under buckling. The laminate response under buckling includes stress and out of plane displacement analysis of the laminate. The stress analysis is going to be achieved by using global-local FEM modeling, whereas the out of plane displacement analysis is going to be achieved by transferring the properties of the local ply drop section FEM models to the global model using a code. This code will calculate the stiffness of each ply drop section and transfer it to the global model. Additionally, the code will be built to work for any blended laminate. Finally, a thermal FEM model will be built in order to investigate the thermal response of the blended laminate during cooling down of the autoclave cycle with the purpose of using it in future blended laminate thermal investigations and to help diminish the saddle type imperfections by testing new configurations in the FEM model.

3.1 Research questions

Research questions have the purpose of helping the author as well as the reader understand the main subject of this thesis project and how to develop it.

FEM modelling for ply drop sections in blended laminates:

- What methodology should be followed in the design of the global FEM blended laminate model?

- What methodology should be followed in the design of local ply drop section FEM models in blended laminates?

- What mesh density should be used for the above models?

- How is the global-local modelling going to be implemented?

- How are the stiffness properties of the ply drop sections going to be measured?

- How are the stiffness properties of the ply drop sections going to be incorporated into the global laminate FEM model?

- What tools are needed to achieve the above?

Effect of ply drops in blended laminates:

- How are the stress results from the local ply drop section FEM models and global FEM model without the ply drops compared?

- How much different is the stiffness of the laminate going to be, if the stiffness of the ply drop sections is included in the FEM model?

- Do the differences in stress and out of plane displacement results between the blended laminate FEM models with and without ply drops, justify the use of the FEM model that includes the ply drops?

Thermal FEM model:

- How is the blended laminate thermal FEM model going to be built?

- What element type is going to be used?

- What mesh density should be used?

- How is the cooling down of the autoclave cycle going to be simulated in the FEM model?

- What is the thermal response of each separate section of the blended laminate during the cooling down in the autoclave cycle?

Chapter 4

Problem definition and methodologies

Blended laminates, are laminates that are divided into different sections and at each section a stacking sequence is assigned, additionally, at the section boundaries there are ply drops so that there is continuity and structural integrity in the laminate. The small area around the section boundaries is called ply drop section. The purpose of this thesis project is to evaluate the effects of ply drops in blended laminates. Firstly, there is going to be a stress analysis of the different ply drop sections found in the blended laminate presented by Gomaa. This analysis is going to be performed using global-local FEM modelling, local referring to the ply drop section FEM models and global to the whole blended laminate FEM model. The blended laminate is under buckling and stress results due to buckling loading in the (local) 3D ply drop section FEM models will be compared to the (global) 2D FEM model results. Secondly, the out of plane displacement of the blended laminate under buckling loading, including the ply drop sections, is calculated. In order to achieve that, a special FEM tool is constructed. The purpose of this FEM tool is to acquire the stiffness properties of the local ply drop sections and transfer them back to the global model in order to accurately calculate the stiffness and the out of plane displacement of the blended laminate. The out of plane displacement results will be compared to the blended laminate FEM model without the ply drop sections. Then, the whole procedure for the calculation of the out of plane displacement of the blended laminate is automated to work on any blended laminate. That means it should automatically acquire the stiffness properties of the ply drop sections and automatically transfer them back to the global model for any blended laminate. Finally, the thermal response of the blended laminate during the cooling down of the autoclave cycle will be studied by building a thermal FEM model. The purpose of this study lies to the fact that the real blended laminate manufactured by Gomaa, had severe imperfections after the autoclave cycle. The reason for this is suspected to be the different thermal expansion-contraction coefficient of each section. Additionally, the FEM model that is built can be used in future projects to help diminish these imperfections. An overview of the methodology followed to solve the problem can be seen in figure 4.2.
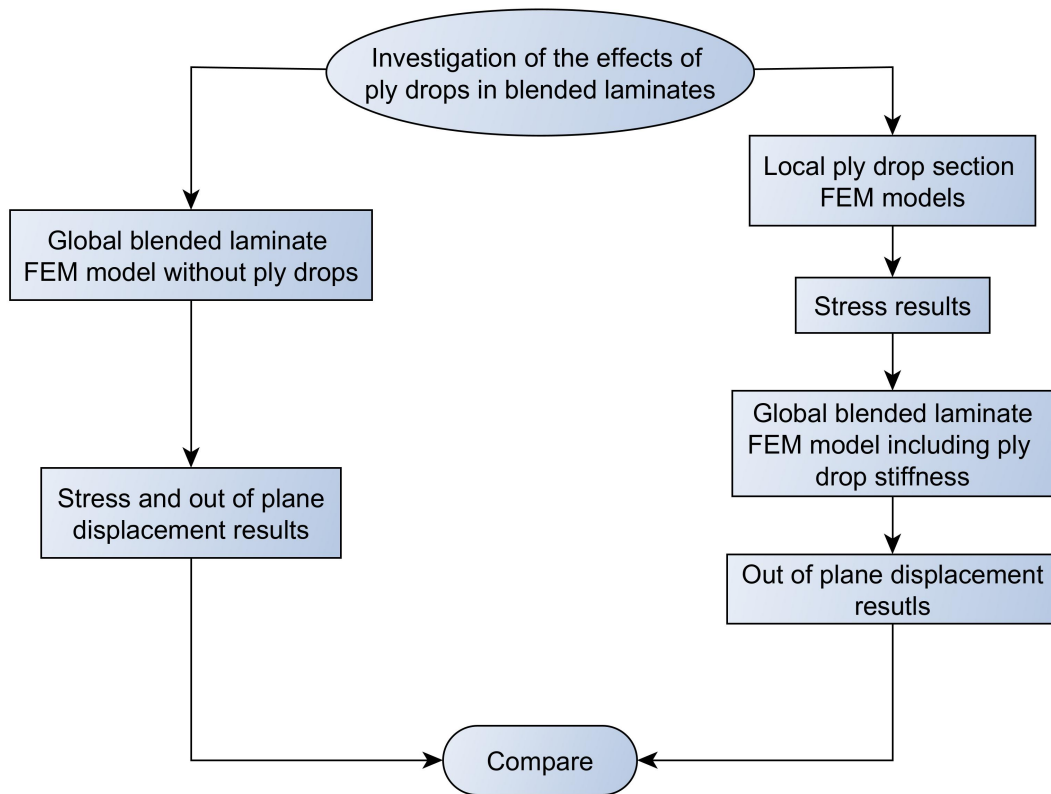
Figure 4.1: Overview of the methodology followed to solve the stress and out of plane displacement problem in the blended laminate.
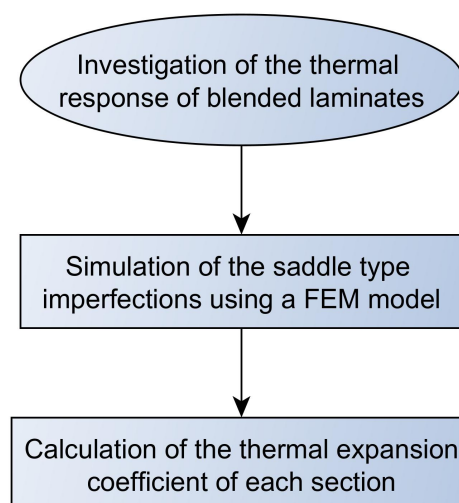
Figure 4.2: Overview of the methodology followed to solve the thermal problem in the blended laminate.

4.1   Global model

The purpose of this section is to analyse how the global blended laminate FEM model is built. This model will eventually be used to execute a non-linear buckling analysis. The displacement results from this analysis will be used as boundary conditions for the local ply drop section FEM models. Additionally, the stress and displacement results from the global laminate will be compared with the results from the local FEM models at the same areas in order to investigate the accuracy of both global and local models.

The global model is a blended laminate with dimensions of 600x400mm and a thickness of 4.96mm, since every section of the laminate has 32 plies with the thickness of 0.155mm each. The laminate is composed of 9 different sections, each one with its own stacking sequence, as explained in section 2.3.7 . The laminate is built using continuum shell elements (SC8R) in order to give a more accurate rotational behaviour compared to conventional shell elements. The buckling load is applied on a node which is coupled to the left side nodes via a coupling constraint. The load application and the boundary conditions are shown in figure 4.3. The material properties used for the carbon fiber plies in the FEM model are taken from testing done by Gomaa. The material properties can be seen in table 4.4. The side edges are simply supported, the right side is fixed and the left side nodes are coupled with the load application point via a coupling constraint. This coupling constraint couples all the degrees of freedom of the load point with the left side of the laminate, U_x, U_y, U_z.
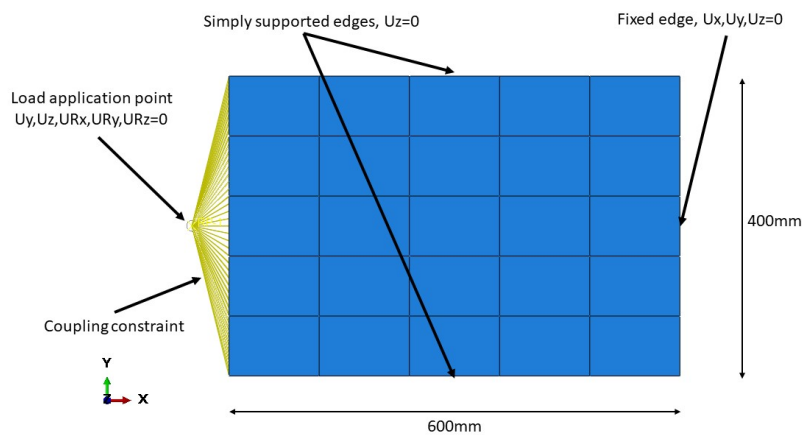
Figure 4.3: The boundary conditions applied on the blended laminate global model.

4.1.1   Mesh convergence study

The mesh convergence of the blended laminate is executed using a Linear perturbation buckle procedure. This step calculates the buckle load of the laminate at a specific eigenvalue, in this case the first eigenvalue. The buckling load is calculated for an increasing number of elements. At the point where the difference between two consecutive buckling loads corresponding to different mesh sizes is less than a specific percentage, the mesh has converged. Search in

literature did not give any specific percentage number at which it can be assumed that the mesh has converged. In general, mesh size is decided by the needs of each simulation. In this case, there is a need for accuracy on the buckling load results and as a consequence, it was decided to use the value of 1% as the difference between two consecutive buckling load values in order to conclude that mesh has converged. Computational time is also an important factor in mesh convergence. However, in this case the difference in computational time between the different mesh sizes was minimal and as a result was not taken into account. In figure 4.4, the buckling load against the number of elements is shown, whereas in figure 4.5 the buckling load against the element size is shown. The difference in percentage between two consecutive buckling loads corresponding to different mesh sizes is shown in table 4.1. As it can be seen in table 4.1, the mesh that corresponds to less that 1% difference, is the one with 2400 elements and an element size of 10mm. The respective buckling load is 111.350 kN.
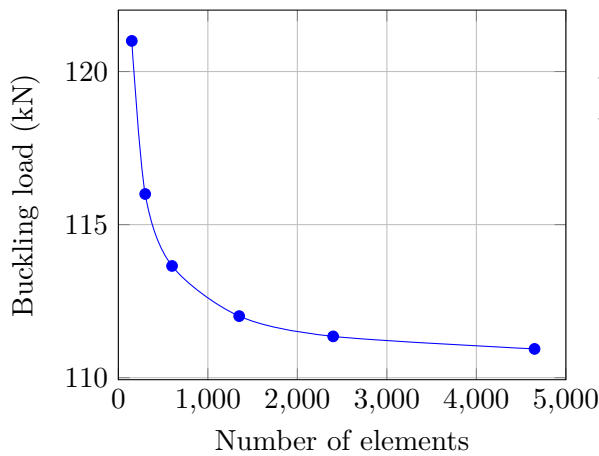
Figure 4.4: Buckling load against number of elements.
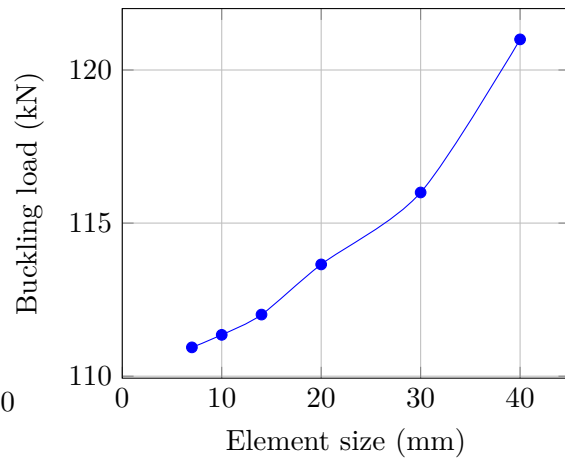
Figure 4.5: Buckling load against element size.

Table 4.1: The difference in percentages between successive buckling loads with different mesh sizes.

Number of elements	element size (mm)	Buckling load (kN)	Difference (%)
150	40	121.048	-
300	30	116.155	4.13
600	20	113.65	2.03
1350	15	112.012	1.44
2400	10	111.35	0.59
4675	7	110.941	0.37

4.2   Local models

The local models refer to the ply drop sections of the blended laminate. In this section, the procedure followed to build the ply drop sections and how the ply drop dimensions are calculated is shown. Then, a mesh convergence study and a boundary sensitivity analysis is executed. The purpose of these local FEM models is first of all to investigate the stress field in the ply drops of the blended laminate and secondly to calculate the stiffness of the ply drop sections in order to eventually calculate the stiffness of the blended laminate including the stiffness of the ply drop sections.

Global-local modeling
The stress analysis of the local ply drop section models is going to be executed utilizing the global-local modeling technique, also called submodeling technique. The global-local modeling technique for this thesis project is used:

- to study a local part of a model, in this case the ply drop section models, with a refined mesh, based on interpolation of the solution from an initial, relatively coarse, global model, which is the blended laminate [1] and

- to obtain an accurate, detailed solution in a local region (ply drop sections) since the detailed modeling of that local region in the global model has negligible effect on the overall solution [1]

4.2.1   FE modelling of blended laminates in literature

Despite the difficulty finding any article concerning FE modelling of blended laminates, many articles were found on FE modelling of ply drops. Despite the fact that laminates composed of a single ply drop is not the same as blended laminates, the methodology for FE modeling of ply drops is very similar to the methodology for blended FEM models and of great importance for this thesis project. Taking a closer look into the most relevant papers, Mortensen and Thomsen translated into an FE model an embedded ply drop consisting of a base sub-laminate, a dropped sub-laminate, a top sub-laminate as well as 3 resin-rich areas between these 3 sub-laminates [21]. The ply drop model can be seen in detail in figure 4.6. The equivalent FE model was composed using 6 and 8 node isoparametric 2D solid elements for the sub laminates and 8 node isoparametric 2d solid elements for the resin rich areas [21]. The FE model can be seen in figure 4.7. The mesh however, is very crude in some areas which is raising doubts about the accuracy of the model.
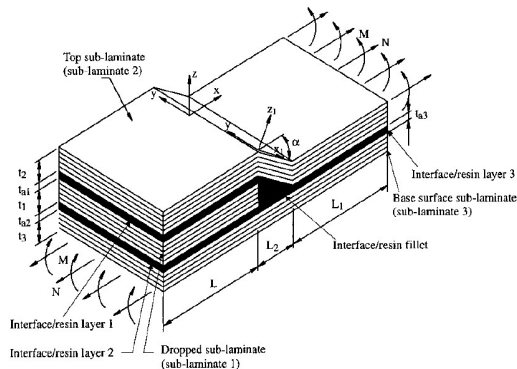
Figure 4.6: The model of an embedded ply drop [21].
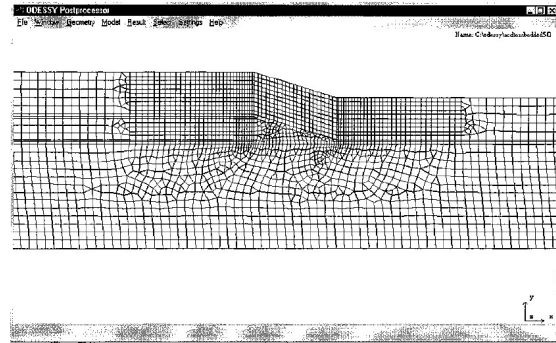
Figure 4.7: The equivalent FE model of an embedded ply drop [21].

Varughese and Mukherjee developed a global local FE model which used 1D elements for the global model and 3D elements for the local ply-drop model. The elements used for the local FE model are the 8 node quadrilateral and 6 node triangular 3D isoparametric elements [32]. The triangular element is used to simulate the resin pocket of the ply-drop whereas the quadrilateral element is used to simulate the plies [32]. The element size used in the FE model is less that or equal to the ply thickness. Additionally, at areas of high stress concentration, the element size is even smaller for more accurate stress/strains computations [32]. The FE model can be seen in figure 4.8. Similarly, Mukherjee and Varughese used eight-noded and 6-noded 3D isoparametric elements in an FE model to simulate a local two ply drop laminate [22]. The two ply drop laminate and the equivalent FE model of Mukherjee and Varughese can be seen in figure 4.9. Cui et al. used a simpler approach in FE modelling of ply drops. Instead of 3D elements, 2D CPS8R shell elements were used at a slice through the thickness of the ply drop laminate [5]. However, there is no comparison between measurements and predictions of this FE model in order to find out how accurate it is. Finally, Botting et al. and Llanos and Vizzini used a combination of solid 8 node elements based on an assumed stress hybrid formulation in combination with solid 6 node isoparametric triangular elements for the resin rich areas of the FE model [4],[17]. All the different types of elements used in the above ply drop FE modelling methods, are summarized in table 4.2.
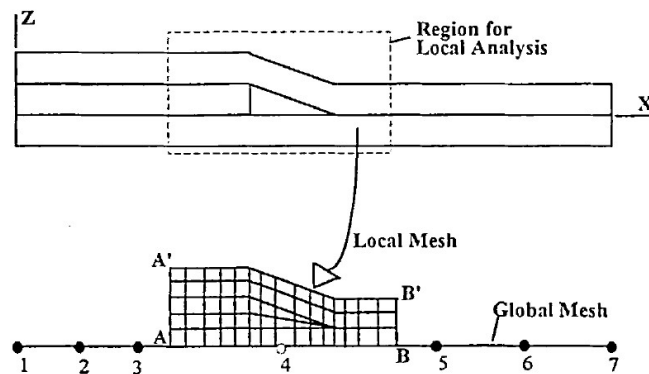
Figure 4.8: The FE model of the global local model [32].
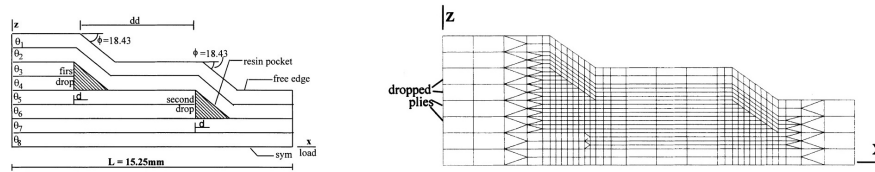
Figure 4.9: The two ply drop laminate and the equivalent FE model [22].

Table 4.2: Element types used in different FE ply drop modelling.

Author	Elements used
Mortensen and Thomsen	mixture of 6 node and 8 node isoparametric 2D solid elements
Varughese and Mukherjee	solid 8 node quadrilateral and 6 node triangular 3D isoparametric elements
Mukherjee and Varughese	solid 8 node quadrilateral and 6 node triangular 3D isoparametric elements
Botting et al.	solid 8 node assumed stress hybrid formulation and 6 node triangular 3D isoparametric elements
Cui et al.	CPS8R shell elements
Llanos and Vizzini	solid 8 node assumed stress hybrid formulation and 6 node triangular 3D isoparametric elements

Taking into account all the information regarding FE modelling of ply drop sections, it was decided to use a combination of 8-node 3D quadrilateral and 6 node 3D triangular elements. The quadrilateral elements will simulate the plies of the laminate whereas the triangular elements the resin-rich pockets in between the plies at the area of the ply drop.

4.2.2 Dimensioning of ply drop sections

Prior to analysing how to dimension ply drop sections in Gomaa's laminate, a review of the dimensions and different sections of the laminate is going to be given. The laminate to be analysed has dimensions of 600x400mm and is composed of 25 sections. All the different sections, the stacking sequence of each section and the global patch interpretation can be seen in figures 2.16, 2.17 and 2.18 respectively. The laminate is symmetric in its plane axes, which means that from the 25 sections, 9 are different and repeated along the 4 quarters of the laminate. In the laminate, there are 14 different ply drop sections, these are:

- Section I-II
- Section III-VI
- Section V-VIII
- Section IV-V-VII-VIII
- Section II-III
- Section IV-V
- Section VI-IX
- Section V-VI-VIII-IX
- Section I-IV
- Section V-VI
- Section I-II-IV-V
- Section II-V
- Section IV-VII
- Section II-III-V-VI

A detailed representation of the ply drop sections on the blended laminate can be seen in figure 4.10.
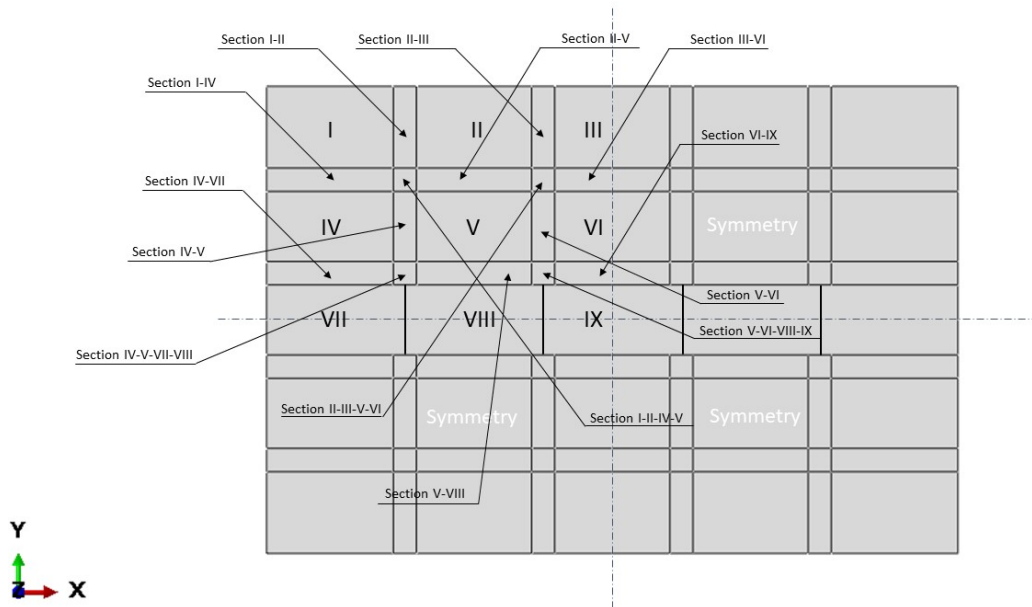
Figure 4.10: Representation of the sections in the blended laminate.

In order to accurately represent the dimensions of the ply drop sections of the blended laminate, microscope pictures of the ply drops were needed. Thankfully, after finishing the manufacturing of the blended laminate, Gomaa had to cut a small portion of the edges of the laminate following the standard manufacturing procedure after the laminate had been manufactured. The material that was cut off the laminate included material from sections I-II, I-IV and IV-VII. In figure 4.11 an example of a microscope picture showing the upper part of section I-II through the thickness can be seen. On the left of the picture is section II and on the right section I. In the microscope picture there are rulers with a specific length in order to understand the scale of the picture. The rest of the pictures taken can be seen in Appendix A.

Figure 4.11: Through the thickness microscope picture from the upper part of Section I-II. On the left of the picture is Section II and on the right Section I.

The range of lengths of all ply drops measured from the microscope pictures are shown in table 4.3. It should be noted that the exact starting and ending point of each ply drop is difficult to measure and as a consequence the measurements are an approximation. Additionally, due to hand lay up manufacturing, every ply drop is a little bit different from each other. Taking into account all the measurements of the ply drops in the microscope pictures, it was decided the lengths of all the ply drops in the FEM models to be 4mm. This value was chosen taking into consideration that this value is close to the mean value of all the ply drops and it is a number that simplifies FEM modelling.

Table 4.3: Ply drop length range in different ply drop sections samples.

	Ply drop lengths range in sample 1	Ply drop length range in sample 2	Ply drop length range in sample 3
Section I-II	2200-4500μm	3250-4000μm	3250-4000μm
Section I-IV	4000-4200μm	4000-4200μm	4000-4200μm
Section IV-VII	4000-4500μm	4000-4500μm	4000-4500μm

4.2.3 FEM models of ply drop sections

Taking into account the literature in section 4.2.1 and the ply drop dimensioning in section 4.2.2, it is now time to build the 3D FEM models for the ply drop sections of Gomaa's blended laminate. The FEM models are built in Abaqus 2017 using one element per laminate ply through the thickness. The material properties used for the carbon fiber plies in the FEM models are taken from testing done by Gomaa. The material properties used in the FEM models to simulate the resin pockets in the ply drops, are shown in table 4.5, whereas the material properties for carbon fiber material can be seen in table 4.4. Each ply has a thickness of 0.155mm meaning that the total thickness of the blended laminate is 4.96mm since every section has 32 plies. The ply drop length in all sections is modeled to 4mm as explained in section 4.2.2.

Table 4.4: M30SC/DT120 carbon fiber material properties.

Material Property	Value	Material Property	Value	Material Property	Value
E11 (GPa)	127.710	v12	0.36	G12 (GPa)	3.1
E22 (GPa)	7.3	v23	0.36	G13 (GPa)	3.1
E33 (GPa)	7.3	v13	0.36	G23 (GPa)	2.69

Table 4.5: Resin material properties

Material Property	Value
E (GPa)	3
v	0.39

The ply drop sections are divided into two categories:

- **Simple ply drop sections**: This category includes ply drop sections in which the plies are dropped in one direction. These ply drop sections are:

  - Section I-II
  - Section II-III
  - Section I-IV
  - Section II-V
  - Section III-VI
  - Section IV-V
  - Section V-VI
  - Section IV-VII
  - Section V-VIII
  - Section VI-IX
  - Section IV-V-VII-VIII
  - Section V-VI-VIII-IX

- **Complex ply drop sections**: This category includes ply drop sections in which the plies are dropped in many directions. These ply drop sections are:

  - Section I-II-IV-V
  - Section II-III-V-VI

For space saving, only one FEM model of each category will be shown here. From the first category section I-II and from the second category section I-II-IV-V will be shown. The rest can be found in Appendix B.

Section I-II

Section I-II is composed of section I with stacking sequence

$$[45/-45/60/-60/45/-45/30/-30/60/-60/0/0/60/-60/0/0]_s$$

and section II with stacking sequence

$$[45/-45/60/-60/60/-60/60/-60/0/0/0/0/60/-60/0/0]_s$$

The FEM model is built by partitioning it as many times as needed in order to create the plies, the ply drops and the resin pockets. Then, each ply is assigned material and orientation properties and the ply drop area is partitioned many times in order to achieve a higher mesh density. The meshing and mesh convergence are explained in the next sections. In order to assign orientation properties in the ply drops, a new orientation system has to be created for each ply drop. In figure 4.12, section I-II is shown through the thickness. On the left of the figure is section I and on the right section II.
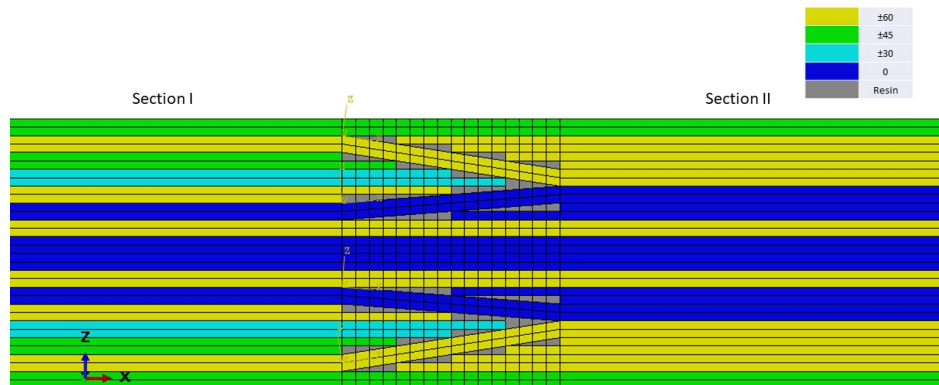
Figure 4.12: FEM model of Section I-II.

Section I-II-IV-V

This ply drop section is composed of 4 different sections. These are:
Section I with stacking sequence

$$[45/-45/60/-60/45/-45/30/-30/60/-60/0/0/60/-60/0/0]_s$$

Section II with stacking sequence

$$[45/-45/60/-60/60/-60/60/-60/0/0/0/0/60/-60/0/0]_s$$

Section IV with stacking sequence

$$[45/-45/60/-60/60/-60/60/-60/60/-60/60/-60/60/-60/60/-60]_s$$

Section V with stacking sequence

$$[45/-45/60/-60/60/-60/60/-60/60/-60/0/0/60/-60/60/-60]_s$$

The procedure to build this section is similar to the one for section I-II but more complex. This is due to the fact that some plies are not dropped only in 1 direction but in 2 at the same time. This complex geometry is made using solid loft and solid extrude features in Abaqus. In figure 4.13, a 3D view of section I-II-IV-V is shown with the name of each section shown above the corresponding section. In the center of the model, the plies are dropped in 2 different directions at the same time, X and Y. In order to better understand the structure of section I-II-IV-V, figure 4.14 shows only the ply drops of section I-II-IV-V hiding the regular plies.
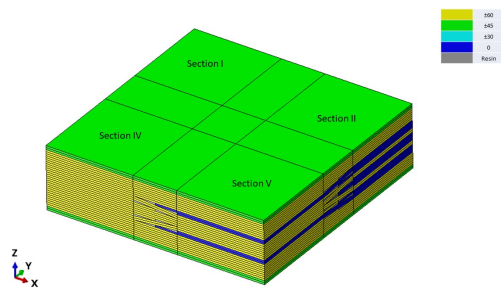
Figure 4.13: FEM model of Section I-II-IV-V.
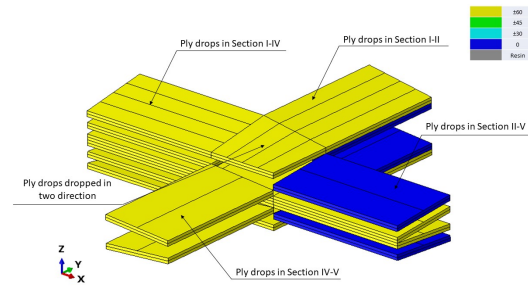
Figure 4.14: FEM model of Section I-II-IV-V showing only the ply drops of the section.

4.2.4   Mesh convergence study

As explained in section 4.2.3, the 14 different ply drop sections are separated into two categories: the simple and the complex ones. Executing a mesh convergence study separately for each ply drop section would be very time consuming and thus it was decided to execute a mesh converge study for one ply drop section of each category, since all the ply drop sections of the same category are very similar. For the simple ply drop section category, section I-II is studied whereas for the complex one, section I-II-IV-V.

Section I-II

The literature review on FE modeling of ply drops in section 4.2.1, concluded that the meshing of the ply drop sections of the blended laminate will be done using a combination of 8 node and 6 node solid elements. The 8 node solid elements are used for the meshing of the whole ply drop section except the parts of the resin pockets which have a triangle shape. It that case, 6 node solid elements are used. In the environment of Abaqus the 8 node and 6 node elements used are the C3D8R, an 8-node linear brick, reduced integration, hourglass control and C3D6 ,a 6-node linear triangular prism. In figure 4.15, the mesh of section I-II is shown including details on the C3D6 element type. In figure 4.16, the dimensions of section I-II are shown. Note that the width of the section has not yet been defined, it is defined in section 4.2.5.
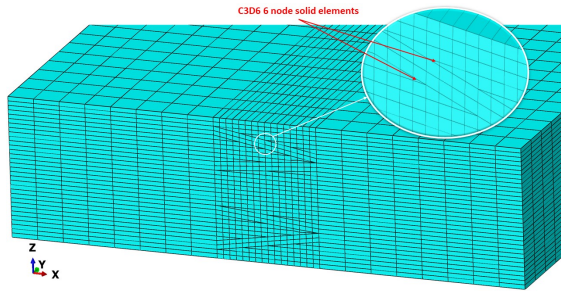
Figure 4.15: Section I-II converged mesh including element details.
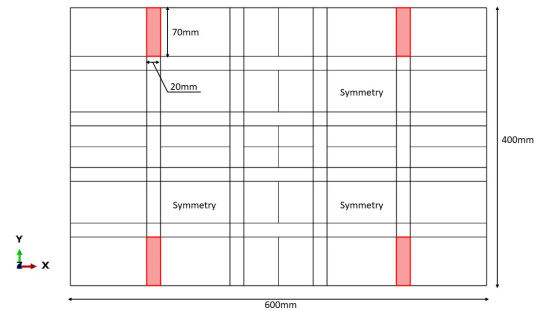
Figure 4.16: Dimensions of section I-II in respect to the blended laminate.

Regarding the mesh convergence study, the maximum stress value at the fiber direction is used as the convergence criteria. In order to run the analysis, all the surfaces of the section, excluding bottom and top ones, have to be assigned the extrapolated values of the displacement field from the global model. This is done by checking the sub-modeling option in the model attributes and then assigning the surfaces that will get the displacement from the global model as a boundary condition. Attention has to be paid in the fact that the position of the local FEM model in the assembly module has to be at the exact same position that the local FEM model is in respect to the global model. This ensures that the right displacement field is assigned in the local FEM model. The analysis is non linear using 100 increments. Since the area around the ply drops is the one that needs more accuracy in the analysis, it was decided to have a denser mesh around this area and a coarser mesh in the area outside the ply drops. That way, the computational time for the analysis is greatly reduced.

The element size for the area outside the ply drops is selected to be 1mm, taking into account the aspect ratio. One element in this area has edge dimensions of 1mm-1mm-0.155mm that gives an aspect ration of 6.45, which is sufficient for accurate calculations. The element size in the ply drop area is selected with the help of a convergence study. By using the non-linear displacement results from the analysis of the global model at 120 kN buckling load, the maximum stress in section I-II is calculated for different mesh sizes. The mesh size at which the max stress has converged is a factor of the difference between two consecutive max stresses of different mesh sizes and the computational time. In figures 4.17 and 4.18, the graphs of the number of elements against max stress and computational time against number of elements are shown. In table 4.6 all the data gathered in one table are shown. Taking into account the computational time and the difference in the max stress between consecutive mesh sizes, the most convenient choice is the mesh size with the 87040 elements. This mesh size is accurate enough but at the same time the computational time is also acceptable.
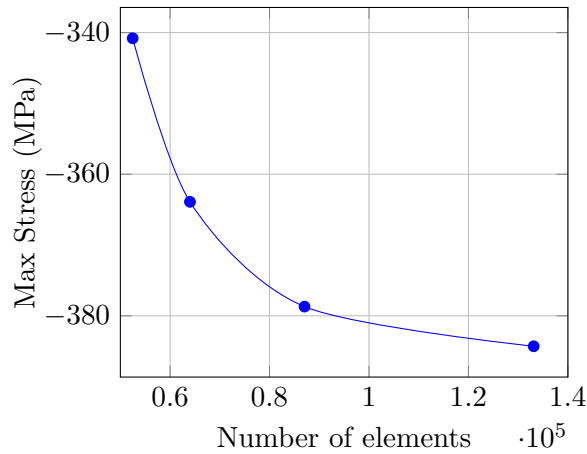
Figure 4.17: Max stress against number of elements.
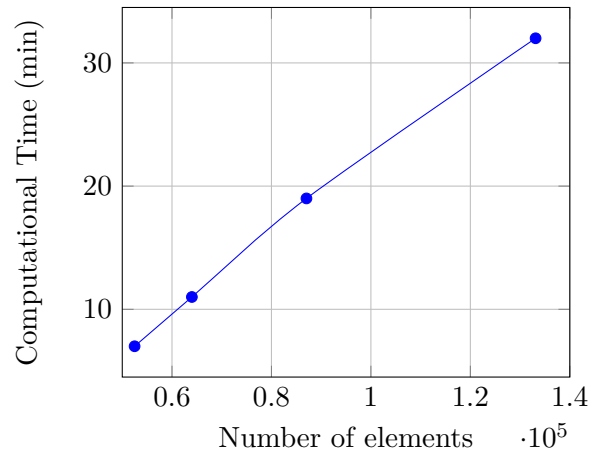
Figure 4.18: Computation time against number of elements.

Table 4.6: All the data calculated for the mesh convergence study.

Number of Elements	Max Stress (Mpa)	Difference (%)	Computational time in cluster (min)
52480	-340.8	-	7
64000	-363.9	6.77	11
87040	-378.7	4.06	19
133120	-384.3	1.47	32

Section I-II-IV-V

The mesh convergence for section I-II-IV-V is executed the same way as in section I-II. The main difference between the two sections is that section I-II-IV-V is composed of 4 difference ply drop sections and at the center of teh section there are plies that are dropped in two directions at the same time. In figure 4.21, the model with the converged mesh can be seen and in figure 4.22 the dimensions of section I-II-IV-V in respect to the blended laminate are shown. More information on how the FEM model is built can be found in section 4.2.1. The element types remain the same as in the case with section I-II and similarly the mesh density is higher in the ply drop sections and coarser in the rest of the model in order to save computational time. In figures 4.19 and 4.20, the graphs of the number of elements against max stress and computational time are shown. In table 4.7 all the data gathered in one table are shown. Taking into account the computational time and the difference in the max stress between consecutive mesh sizes, the most convenient choice is the mesh size of 21248 elements, since it is accurate enough and the computational time is acceptable.
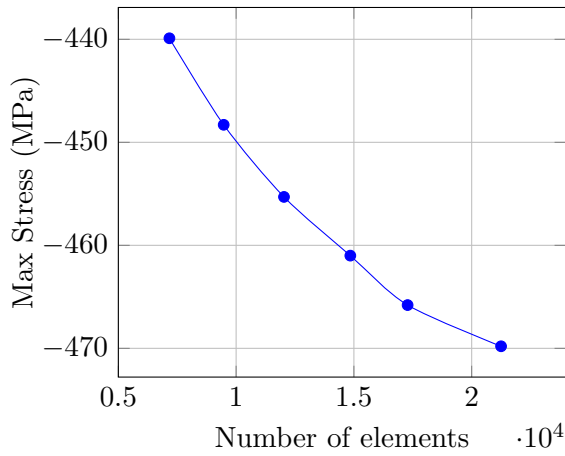
Figure 4.19: Max stress against number of elements.
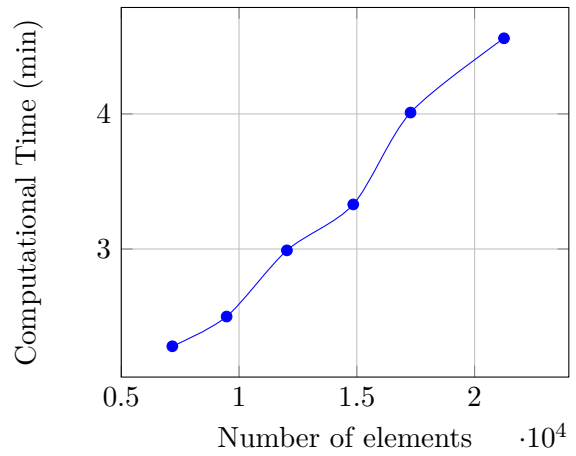
Figure 4.20: Computation time against number of elements.

Table 4.7: All the data calculated for the mesh convergence study.

Number of Elements	Max stress (Mpa)	Difference (%)	Computational time (min)
7168	-439.9	-	2.28
9472	-448.3	1.90	2.5
12032	-455.3	1.56	2.99
14848	-461	1.25	3.33
17280	-465.8	1.04	4.01
21248	-469.8	0.85	4.56
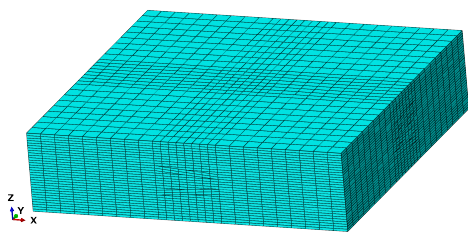
Figure 4.21: Section I-II-IV-V converged mesh.
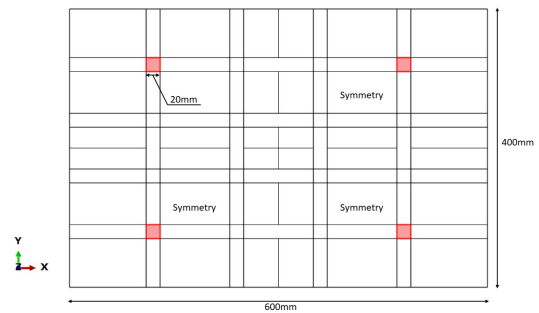
Figure 4.22: Dimensions of section I-II-IV-V in respect to the blended laminate.

4.2.5 Boundaries sensitivity study

In section 4.2.4, the width of the ply drop sections is shown to be 20mm (figures 4.16, 4.22). However, this value is not randomly chosen but was chosen after a boundary sensitivity study. In this study the max stress value at fiber direction is calculated for different section widths. The optimum width is chosen taking into account the max stress difference between two consecutive analysis with different section widths, the number of elements and the computational time. Considering that a boundary sensitivity study for all 14 ply drop sections would be very time consuming and assuming that the boundary width would have the same effect in all ply drop sections, it was decided to execute a boundary sensitivity study only for section I-II. In figures 4.23 and 4.24, the graphs of the section width against max stress and computational time respectively, are shown. In table 4.8 all the data gathered in one table are shown. Taking into account the computational time and the difference in the max stress between consecutive sections widths, it was decided to chose the section width of 20mm since it has the best trade off between computational time, max stress accuracy and number of elements.
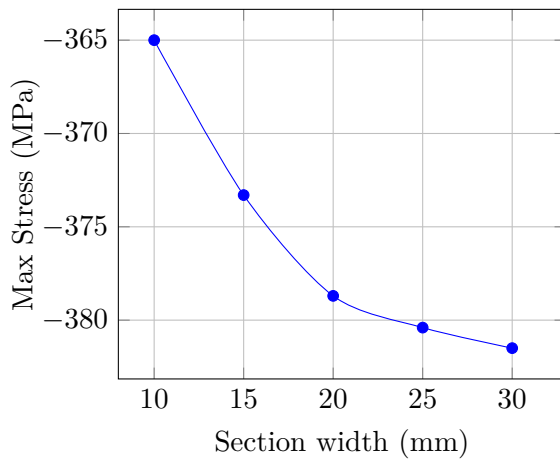
Figure 4.23: Max stress against section width.
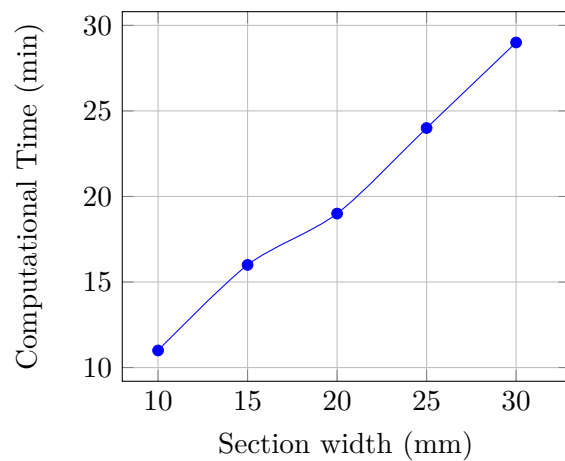
Figure 4.24: Computation time against Section width.

Table 4.8: All the data calculated for the boundaries sensitivity study.

Section width (mm)	Max Stress (MPa)	Difference (%)	Number of elements	Coputational time in cluster (min)
10	-365	-	61440	11
15	-373.3	2.27	71680	16
20	-378.7	1.45	87040	19
25	-380.4	0.45	102400	24
30	-381.5	0.29	112640	29

4.3   Tool to calculate stiffness in blended laminates

The purpose of this chapter is to investigate the effect of the ply drop sections in the out of plane displacement of blended laminates. In order to achieve that, the stiffness properties of the ply drop sections are extracted using the FEM models in section 4.2.3. After calculating the stiffness properties of the ply drop sections, these properties have to be put into the global blended laminate model. This is achieved by using conventional laminates (without ply drops) with stiffness properties equivalent with the ones from the ply drop sections. These laminates will take the place of the ply drops in the global blended laminate. An overview of the procedure followed in this chapter is shown in figure 4.25. The fist step is to create a stiffness calculator. This calculator should be able to extract the stiffness properties of any laminate that its properties cannot be calculated using CLT. With the help of the stiffness calculator, the stiffness properties of all the ply drop sections are calculated. Next step is to create conventional laminates that have properties equivalent to the ply drops in the different ply drop sections. Additionally, a verification that the equivalent laminates have the right stiffness properties is needed. Then, the automation of the whole process is needed so that it can work on any blended laminate with any ply drop sections. Finally, the next step is to use the tool to calculate and put the stiffness properties back to the global model.
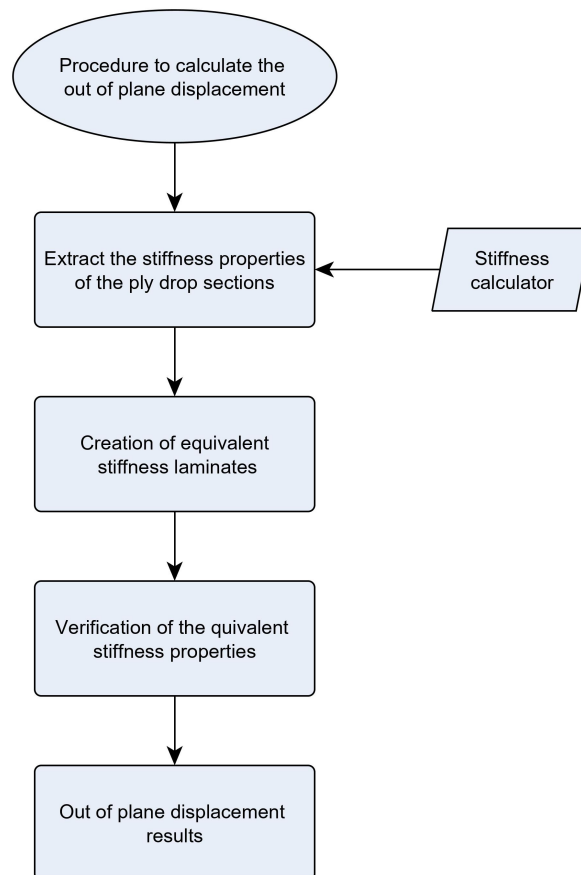
Figure 4.25: An overview of the procedure followed to calculate the out of plane displacement.

4.3.1 Stiffness calculator

In order to successfully calculate the out of plane displacement of the blended laminate, the stiffness properties of the ply drop sections have to be calculated. However, the ply drop section stiffness properties cannot be calculated using CLT, since the ply drops extend out of the XY plane. Thus, there is a need for a FEM tool that can accurately calculate the stiffness properties of unconventional laminates. The term unconventional means that the stiffness properties cannot be expressed using CLT.

This FEM tool functions similarly to the Representative Volume Element theory (RVE). In this theory, the stiffness properties of a small part of a structure, called unit cell, are acquired. This unit cell is in the micro-scale, it is repeated everywhere in the structure and it has stiffness properties that can not be calculated using conventional methods like CLT. In order to acquire the stiffness properties, specific FEM analysis and post processing of the results are done. The tool presented here, has similar function with the difference that it works in the macro-scale, directly calculating the stiffness of each FEM structure. The way acquiring the stiffness properties of the structure is by executing specific analysis and then calculating the stiffness from the post processing of the results. 6 models are needed to calculate all the necessary stiffness and poisson ratios properties. In their paper, Omairey et al. present all these 6 models needed for the calculation of all properties, which are shown in figure 4.26 [23]. All the procedure and post processing is automatically executed in a python code. In the next sections, a detailed explanation of how the code works is presented. An overview of the procedure is presented in figure 4.27.
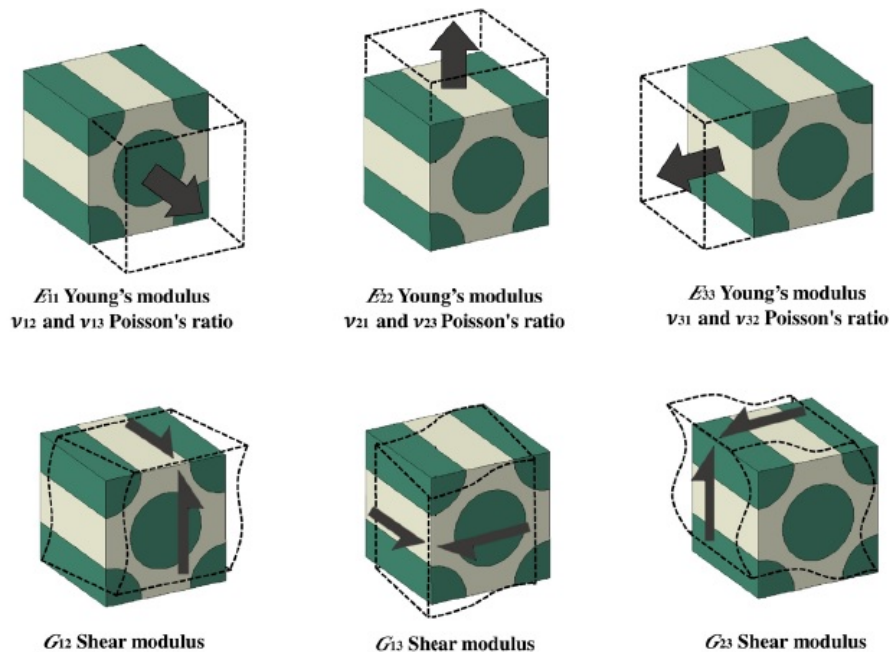
Figure 4.26: An overview of all the analysis needed to calculate the properties of a FEM model [23].
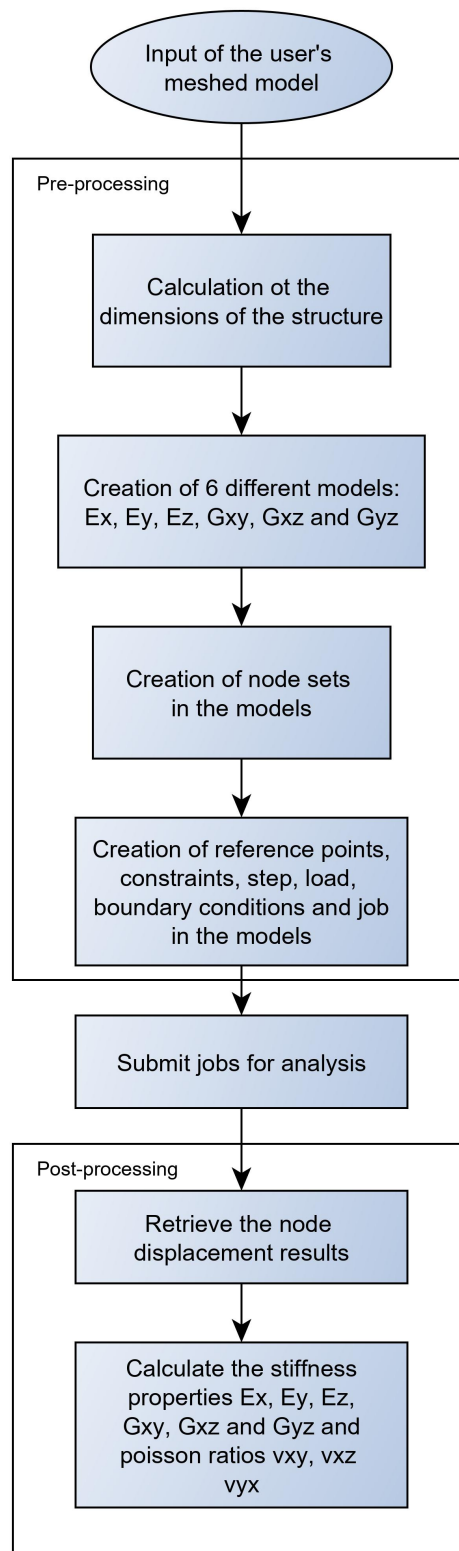
Figure 4.27: An overview of the procedure followed to calculate the stiffness of a structure.

Pre-processing

Pre-processing includes all the necessary steps to prepare the different FEM models for the analysis needed to calculate the stiffness properties. These steps are explained below.

• **Calculation of the dimensions of the structure**. In this step, the dimensions of the structure are calculated by extracting the coordinates of the edges of the structure. Accordingly, the height, width and length dimensions are calculated.

• **Creation of different models**. 6 different models are needed to calculate the necessary stiffness properties. These models are named E_x, E_y and E_z which calculate young's modulus E_x, E_y and E_z, poison ratios v_{xy}, v_{yz} and v_{xz}. Then, there are the models G_{xy}, G_{xz} and G_{yz} that calculate shear modulus G_{xy}, G_{xz} and G_{yz}. Here it has to be noted that poisson ratios v_{yx}, v_{zy} and v_{zx} are calculated using the orthotropic equations 4.1, since Abaqus uses the same procedure.

• **Creation of node sets**. The purpose of this step is to create the necessary node sets in all 6 models. These node sets will later be used for the creation of boundary conditions, constraints and load applications. The node sets are explained in more detail in the next step.

• **Creation of reference points, constraints, step, load and boundary conditions** in each model. Each of the 6 models mentioned above, need different application of boundary conditions, reference points, constraints, etc, in order to calculate the different stiffness properties, two examples are presented, one for E_x model and one for G_{xy} model. All the other models are similar to these two models.

The E_x model calculates the E_x young's modulus and v_{xy} poisson ratio. In figure 4.28, all the necessary node sets used for the application of the boundary conditions and constraints are shown. The load is applied to the X direction on a node which is coupled with the edge nodes via a coupling constraint in order to transfer the load to the structure. The boundary condition on the left end of the model, is X=0. The displacement the structure is subjected to in to order to calculate the stiffness properties, is shown in figure 4.29.
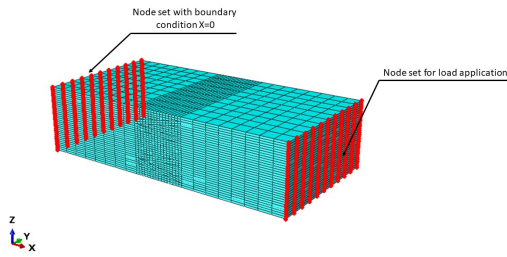
Figure 4.28: Node sets used for the E_x model.
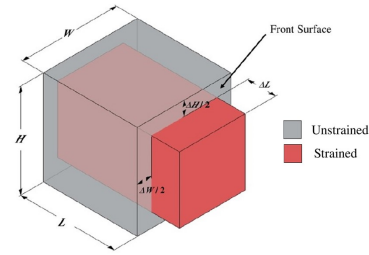
Figure 4.29: The displacement the structure is subjected to in order to calculate the young's modulus E_x and poisson ratio v_{xy} [23].

The G_{xy} model calculates the G_{xy} shear modulus property. This is achieved by applying pure shear on the structure. In figure 4.30, all the necessary node sets used for the application of the boundary conditions and constraints are shown. Similarly with the E_x model, the load is applied in a node which is coupled to the respective node sets using coupling constraints. The displacement the structure is subjected to in to order to calculate the shear modulus, is shown in figure 4.31.
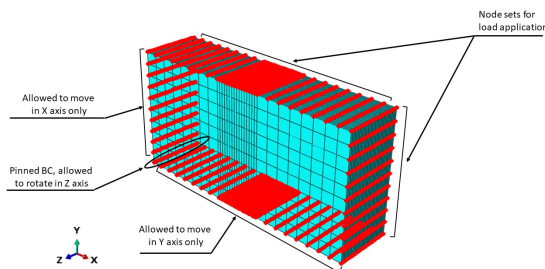
Figure 4.30: Node sets used for the G_{xy} model.
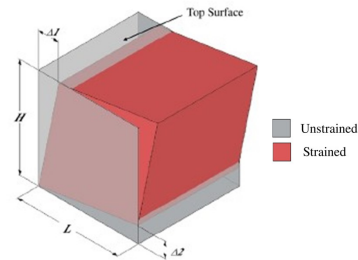
Figure 4.31: The displacement the structure is subjected to in order to calculate the shear modulus G_{xy} and poisson ratio v_{xy} [23].

Job analysis and post-processing

When the pre-processing phase has finished, the job for each model is submitted for analysis. When the jobs are finished, the post-processing phase begins. In this phase, stiffness property values are calculated. Based on the two examples presented in the pre-processing phase, E_x and G_{xy}, the calculations for the extraction of the stiffness properties are presented.

Regarding E_x model, the equations used in the code are:

$$E_x = \frac{Stress}{Axial\ Strain} = \frac{\frac{Axial\ force}{Front\ surface\ area(HxW)}}{\frac{\Delta L}{L}}$$

$$v_{xy} = \frac{-Transverse\ strain}{Axial\ Strain} = \frac{\frac{\Delta H}{H}}{\frac{\Delta L}{L}}$$

$$v_{xz} = \frac{-Transverse\ strain}{Axial\ Strain} = \frac{\frac{\Delta W}{W}}{\frac{\Delta L}{L}}$$

where H, W, ΔL, L, ΔH, ΔW are shown in figure 4.29.

Regarding G_{xy} model, the equations used in the code are:

$$G_{xy} = \frac{Shear\ Stress}{Tensors\ of\ shear\ Strain} = \frac{\frac{Force\ in\ top\ surface}{Top\ surface\ area(LxW)}}{\frac{\Delta 1}{H} + \frac{\Delta 2}{L}}$$

where H, W, Δ1, L, Δ2 are shown in figure 4.31.

4.3.2   Verification of the code in orthotropic material model

The verification of the code for models using orthotropic material, is done using a 3D model in abaqus. The procedure to verify that the code works is done by assigning random material stiffness properties in the model and then the code is used to verify that it works correctly by extracting the same property values as the ones assigned. The results of the comparison are shown in table 4.9. As it can be seen, all the value differences are less than 1% which verifies that the code works accurately enough.

Table 4.9: Comparison of stiffness properties for an orthotropic material model.

	Assigned material values	Values from code	difference (%)
E_x (Mpa)	150000	149970	0.02
E_y (Mpa)	50000	50000	0
E_z(Mpa)	25000	25000	0
v_{xy}	0.3	0.3006	0.2
v_{xz}	0.15	0.150089976	0.059
v_{yz}	0.2	0.201	0.5
v_{yx}	0.1	0.100220044	0.22
v_{zx}	0.025	0.02502	0.08
v_{zy}	0.1	0.1005	0.5
G_{xy} (Mpa)	10000	10000	0
G_{xz} (Mpa)	7000	6997	0.042
G_{yz} (Mpa)	5000	4997.5	0.05

4.3.3   Verification of the code in laminates

In order to verify that the stiffness properties extracted from the code are correct in lamiantes, the equivalent stiffness properties of a laminate calculated with CLT are compared to the ones

calculated with the code. The stacking sequence chosen for the laminate is section I, taken from the blended laminate. There is no specific reason for choosing this stacking sequence, this can be done with any stacking sequence. The stacking sequence of the laminate is:

$$[45/-45/60/-60/45/-45/30/-30/60/-60/0/0/60/-60/0/0]_s$$

Using CLT, the abd matrix is calculated and then the equivalent properties of the laminate are calculated. More information on the equations to calculate the equivalent laminate properties can be found in section 2.1.1. Then, the same properties are calculated by applying the code in the 3D FEM model of section I. It has to be noted here that CLT has some assumptions that do not exist in 3D models. The most important for this case are:

- The normals to the mid-plane remain straight and normal to the midplane even after deformation.

- The normals to the mid-plane do not change their lengths.

Taking into account the above assumptions of CLT, just for this case, some extra boundary conditions were inserted in the code, which force the sides of the laminate to move as one, since in the 3D laminate model, each ply has some degree of independency when it deforms. That way, the behaviour of the laminate is closer to the assumptions of CLT. However, despite the extra boundary conditions, there is still some independent deformation of each ply of the laminate internally, which does not allow for an one to one comparison between CLT and the code. Nevertheless, the comparison was carried forward and the results are presented in table 4.10 for the case with the extra boundary conditions and without. It can be seen that the difference between CLT and 3D model is very small for the case where the extra boundary conditions are enforced in the 3D model to simulate the CLT assumptions.

Table 4.10: Comparison of stiffness properties between CLT and the code presented in the previous section.

	CLT properties		3D properties usign code		Difference (%)	3D properties using code and the extra BCs to simulate CLT		Difference (%)
E_x	46451.37	MPa	45511.9	Mpa	2.02	46103.37	MPa	0.74
E_y	34116.25	MPa	29394.7	MPa	13.83	33199.45	MPa	2.68
G_{xy}	21587.87	MPa	22118.76	MPa	2.45	22118.761	MPa	2.45
v_{xy}	0.50395		0.499634		0.85	0.504611		0.13

4.3.4 Equivalent stiffness laminates

Having verified that the code calculating the stiffness of a model is working, it is time to use it to find a way to build laminates with equivalent stiffness to the ply drop section models. The equivalent stiffness laminates should be built in a way that works in the global blended laminate FEM model. That means, all of their plies should be straight and parallel to each other in order to form a stacking sequence that can be combined with continuum shell elements, the same way the original global blended laminate FEM model is built. In total, 3 different methods to build equivalent laminates are presented and compared. All of these

different methods are compared using ply drop section I-II as a testbed, since using all 14 ply drop sections as a testbed would be very time consuming. In order to verify that the selected method works for all sections, it is also tested on another two of the most complex ply drop sections.

Method 1

In the first method, the stiffness properties of each ply drop in each ply drop section are measured using the stiffness calculator code and then the ply drops are replaced by unidirectional laminates of the same dimensions with all its plies having 0° fiber direction. That way, both laminates have the same in-plane properties. The rest of the plies from the ply drop section remain the same. Now, all the plies are straight and parallel to each other. The procedure is shown schematically in figure 4.32.
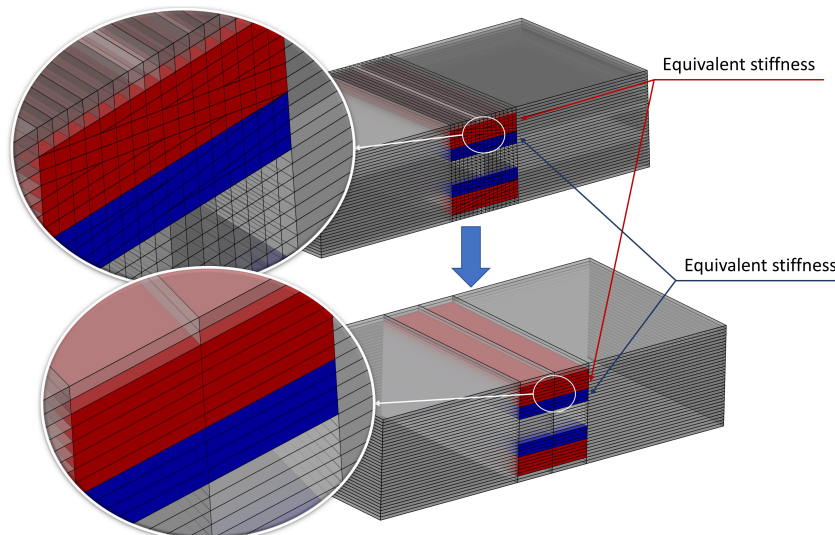
Figure 4.32: An overview of method 1 on building an equivalent stiffness laminate for ply drop section I-II.

Method 2

In method 2, each ply drop is divided in two parts in the x axis and each part is measured for stiffness properties using the stiffness calculator code. Similarly to method 1, all ply drop parts are replaced by unidirectional laminates of the same dimensions with all its plies having 0° fiber direction and as a consequence similar in plane properties. The procedure is shown schematically in figure 4.33.
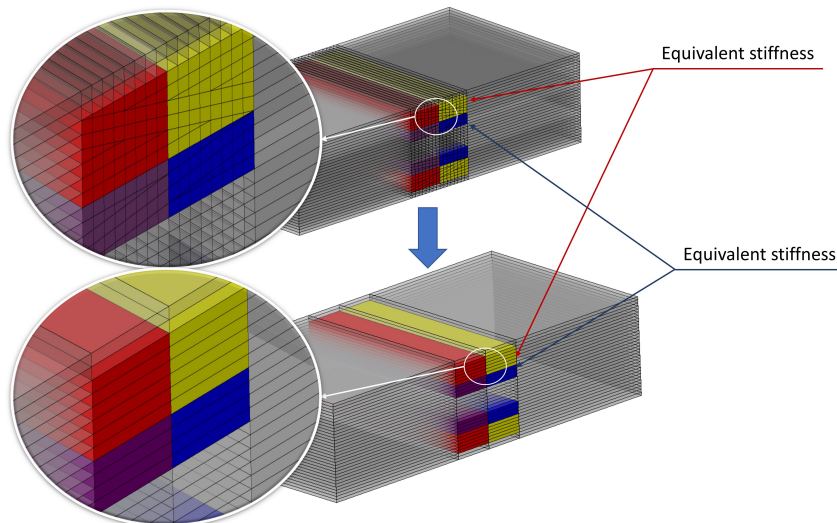
Figure 4.33: An overview of method 2 on building an equivalent stiffness laminate for ply drop section I-II.

Method 3

In method 3, the stiffness of all the ply drops in the section are measured as one structure using the stiffness calculator code. Similarly to all previous methods, the structure that contains all the ply drops is replaced by a unidirectional laminate of the same dimensions with all its plies having 0° fiber direction and the same in plane properties. The procedure is shown schematically in figure 4.34.
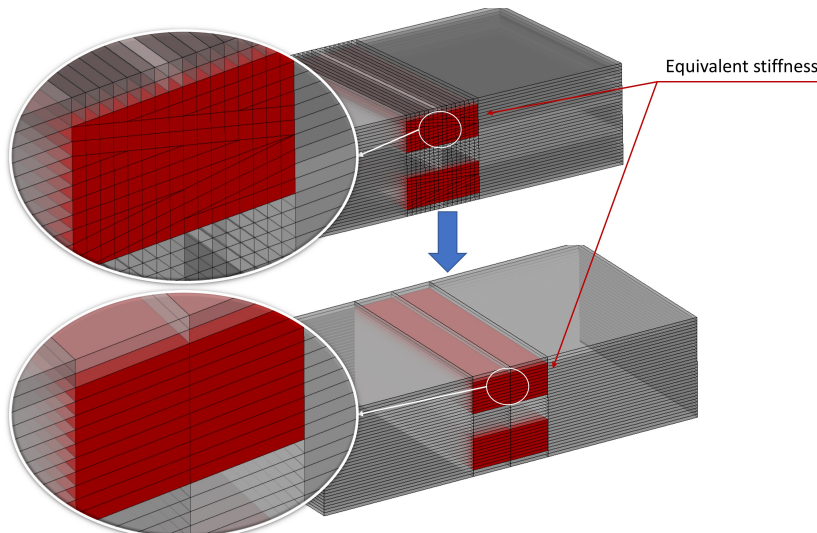
Figure 4.34: An overview of method 3 on building an equivalent stiffness laminate for ply drop section I-II.

Notes on measuring the stiffness of the ply drops

In order to measure the stiffness of the ply drops in each ply drop section, the stiffness calculator code presented in previous section is used. This code however, works only on symmetric and balanced laminates. Each ply drop in the different ply drop sections, has two parts, one normal and its symmetric one, which are separate one from the other in most cases. In order to measure the stiffness of one ply drop, the symmetric part is needed as well, that means, in each ply drop FEM model the symmetric part has to be added in order the measurement to be correct, otherwise the coupling effects due to the asymmetry will produce curvatures that will alter the stiffness measurements.

4.3.5 Comparison of in-plane stiffness properties

In order to chose which method is more accurate, the in-plane stiffness properties of the equivalent laminate of section I-II for each different method and the original section I-II laminate are measured using the stiffness calculator code and then are compared. The results from the comparison for each method can be seen in tables 4.11, 4.12 and 4.13 for methods 1, 2 and 3 respectively. Note that poisson ratios v_{yx}, v_{zx} and v_{zy} are calculated using poisson ratios v_{xy}, v_{xz} and v_{yz} and the young's modulus E_x, E_y, E_z since abaqus does it this way. The equations are:

$$v_{yx} = v_{xy}\frac{E_y}{E_x}, \ v_{zx} = v_{xz}\frac{E_z}{E_x}, \ v_{zy} = v_{yz}\frac{E_z}{E_y} \tag{4.1}$$

Table 4.11: Comparison of stiffness properties between section I-II and its equivalent laminate for method 1.

	Section I-II		Equivalent laminate for section I-II		Error (%)
E_x	47659.42	MPa	46718.59	MPa	1.97
E_y	32934.94	MPa	31740.69	MPa	3.63
E_z	8006.31	MPa	7992.56	MPa	0.17
G_{xy}	19320.65	MPa	18890.12	MPa	2.23
G_{xz}	2831.07	MPa	2827.588	MPa	0.12
G_{yz}	2782.82	MPa	2766.085	MPa	0.60
v_{xy}	0.4434		0.4346		1.98
v_{xz}	0.292935		0.2886		1.48
v_{yz}	0.30401		0.3084		1.44
v_{yx}	0.306411		0.295268		3.64
v_{zx}	0.04921		0.049373		0.33
v_{zy}	0.073903		0.077658		5.08

Table 4.12: Comparison of stiffness properties between section I-II and its equivalent laminate for method 2.

	Section I-II		Equivalent laminate for section I-II		Error (%)
E_x	47659.42	MPa	47309.61	MPa	0.73
E_y	32934.94	MPa	31669.66	MPa	3.84
E_z	8006.31	MPa	7983.76	MPa	0.28
G_{xy}	19320.65	MPa	19050	MPa	1.40
G_{xz}	2831.07	MPa	2825.09	MPa	0.21
G_{yz}	2782.82	MPa	2763.2	MPa	0.71
v_{xy}	0.4434		0.438849		1.03
v_{xz}	0.292935		0.317052		8.23
v_{yz}	0.30401		0.30329		0.24
v_{yx}	0.306411		0.293771		4.13
v_{zx}	0.04921		0.053504		8.73
v_{zy}	0.073903		0.076458		3.46

Table 4.13: Comparison of stiffness properties between section I-II and its equivalent laminate for method 3.

	Section I-II		Equivalent laminate for section I-II		Error (%)
E_x	47659.42	MPa	45499.48	MPa	4.53
E_y	32934.94	MPa	31651.73	MPa	3.90
E_z	8006.31	MPa	8001.73	MPa	0.06
G_{xy}	19320.65	MPa	18673.77	MPa	3.35
G_{xz}	2831.07	MPa	2938.57	MPa	3.80
G_{yz}	2782.82	MPa	2759.41	MPa	0.84
v_{xy}	0.4434		0.44577		0.53
v_{xz}	0.292935		0.292		0.32
v_{yz}	0.30401		0.28307		6.89
v_{yx}	0.306411		0.3101		1.20
v_{zx}	0.04921		0.051352		4.35
v_{zy}	0.073903		0.071562		3.17

4.3.6 Comparison of out of plane stiffness properties

One characteristic of laminates is that their out of plane stiffness properties can be completely different from their in plane stiffness properties. Plies with different fiber angle orientation have different stiffness properties in respect to the principal direction and depending on their height position in the laminate, they can have different moment of inertia which is translated to different bending stiffness matrix, or D matrix as it is called in CLT. The D matrix can be seen in equation 4.2. In order to compare the out of plane stiffness of laminates, the values of the D matrix have to somehow be compared. Since all the laminates to be compared are

symmetric and balanced, D matrix values D_{16} and D_{26} are very small in comparison to the other values and they are neglected. The values left for comparison are D_{11}, D_{12}, D_{22}, D_{66}. Value D_{12} is also neglected since it is a direct outcome of D_{11} and D_{22} values. So, what is finally left for comparison are values D_{11}, D_{22} and D_{66}, which are related to pure bending for D_{11} and D_{22} and torsion for D_{66}. Normally, pure bending stiffness is measured using a 3 or 4 point bending test. However, in this case the ply drop sections have very small dimensions and as a consequence, 3 or 4 point bending testing would be invalid.

$$\begin{bmatrix} M_{xx} \\ M_{yy} \\ M_{xy} \end{bmatrix} = \begin{bmatrix} D_{11} & D_{12} & D_{16} \\ D_{12} & D_{22} & D_{26} \\ D_{16} & D_{26} & D_{66} \end{bmatrix} \begin{bmatrix} \kappa_x \\ \kappa_y \\ \kappa_{xy} \end{bmatrix} \tag{4.2}$$

So, in order to compare the D matrix values, 3 different FEM models are used. In these FEM models, the same rotation moments are applied in each equivalent laminate built with a different method and the reaction moments are measured. Two laminates with exactly the same bending stiffness should have no difference in their reaction moment values under the condition that the rotational moment is the same for both models. The FEM models used here do not have the same dimensions as the ply drop sections since there is no reason to do so. All it's needed is stiffness properties comparison, so a smaller part of the ply drop sections is needed. As a result, it was decided models to have dimensions of 20x20mm, since 20mm is the width limit calculated in the boundaries sensitivity study in section 4.2.5.

M_{xx} moment FEM model

This model respresents the D_{11} bending stiffness value. The edge of the laminate on the X axis is fixed and on the opposite side a moment is applied with a rotation of 0.05 radians defined as a boundary condition. The moment is applied on a node which is coupled with the edge nodes via a coupling constraint. The FEM model can be seen in figures 4.35 and 4.36.
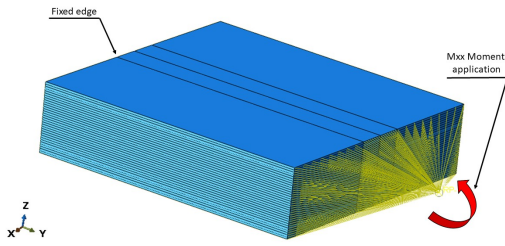
Figure 4.35: M_{xx} moment application FEM model.
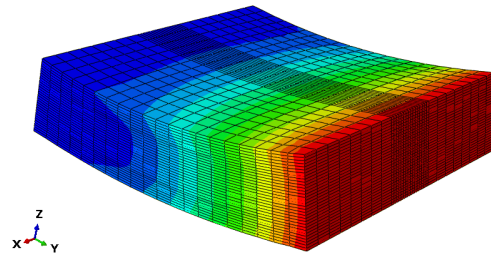
Figure 4.36: The displacement result of M_{xx} moment application.

M_{yy} moment FEM model

This case represents the D_{22} bending stiffness value. Similarly to M_{xx} moment FEM model, the edge of the laminate on the y axis is fixed and on the opposite side a moment is applied

with a with a rotation of 0.05 radians as a boundary condition. The application of the moment is the same as the M_{xx} model. The FEM model can be seen in figures 4.37 and 4.38.
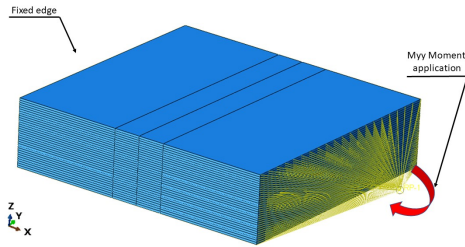
Figure 4.37: M_{yy} moment application FEM model.
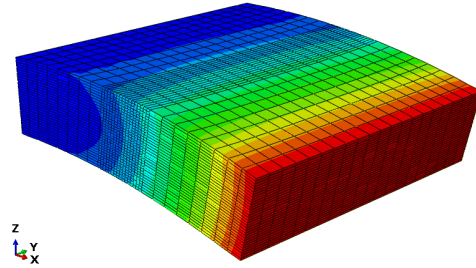
Figure 4.38: The displacement result of M_{yy} moment application.

M_{xy} moment FEM model

This model represents the D_{66} bending stiffness value. The edge on the y axis is fixed and on the opposite side, a torsional fixed moment is applied with a rotation of 0.05 radians as a boundary condition on a node coupled with the nodes on the edge via a coupling constraint. The application of the moment is the same as the M_{xx} model. The FEM model can be seen in figures 4.39 and 4.40.
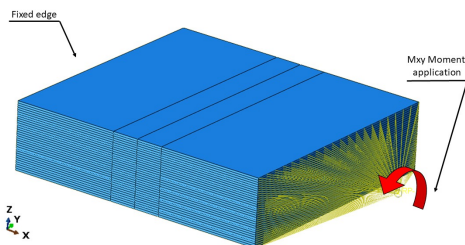
Figure 4.39: M_{xy} moment application FEM model.
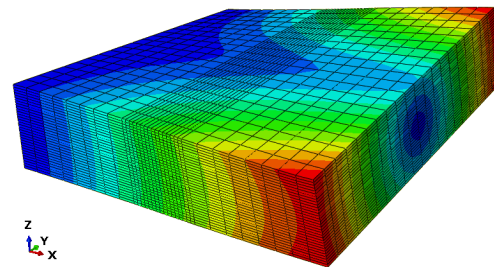
Figure 4.40: The displacement result of M_{xy} moment application.

Reaction moment results

In table 4.14, all the reaction moment results concerning section I-II and the 3 different equivalent laminates built with the methods presented in section 4.3.4, are shown.

Table 4.14: Comparison of reaction moments between section I-II and its equivalent laminates for methods 1, 2 and 3.

	Section I-II	Equivalent of section I-II using method 1	Error (%)	Equivalent of section I-II using method 2	Error (%)	Equivalent of section I-II using method 3	Error (%)
M_{xx} (Nm)	19240	18340	4.68	18280	4.99	17980	6.55
M_{yy} (Nm)	13620	13410	1.54	13680	0.44	14100	3.52
M_{xy} (Nm)	29784	29795	0.04	29906	0.41	29350	1.46

4.3.7 Selection of the most accurate method

In order to decide which of the 3 methods presented in section 4.3.4 is the most accurate, the addition of the errors for the in-plane and out of plane comparison with original section I-II, are added for each method. Additionally, the computational time for the stiffness calculator code to to calculate the stiffness properties of the ply drops in each method, is added to the previous sum. The method with the smallest total number is the one selected. At this point, it has to be noted that the error values for the moment reactions (M_{xx}, M_{xy}, M_{yy}) which represent the out of plane displacement stiffness, have a weight coefficient of 2, since the blended laminate is under buckling loading and the out of plane properties play a major role in the final outcome. All the errors for all the methods as well as the computational times, are presented in table 4.15. Looking at the results, it can be seen that method 1 is accurate but not the fastest, whereas method 3 is the fastest but not the most accurate. The final choice is method 1 since it has the smallest total error + computational time number. This basically mean that it is the best trade off between accuracy and computational time.

Table 4.15: Sum of all the errors and the computational time for methods 1, 2 and 3. The errors referring to the moment reactions, have a weight coefficient of 2.

	Method 1	Method 2	Method3
E_x error(%)	1.97	0.73	4.53
E_y error(%)	3.63	3.84	3.90
E_z error(%)	0.17	0.28	0.06
G_{xy} error(%)	2.23	1.40	3.35
G_{xz} error(%)	0.12	0.21	3.80
G_{yz} error(%)	0.60	0.71	0.84
v_{xy} error(%)	1.98	1.03	0.53
v_{xz} error(%)	1.48	8.23	0.32
v_{yz} error(%)	1.44	0.24	6.89
v_{yx} error(%)	3.64	4.13	1.20
v_{zx} error(%)	0.33	8.73	4.35
v_{zy} error(%)	5.08	3.46	3.17
M_{xx} error(%)x2	9.36	9.98	13.1
M_{xy} error(%)x2	3.08	0.88	7.04
M_{yy} error(%)x2	0.08	0.82	2.92
Computation time (min)	5.82	10.37	2.58
sum	41.02	55.04	58.55

4.3.8 Verification of the method in other ply drop sections

In previous sections, a method was presented on how to built laminates with equivalent stiffness properties in laminates with ply drops. The method was verified using ply drop section I-II. However, in order to verify that this method works for all the other sections as well, it is tested against two more ply drop sections. These are section I-II-IV-V and section IV-V. The reason for choosing these ply drop sections for verification, is because of the large

number of ply drops. The results for section I-II-IV-V and section IV-V are presented in tables 4.16 and 4.17 respectively. Looking at the results, section I-II-IV-V seems to have more that one values where the error is higher than 10%. A possible explanation for this can be the large number of ply drops in this ply drop section, which is 14 in total, including the symmetric ones. Even if the equivalent stiffness for each ply drop has a small error, the high number of ply drops will lead to higher total error in the whole equivalent ply drop section. Future investigation is needed on how to lower the errors in the stiffness calculator code for sections with a large number of ply drops.

Table 4.16: Section I-II-IV-V stiffness properties compared to the equivalent laminate stiffness properties.

	Section I-II-IV-V	Equivalent of section I-II-IV-V	Error (%)
E_x (MPa)	27985.86	27784.57	0.72
E_y (MPa)	34849.26	34775.03	0.21
E_z (MPa)	7835.2	7800.73	0.44
G_{xy} (MPa)	20472.44	20305.55	0.82
G_{xz} (MPa)	2757.45	3025.01	9.70
G_{yz} (MPa)	2764.9	2706.59	2.11
v_{xy}	0.4018	0.4362	8.56
v_{xz}	0.3689	0.362	1.87
v_{yz}	0.2143	0.2418	12.83
v_{yx}	0.50	0.55	9.12
v_{zx}	0.10	0.101	1.59
v_{zy}	0.05	0.056	12.58
M_{xx} (Nm)	20420.00	18210.00	10.82
M_{yy} (Nm)	10960.00	10660.00	2.74
M_{xy} (Nm)	29880.00	29010.00	2.91

Table 4.17: Section I-IV stiffness properties compared to the equivalent laminate stiffness properties.

	Section I-IV	Equivalent of section I-IV	Error (%)
E_x (MPa)	28064.47	27571.71	1.76
E_y (MPa)	22870.73	22189.23	2.98
E_z (MPa)	7863.52	7851.38	0.15
G_{xy} (MPa)	22167.3	22260.6	0.42
G_{xz} (MPa)	2673.16	2843.24	6.36
G_{yz} (MPa)	2779.04	2775.4	0.13
v_{xy}	0.5402	0.5419	0.31
v_{xz}	0.3012	0.2865	4.88
v_{yz}	0.3585	0.3693	3.01
v_{yx}	0.44	0.44	0.94
v_{zx}	0.08	0.08	3.33
v_{zy}	0.12	0.13	6.01
M_{xx} (Nm)	15990.00	15140.00	5.32
M_{yy} (Nm)	11780.00	11870.00	0.76
M_{xy} (Nm)	29850.00	29960.00	0.37

4.3.9 Automation of the process

The purpose of this chapter is to automate the process of calculating the out of plane displacement for any blended laminate. This is done in a python code and includes the calculation of the stiffness of the ply drop sections, the building of the equivalent stiffness laminates, the assigning of the equivalent stiffness properties in the FEM model of the blended laminate and the execution of the analysis. However, not all the process is still automated and some procedures have to be done by the user. These procedures are:

- The building of the 3D ply drop FEM models. Still there is not a code that can automatically build the ply drops taking as an input the length of the ply drops. This could be a future project. Additionally, the ply drop FEM model must have its symmetric counterpart, other wise the code calculating the stiffness will calculate wrong results due to asymmetry and coupling effects. The ply drop length does not have to be the same as the length of the ply drop section.

- Position of the ply drop in the assembly module. It should be noted that the position of the ply drops in the assembly module should be at the exact same position where the ply drop is in respect to the blended laminate. This is because the code assigns the stiffness properties of the ply drop sections according to their position in the assembly module.

- The user has to make the partitions where the ply drop sections are located in the blended laminate and re-mesh the model. This feature can be automated in the future.

- The name of each ply drop should be specific and not random. For example, if ply drop section I-II has 2 ply drops, then the name of each ply drop should be "Section_I_II-plydrop1" for the first ply drop and "Section_I_II-plydrop2" for the second ply drop. The same applies for the rest of the ply drop sections.

- The names of the stacking sequences of the sections in the blended laminate, should be named specifically and not randomly. For example the stacking sequence of section I should be named "Section_I".

- The blended laminate model should be first in the list of models in the abaqus.cae file and the rest of the models should be only the ply drop models, without any extra model.

An overview of how the code automates the whole process is shown in figure 4.41.
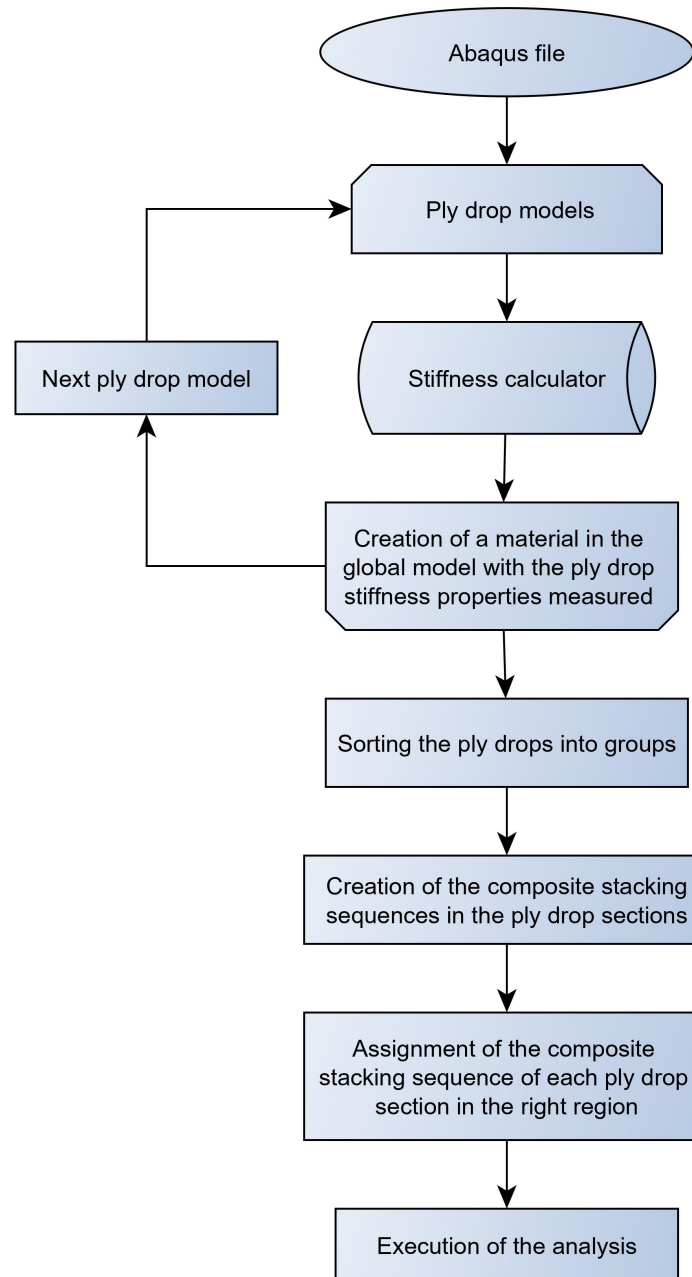
Figure 4.41: An overview of the automation process to calculate the out of plane displacement of a blended laminate.

A short explanation for each process of the code follows.

- **Ply drop models**. This process loops through all the ply drop models in the Abaqus file.

- **Stiffness calculator**. This is the code presented in section 4.3.1 which calculates all

the stiffness properties of a FEM model.

- **Creation of a material in the global model with the ply drop stiffness properties measured**. This procedure creates a material in the global blended model with the same name as the respective ply drop and it puts the stiffness property values calculated using the stiffness calculator in the previous step.

- **Sorting the ply drops into groups**. This process sorts the ply drop names into groups of ply drops from the same ply drop section. For example, ply drop FEM models "Section_I_II-plydrop1" and "Section_I_II-plydrop2" are put in the same list. At the end, there should be equal number of lists and ply drop sections. All these lists are put in another list called groups.

- **Creation of the composite stacking sequences in the ply drop sections**. In this process, the code fills the data for the stacking sequence of each ply drop section with the right information. Firstly, it extracts the position of each ply drop in space. Then, according to this position, the material with the same name with the ply drop name, is put in the plies that occupy the same space in the stacking sequence as the ply drop through the thickness of the laminate. All the fiber directions for these particular plies are set to 0°. The rest of the plies are filled with the data from the stacking sequence of one of the two sections that compose this particular ply drop section since they are common. The code understands which section to choose from the name of the ply drop.

- **Assignment of the composite stacking sequence of each ply drop section in the right region**. From the previous step, the code has extracted the position of the ply drops in space and has created the ply drop section stacking sequences. Knowing the in plane position of each ply drop, the code assigns the ply drop section stacking sequences at the right regions.

4.4 Thermal Global Blended FEM model

The purpose of this section is to investigate the thermal response of the blended laminate during cooling down in the autoclave and create a model that can simulate the imperfections due to cooling down, as presented in the thesis of Gomaa. Additionally, the thermal response of each section of the laminate will be studied separately in order to find out if the different expansion coefficients of each section is the reason for the saddle type imperfections in the blended laminate, as Gomaa implied in his thesis. The FEM model is built in Abaqus using S4RT, 4-node thermally coupled doubly curved, reduced integration, hourglass control, finite membrane strains shell elements. In order to simulate the cooling down of the autoclave, a similar method to Mattioni et al. is followed [19]. In this method, the laminate is fixed at the center node and an initial and final temperature is applied to all the nodes of the model. This leads to mechanical loading due to the temperature difference. The initial temperature is applied with a predefined field and the final temperature is applied as an interaction, using a surface film condition at the surface of the blended laminate. The surface film condition should be applied to both sides of the surface of the blended laminate, otherwise the laminate will get invalid displacements. The initial temperature was set to 120 degrees Celsius according to the autoclave temperature cycle that Gomaa provided in his thesis. The autoclave cycle can be seen in figure 4.42. The final temperature is set to the room temperature, which is 25 degrees Celsius. The analysis is non-linear using a coupled temperature-displacement step and 89 increments. Unfortunately, no thermal properties of the material used in the blended laminate was found and as a result, carbon fiber material properties found in literature were used instead. The thermal material properties used can be seen in table 4.18.
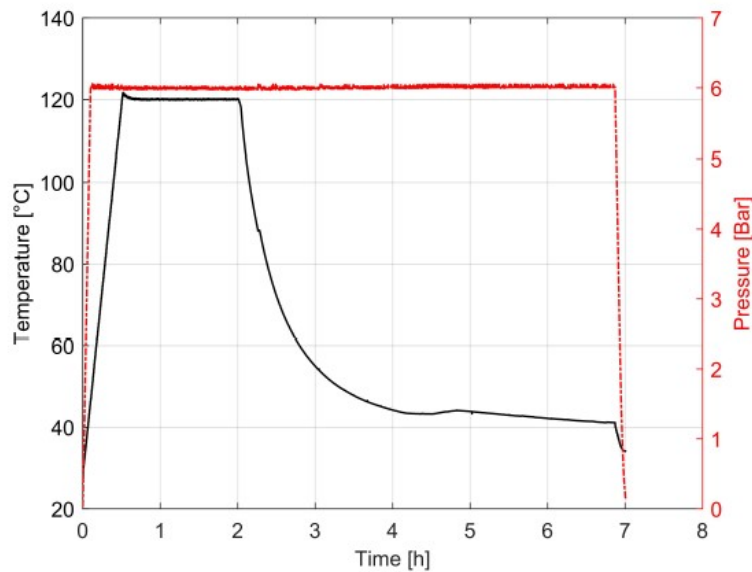
Figure 4.42: The autoclave cycle used for the blended laminate [19].

Table 4.18: The thermal material properties used in the analysis.

Material properties	Values	Units
Thermal conductivity k_{11}	2	W/mmC^o
Thermal conductivity k_{22}	0.2	W/mmC^o
Thermal conductivity k_{33}	0.2	W/mmC^o
Density	$1.5\ 10^{-6}$	Kg/mm^3
Expansion coefficient a_{11}	$-1.2\ 10^{-5}$	-
Expansion coefficient a_{22}	$3.4\ 10^{-5}$	-
Expansion coefficient a_{33}	$3.4\ 10^{-5}$	-
Specific heat	904	J/KgC^o

4.4.1 Composite stacking sequence in thermal FEM model

The stacking sequence of each section in the blended FEM model has 32 plies. However, Abaqus has a limitation of 20 integration points when using S4RT shell elements. Even if one integration point is used per ply, they still exceed the limitation of 20 integration points for the whole stacking sequence. In order to solve this limitation, the stacking sequence of each section was simplified in a way that it does not affect the general stacking sequence characteristics. The simplification is that pairs of $\pm$ plies of the same orientation can become single plies of same orientations with different signs and double the thickness. The simplified stacking sequence still remains symmetric and balanced but it has less integration points. For example if a stacking sequence has 2 pairs of $\pm 60^o$ plies, one becomes $+60^o$ and the other -60° with double the normal thickness, so that the stacking sequence remains symmetric and balanced. In order to verify that this simplification works, a stacking sequence is simplified and a thermal analysis is run for both simplified and original stacking sequences. Then, the displacement results are compared. The thermal model that is used for this analysis, has dimensions of 120x80mm, the initial temperature is 120 degrees Celsius and the final temperature is 25 degrees Celsius.
The original stacking sequence with $t_{ply} = 0.155mm$ is:

$$[45/-45/60/-60/60/-60/45/-45/0/0]_s$$

and the simplified one with $t_{ply} = 0.31mm$ is:

$$[45/60/-60/-45/0]$$

The results from the thermal analysis are shown in table 4.19. It can be seen that results are exactly the same for both stacking sequences which proves that the simplification works.

Table 4.19: Difference in displacement due to thermal loading between original and simplified stacking sequence.

	Displacement in X (mm)	Displacement in Y (mm)	Ply thickness (mm)
Original stacking sequence $[45/-45/60/-60/60/-60/45/-45/0/0]_s$	0.02538	0.01692	0.155
Simplified stacking sequence $[45/60/-60/-45/0]_s$	0.02538	0.01692	0.31
Difference (%)	0	0	

The blended laminate has a total of 25 stacking sequences. Due to symmetry in the in-plane axes, there are 9 stacking sequences repeated for each quarter of the laminate (see figures 2.17 and 2.18 for more info). From these 9 stacking sequences, 4 are different. In tables 4.20, 4.21, 4.22 and 4.23, the simplification done for each stacking sequence is presented so that the number of integration points in any stacking sequence is equal or less than 20. Only the symmetric parts of the stacking sequences are shown. The simplified stacking sequences still remain symmetric and balanced.

Table 4.20: Simplified stacking sequence for Sections I and III.

Section I and III			
Original stacking sequence		Simplified stacking sequence	
Ply thickness	Orientation	Ply thickness	Orientation
0.155	45	0.31	45
0.155	-45		
0.155	60	0.31	60
0.155	-60		
0.155	45	0.31	-45
0.155	-45		
0.155	30	0.155	30
0.155	-30	0.155	-30
0.155	60	0.31	-60
0.155	-60		
0.155	0	0.31	0
0.155	0		
0.155	60	0.155	60
0.155	-60	0.155	-60
0.155	0	0.31	0
0.155	0		
Total integration points	32		20

Table 4.21: Simplified stacking sequence for Section II.

Section II			
Original stacking sequence		Simplified stacking sequence	
Ply thickness	Orientation	Ply thickness	Orientation
0.155	45	0.155	45
0.155	-45	0.155	-45
0.155	60	0.31	60
0.155	-60		
0.155	60	0.31	-60
0.155	-60		
0.155	60	0.31	60
0.155	-60		
0.155	0	0.31	0
0.155	0		
0.155	0	0.31	0
0.155	0		
0.155	60	0.31	-60
0.155	-60		
0.155	0	0.31	0
0.155	0		
Total integration points	32		18

Table 4.22: Simplified stacking sequence for Sections IV,VI,VII,VIII and IX.

Section IV, VI, VII, VIII and IX			
Original stacking sequence		Simplified stacking sequence	
Ply thickness	Orientation	Ply thickness	Orientation
0.155	45	0.155	45
0.155	-45	0.155	-45
0.155	60	0.31	60
0.155	-60		
0.155	60	0.31	-60
0.155	-60		
0.155	60	0.31	60
0.155	-60		
0.155	60	0.31	-60
0.155	-60		
0.155	60	0.31	60
0.155	-60		
0.155	60	0.31	-60
0.155	-60		
0.155	60	0.155	60
0.155	-60	0.155	-60
Total integration points	32		20

Table 4.23: Simplified stacking sequence for Section V.

Section V			
Original stacking sequence		Simplified stacking sequence	
Ply thickness	Orientation	Ply thickness	Orientation
0.155	45	0.155	45
0.155	-45	0.155	-45
0.155	60	0.31	60
0.155	-60		
0.155	60	0.31	-60
0.155	-60		
0.155	60	0.31	60
0.155	-60		
0.155	60	0.31	-60
0.155	-60		
0.155	0	0.31	0
0.155	0		
0.155	60	0.31	60
0.155	-60		
0.155	60	0.31	-60
0.155	-60		
Total integration points	32		18

4.4.2 Convergence study

A convergence study is executed in order to find the mesh size for the thermal FEM model. The convergence value is the out of plane displacement. At this point, it has to be noted that Gomaa stated in his thesis that when the blended laminate finished the autoclave cycle, it was straight without any visual imperfections but in an unstable state. By the moment he touched it, it went into an equilibrium position of saddle type. The same happens with the FEM simulation. If there is no external force on the blended laminate, there is no out of plane displacement. In order to force the laminate into an equilibrium position, a very small out of plane force is applied at one of the 4 edges of the laminate. The same methodology is followed by Mattioni et al. as well [19]. The force magnitude is only 0.01N but is sufficient to drive the blended laminate into its equilibrium position. In figures 4.43 and 4.44, the out of plane displacement against the number of elements and element size respectively, are shown. Additionally, in table 4.24, all the data for mesh convergence are gathered in one table. The convergence criteria was decided to be the less than 1% difference between consecutive out of plane displacements of different mesh sizes. Thus, the mesh size of 1200 elements was selected.
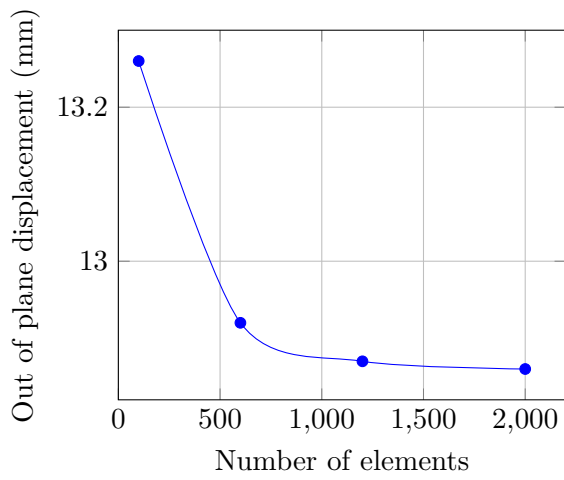
Figure 4.43: Out of plane displacement against number of elements.
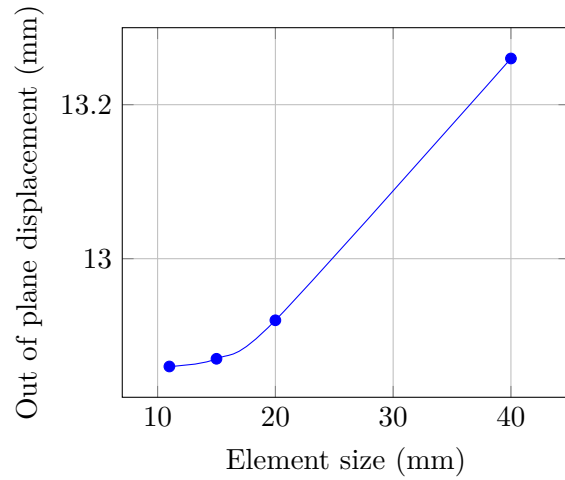
Figure 4.44: Out of plane displacement against element size.

Table 4.24: The difference in percentages between consecutive out of plane displacements of different mesh sizes.

Number of elements	Element size (mm)	max U3 (mm)	Difference (%)
100	40	13.26	-
600	20	12.92	2.56
1200	15	12.87	0.39
2000	11	12.86	0.08

Chapter 5

Results

5.1 Global FEM model

5.1.1 Non-Linear analysis

Using the model built in section 4.1, it is time to accurately calculate the out of plane displacement and the ply stresses of the global FEM model. Geometric non-linear analysis is used with a step of 100 increments, so that the recalculation of the stiffness matrix in each increment is accurate enough. The load is set to 120 kN which is higher than the buckling load calculated in section 4.1.1 , which is 111.350 kN. The applied load is higher that the buckling load in order to investigate the post buckling region of the blended laminate as well. The mesh size and the type of elements used remain the same as in the model in section 4.1.1. Additionally, the introduction of an imperfection is needed, otherwise the laminate will never buckle in the out of plane direction. The imperfection introduced is 1% of the out of plane displacement for the first eigenvalue of the linear perturbation analysis executed in section 4.1.1. The results of the non linear analysis for the out of plane displacement of the blended laminate at 120 kN buckling load are shown in figure 5.1. The stress results at fiber direction, for the first ply of each section of the blended laminate, are shown in figure 5.2. The stress results for the rest of the 31 plies of all sections can be seen in Appendix C. The ply numbering in the stress results is defined as follows: the 1st ply is the ply closest to the bottom and the 32nd ply is the ply closest to the top. Additionally, in figure 5.3, the displacement of the laminate against the buckling load is shown. It is obvious from figure 5.2 that no stress continuity exists between the different sections of the blended laminate. This is due to the simplified global blended laminate model, which does not model the ply drop sections, but instead there is a sudden change in the stacking sequence between sections which in reality is impossible to happen since the laminate would have no structural integrity.
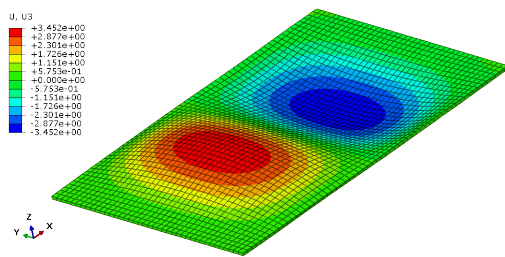
Figure 5.1: The out of plane displacement of the blended laminate at 120 kN buckling load. The legend is in mm.
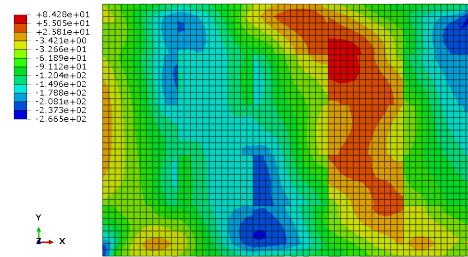
Figure 5.2: Stress results at fiber direction for ply 1 of all sections of the blended laminate at 120 kN buckling load. The legend is in MPa.
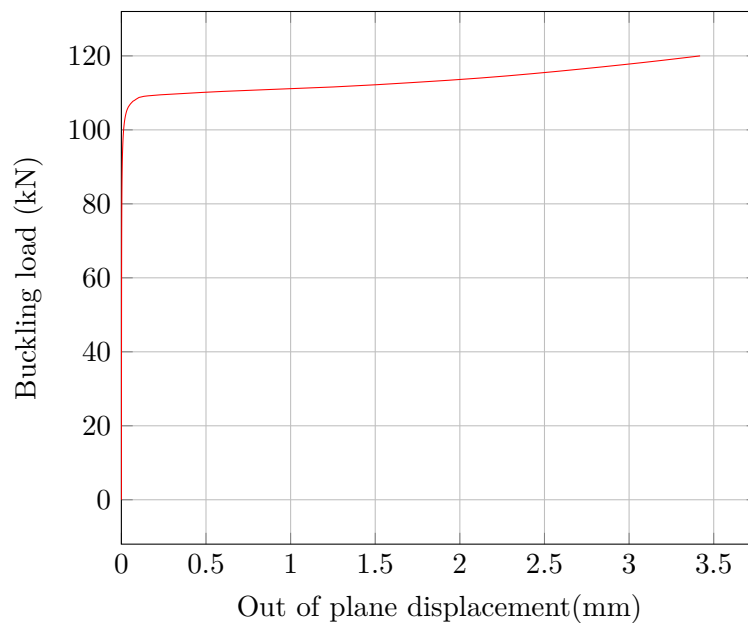
Figure 5.3: Out of plane displacement of the global blended laminate FEM model.

5.1.2 Discussion

The FEM model presented above, is built similarly to the one used by Gomaa with the difference that Gomaa's model is longer, wider and included the resin blocks used in the buckling testing since it was intended to simulate the buckling testing results, something that was not the case in this thesis project [7]. The FEM model results taken from the FEM model presented above, are used as a benchmark in order to compare the stress and out of plane displacement results from this model and the one including the ply drop sections.

5.2 Local FEM models results

5.2.1 Non-linear analysis results

Having defined the mesh density and section width in section 4.2.3, the non-linear analysis for all the ply drop sections can be executed. As explained previously, global-local modeling is used for the analysis of the local ply drop sections, which means that the extrapolated values of the displacement results from the global blended FEM model are used as boundary conditions for the ply drop section FEM models. The analysis is non-linear with 100 increments. The stress field at fiber direction for section I-II is shown in figure 5.4. The results for the rest of the 13 sections can be found in Appendix D.
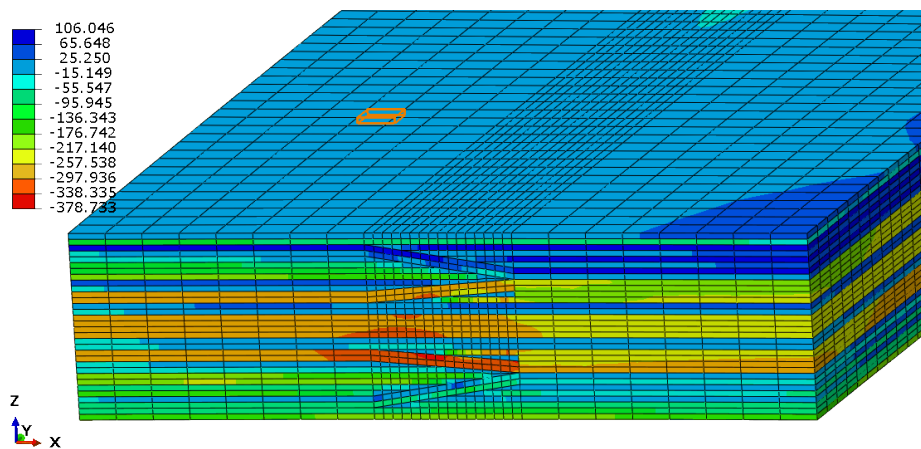
Figure 5.4: Stress results of section I-II. The legend is in MPa.

5.2.2 Results comparison and discussion

In this section, the results from the local ply drop section FEM models and the results from the global FEM model at the same area, are compared. In table 5.1, the results from both models are shown. Looking at table 5.1, it can be seen that in sections where the maximum stress location is outside the ply drop area, the difference for the value of max stress between global and local FEM models is in the range of 1 to 22%. On the other hand, when the max stress location is in the ply drop area, which of course does not exist in the global FEM model, the difference of max stress between global and local FEM models is in the range of 18 to 54%. This is logical taking into account the fact that there is a completely different design approach in both FEM models and also the fact that the mesh density in the local ply drop section FEM models is much higher. The global model uses 2D continuum shell elements with a stacking sequence whereas the local ply drop section models use 3D solid elements with one element per ply and detailed representation of the ply drops. Additionally, the max stress location in both global and local FEM models is in the same ply, except for two sections. In the majority of the cases, the max stress for both global and local models is at 0° plies, which makes sense since they have the highest stiffness in the direction of the buckling load. In the two cases that the location of the max stress is not at 0° plies, that did not happen because there are no 0° plies in these ply drop sections (Sections IV-VII and

VI-IX). Instead, these two sections are composed of primarily $\pm 60^o$ plies except the top and bottom 2 plies which are $\pm 45^o$, as in all sections. The most vulnerable ply drop sections, from a max stress point of view, are the ones with the most complex geometries. These are Sections I-II-IV-V and II-III-V-VI. These are also the ply drop sections in which the max stress difference between global and local FEM models models is the highest, around 50 to 54%. When Gomaa C-scanned the blended laminate after the buckling failure test, the regions where the laminate failed, include the region where section II-III-V-VI is located as it can be seen in figure 5.5. This ply drop section has the highest stress of all sections. Of course the load in this analysis is 120 kN, which is less than the buckling load used by Gomaa to fail test the laminate, which was much higher. Additionally, there were resin blocks at the edges of the laminate, which slightly alter the boundary conditions. All that means the first ply failure of the laminate could have happened in section II-III-V-VI. Unfortunately, there is no data for the compressive strength in fiber direction of the carbon fiber material used in this analysis, in order to use failure criteria. Maybe in future projects the material properties can be extracted from testing and the use of failure criteria will be possible.

Table 5.1: Max stress values and location of all the sections for both global and local ply drop section models. The ply numbers are measured from bottom to top.

Ply drop Section	Global Blended model max stress results (MPa) and location		Local model max stress results (MPa) and location		Difference (%)
I-II	-297.4	at ply 11 (0^0)	-378.7	at plydrop 11 (0^0)	27.34
II-III	-331.3	at ply 11 (0^0)	-405.4	at plydrop 11 (0^0)	22.37
I-IV	-311.4	at ply 22 (0^0)	-339.4	at ply 22 (0^0)	8.99
II-V	-307.4	at ply 9 (0^0)	-320.5	at ply 9 (0^0)	4.26
III-VI	-348	at ply 11 (0^0)	-352.4	at ply 11 (0^0)	1.26
IV-V	-238	at ply 11 (0^0)	-282.8	at plydrop 11 (0^0)	18.82
V-VI	-257.1	at ply 11 (0^0)	-297	at ply 11 (0^0)	15.52
IV-VII	-206.4	at ply 1 (45°)	-263.9	at plydrop 23 (-60°)	27.86
V-VIII	-281.1	at ply 11 (0^0)	-344.8	at ply 11 (0^0)	22.66
VI-IX	-230.2	at ply 2 (-45°)	-284.6	at plydrop 9 (60°)	23.63
I-II-IV-V	-303.8	at ply 11 (0^0)	-469.8	at plydrop 11 (0^0)	54.64
II-III-V-VI	-338.7	at ply 11 (0^0)	-507.9	at plydrop 11 (0^0)	49.96
IV-V-VII-VIII	-239.8	at ply 11 (0^0)	-276.3	at ply 11 (0^0)	15.22
V-VI-VIII-IX	-261.5	at ply 11 (0^0)	-295.6	at ply 11 (0^0)	13.04

Figure 5.5: The failure location of the blended laminate Gomaa tested [7].

5.3 Out of plane displacement results including ply drops

5.3.1 Blended laminate built by Gomaa

The automated code built in section 4.3.9, is tested in the FEM model of the blended laminate Gomaa built. The results are shown in figure 5.6 in comparison with the out of plane displacement of the blended laminate FEM model without the ply drop sections, presented in section 5.1.1. It can be seen that the maximum displacement is higher in the blended laminate including the ply drops, which makes sense since the ply drop sections have lower stiffness than the idealised situation where there are no ply drops and there is a sudden change in the stacking sequence. The lower stiffness is due to the existence of resin pockets in the ply drops as well as the fact that the ply drops are not parallel to the load application, which lowers the in-plane stiffness properties of the laminate. In table 5.2, the stiffness and out of plane displacement comparison between the blended laminate with and without ply drops is shown. The difference in stiffness is small, only 0.7%. The lower stiffness in the blended laminate with the ply drops has also affected the curve of the out of plane displacement which is 6% higher in the blended laminate with the ply drops. The transition from linear displacement to buckling is smoother in the blended laminate with the ply drops in comparison to the the one without.
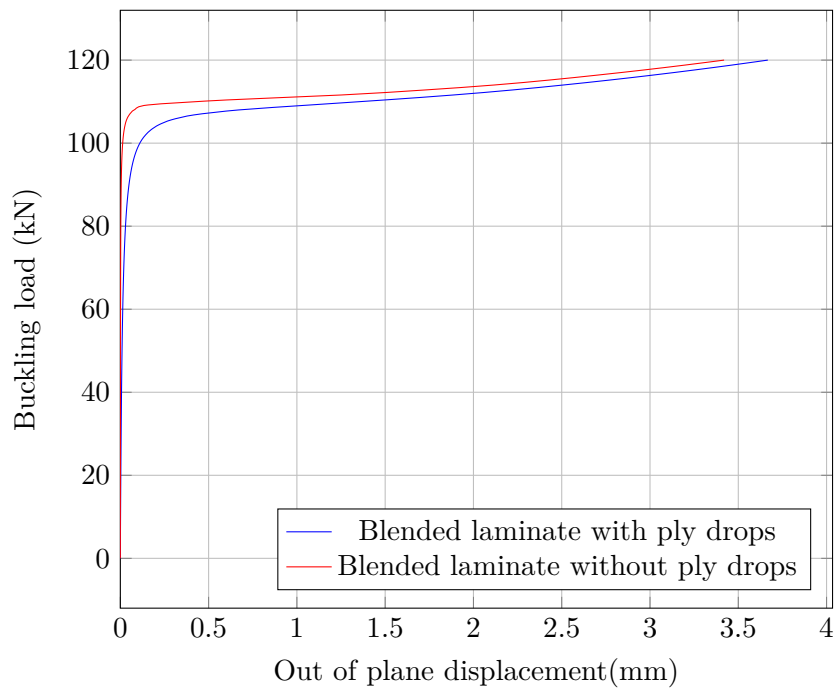
Figure 5.6: Comparison of out of plane displacement between blended laminate with and without ply drops.

Table 5.2: Stiffness and out of plane displacement comparison between blended laminate with and without ply drops.

Laminate	Stiffness (kN/mm)	Difference (%)	Out of plane displacement at 120 kN (mm)	Difference (%)
Blended without ply drops	95.23	-	3.45	-
Blended laminate with plydrops	94.48	-0.7	3.66	6.08

5.3.2 Blended laminate with varying number of sections

The code built in section 4.3.9 is supposed to work on any blended laminate configuration with any number of sections. This means it should automatically calculate the ply drop properties, build the necessary ply drop section stacking sequences and do all the necessary calculations. In order to verify that the code works, it is tested on different blended laminate configurations, all based on the dimensions of the blended laminate built by Gomaa, 600mm x 400mm. For time saving purposes, the properties of each ply drop in each different configuration are not calculated using the method explained in section 4.3.1 but are calculated by averaging the ABD matrices from the ply drops that compose each ply drop section. This method will not give accurate results, since it is not properly simulating the resin pockets and the geometry of the ply drops. However, the purpose of this section is not the accuracy of the results but to verify that the code works on different blended laminate configurations. In table 5.3, the buckling load and the out of plane displacement results of different blended laminate configurations are shown, including the results with and without the ply drop sections. The differences shown in table 5.3 are a lot smaller than in reality, due to not properly simulating the ply drop geometry. Nevertheless, the code worked perfectly for all different configurations of table 5.3, proving that it can be used on any blended configuration.

Table 5.3: Buckling load and out of plane displacement comparison between different blended laminate configurations.

Sections configuration	Buckling load		difference (%)	out of plane displacement		difference (%)
	without plydrops	with plydrops		without plydrops	with plydrops	
4x4	106.052	105.899	0.14	1.075	1.065	0.93
5x5	112.971	112.14	0.74	1.197	1.178	1.59
7x7	133.662	135.301	1.23	1.373	1.383	0.73
9x9	132.722	133.698	0.74	1.357	1.38	1.69
5x3	76.189	76.715	0.69	1.49	1.554	4.30
5x7	128.858	128.726	0.10	1.368	1.356	0.88
5x9	136.752	136.308	0.32	1.327	1.314	0.98
3x5	112.445	111.921	0.47	1.206	1.19	1.33
7x5	127.888	127.814	0.06	1.449	1.434	1.04
9x5	128.023	127.964	0.05	1.304	1.297	0.54

5.3.3 Discussion

Looking at the results, it is clear that the stiffness difference between the blended FEM model with and without ply drops is very small, only 0.7%. Nevertheless, this stiffness difference is translated to a 6% difference in the out of plane displacement at 120 kN, which justifies the use of the FEM model with the ply drop sections, if accuracy in the out of plane displacement results is needed. However, if a blended laminate is composed of a large number of sections, then the difference between FEM models with and without ply drops would have been even

higher due to the higher amount of sections with ply drops and resin pockets, which makes the use of the FEM model with the ply drops preferable. In case the number of ply drop sections is very small, the simple FEM model without the ply drop sections, is more preferable, since much less time is needed to built and solve it whereas the difference in the results between the FEM models with and without ply drops would have been even smaller. Additionally, The code built in section 4.3.9 is verified that it can work on any blended laminate configuration by applying it on many different blended cases without any issue.

5.4 Thermal FEM model results

5.4.1 Simulating the saddle type imperfections of the blended laminate

The FEM model presented in section 4.4 is used to simulate the saddle type imperfections of the blended laminate during cooling down in the autoclave cycle. As explained in section 4.4, there is no data available for the thermal properties of the material used in the blended laminate. As a result, all the properties in table 4.18 were taken from literature, which makes them inaccurate for the purpose of this study. This leaves no other possibility but to reverse engineer the thermal expansion coefficient properties using the saddle type out of plane displacement measurements done by Gomaa in the blended laminate, after the autoclave cycle. It has to be noted that the blended laminate Gomaa manufactured, has slightly different dimensions, so that the resin blocks can be attached at the edges for testing purposes. The length is 700mm instead of 600mm and the width is 415mm instead of 400mm, so that material can be cut off after manufacturing, as a standard laminate manufacturing procedure. The FEM model used in this section, was also updated to these dimensional values. In figures 5.7 and 5.8, the out of plane displacement results from the FEM model and the real measurements of the laminate are shown. The expansion coefficients that reversed engineered in the FEM model are:

$$a_{11} = -0.7\ 10^{-5},\ a_{22} = 2.9\ 10^{-5}\ and\ a_{33} = 2.9\ 10^{-5}$$

As it can be seen, the displacement field is similar in both FEM model and real laminate. However, despite the fact that the maximum displacement is the same, the minimum displacement is different. FEM model shows 3.51mm minimum displacement, whereas the measurements in the real laminate show 5.08mm. A possible explanation could be the asymmetry in the displacement field of the manufactured laminate. This asymmetry could exist due to tiny ply mismatches during manufacturing using the hand lay-up technique. All in all, the FEM model succeeded in simulating qualitatively and almost quantitatively the general displacement field of the laminate after the autoclave cycle.
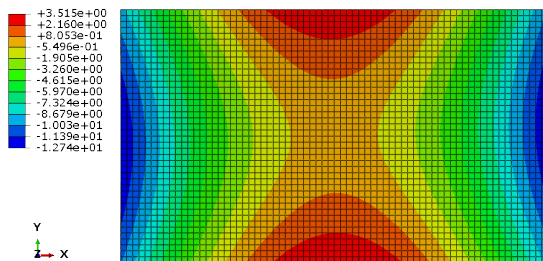
Figure 5.7: The out of plane displacement of the blended laminate at after the autoclave cycle from the FEM model. The legend is in mm.
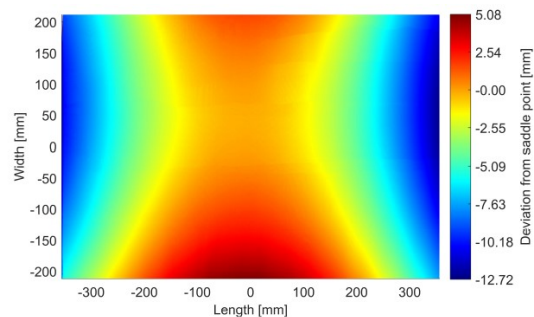
Figure 5.8: The out of plane displacement of the blended laminate after the autoclave cycle measured by Gomaa. The legend is in mm.

5.4.2   Thermal expansion coefficient of each section

In order to verify that the saddle type imperfections are caused due to the different section expansion coefficients, a thermal analysis was run for each section of the blended laminate. The FEM model and thermal properties used in this model are the same as in section 5.4.1 with the only difference that the model has only one section and there is no out of plane force. The dimensions of all sections are 120x80mm. The temperatures used here are the same as in all previous thermal FEM models, 120 degrees Celsius as a starting temperature and 25 degrees Celsius as the final temperature. In table 5.4, the displacement in X and Y direction of each section, as well as the calculated expansion coefficient of each section are presented. It should be noted that from the total 25 sections of the laminate, due to symmetry, there are 9 different sections. From these 9 sections, there are 4 different stacking sequences. Assuming that the expansion of the sections is linear, the equations used to calculate the expansion coefficients for each section are:

$$a_x = \frac{Displacement\ in\ X}{Length\ \Delta T}$$

$$a_y = \frac{Displacement\ in\ Y}{Width\ \Delta T}$$

$$\Delta T = 25 - 120 = -95\ degrees\ Celsius$$

The results in table 5.4 show a clear evidence of thermal expansion mismatch between the different sections of the blended laminate. In particular, sections IV, VI, VII, VIII and IX have negative displacement in X direction and at the same time sections I, II, III and V have positive displacement in X. This causes a thermal pre-stress in the laminate which results in the saddle type imperfections. In Y directions there is still a mismatch in displacement values but all sections have positive displacement.

Table 5.4: Displacement results and expansion coefficients for all sections of the blended laminate during the simulation of cooling down in the autoclave cycle.

	Displacement in X (mm)	Displacement in Y (mm)	a_x	a_y
Section I and III	0.062	0.025	-5.42E-06	-3.25E-06
Section II	0.059	0.027	-5.22E-06	-3.51E-06
Section IV,VI,VII,VIII and IX	-0.128	0.088	1.12E-05	-1.16E-05
Section V	0.012	0.051	-1.06E-06	-6.64E-06

5.4.3   Discussion

In this section, a thermal FEM model was built to simulate the thermal response of blended laminates during the cooling down in the autoclave cycle. The thermal FEM model was built using 2D coupled temperature-displacement elements. Due to the fact that abaqus has a limit of 20 integration points in the stacking sequence used for that particular elements, the stacking sequences of all the sections had to be modified in such way that they would not lose their thermal properties and at the same time have a maximum of 20 integration points. The blended laminate FEM model was based on the laminate that Gomaa manufactured for his thesis and the results of the out of plane displacement of the FEM model and real out of

plane displacement data taken from Gomaa's thesis, showed a clear qualitative and almost quantitative match. This concludes to the fact that similar FEM models can be used in future projects to investigate the response of blended laminates with different configurations as well as test different methods to diminish the saddle type imperfections on this laminate or other blended laminates without the need to manufacture it.

Chapter 6

Conclusions and recommendations

In this thesis project, a blended laminate built by Gomaa is extensively investigated under buckling loading using FEM analysis. The design of the laminate ply drops in the different ply drop section FEM models was achieved by measuring the ply drop dimensions in microscope pictures taken from samples of the manufactured blended laminate. Stress analysis done in the ply drop section FEM models using global-local modeling technique, showed that stresses in some sections are 54% higher than stress values taken from the simplified FEM model without the ply drop sections. Additionally, a code was created to automatically calculate the out of plane displacement of the laminate including the stiffness properties of the ply drops. The total stiffness of the FEM model with the ply drops was measured to be 0.7% lower than the FEM model without the ply drop sections. Similarly, the out of plane displacement of the FEM model including the ply drop sections was higher than the FEM model without the ply drop sections at the same load by 6%. Finally, a thermal FEM model was built to simulate the saddle type imperfections caused by the cooling down of the autoclave cycle and the expansion coefficients of the different sections of the laminate were measured and found out to be very different in some cases.

6.1   Conclusions

The investigation of the mechanical effects of the ply drops in the blended laminate Gomaa built, led to some interesting conclusions. As far as stresses in blended laminates are concerned, the stresses in the local ply drop section FEM models were considerably higher (up to 54% higher) than in the simple global FEM model that does not incorporate the ply drop geometries. This difference in stress value is justified by the fact that the ply drop section FEM models have complex 3D geometries which include all the different ply drops as well as the resin pockets. In such complex geometries, the stress mechanisms are very different from the ones in the simple global FEM model, where there are no ply drops, all plies are straight and parallel and there is no continuity between the stacking sequences of the different laminate sections. This leads to the conclusion that in order to have accurate stress results

in blended laminates, complex 3D FEM models of the ply drop sections of that particular blended laminate need to be built and investigated.

Regarding stiffness and out of plane displacement in blended laminates, the difference between the FEM model including the stiffnesses of the ply drops and the simpler one without any ply drops, depends on the number of sections. In the particular case of the laminate that Gomaa built, which is composed of 25 sections, the differences in stiffness and out of plane displacement are relatively small (0.7% and 6% respectively). However, with increasing number of sections, the difference in stiffness and out of plane displacement between the complex and simple FEM models increases. For example, if a blended laminate has 100 sections, the difference between the complex and simple FEM models would be much higher than the difference in the laminate that Gomaa built. This leads to the conclusion that if the number of sections in a blended laminate is small (for example less than 20), then there is no need for a complex FEM model that includes the stiffnesses of the ply drops, except very accurate results are needed. On the contrary, blended laminates with large number of sections need a FEM model which includes the stiffnesses of the ply drop sections, otherwise the results, especially for the out of plane displacement, could be significantly higher.

As far as the thermal FEM model is concerned, it was built using 2D coupled temperature-displacement elements and the results showed a qualitative and almost quantitative match between the FEM model results and real out of plane displacement data due to imperfection taken from Gomaa's thesis. This proves that FEM modelling can be used to simulate saddle type imperfections in blended laminates due to thermal stresses caused by the stiffness mismatch of the different laminate sections. Additionally, the investigation of the thermal expansion of each laminate section showed that the different sections of the blended laminate have different thermal expansion coefficients which confirmed that the reason for the saddle type imperfections is indeed the different thermal expansion coefficients. This leads to the conclusion that the thermal FEM model can be used in future projects to investigate the thermal response of other blended laminates. It can also be used to diminish the saddle type imperfections by testing different blended configurations on the FEM model and as such not having the need to manufacture each different configuration, which can save time and money.

6.2   Recommendations for future work

- **Use of the thermal model presented in this thesis to diminish the saddle type imperfections**. The laminate Gomaa built, experienced severe saddle type imperfections due to different expansion coefficients of the sections composing the laminate. New ideas on how to diminish these imperfections can be tested in the thermal model to prove that they are working. One possible idea is to increase the section resolution of the blended laminate. What that means is that the number of sections will increase from 25 that is at the moment to a higher number. The higher number of sections will increase the manufacturing complexity of the laminate but will also decrease the thermal displacement differences between the sections due to smaller section size. This will still lead to imperfections during the autoclave cooling down but they will be much smaller, ideally small enough that will not alter the shape of the laminate.

- **Improve the code that calculates the out of plane displacement of the laminate with the stiffness properties of the ply drop sections**. Some of the functions

that could be included in the code are to automatically design the ply drop sections by taking as input the length of each ply drop, the ply thickness, the depth of each ply drops, the position in respect to the laminate, the stacking sequences of the sections that compose the ply drop section as well as the specific plies that are dropped. The code should automatically sketch the ply drop section, extrude it to the desired thickness, execute partitioning commands where necessary, apply the desired properties and finally mesh the part. This should considerably diminish the time needed to create the ply drop section FEM models and will also make fast experimentation with different ply drop section designs possible.

- **Improve the code that calculates the stiffness properties**. Despite the fact that the code is accurate in calculating the stiffness properties of the different ply drops, there is still some error in the calculations. This error is multiplied in some ply drop sections due to the high number of ply drops existing in these particular ply drop sections, leading up to a maximum of 10% error. In order to diminish that, the accuracy of the code calculating the stiffness properties has to be improved. One way to achieve that, is by altering the boundary conditions of the FEM models that calculate the stiffness properties. In the current code, the boundary conditions are applied per side of the part, which means that a boundary condition is applied to all the nodes of a specific part side. This could be altered so that the nodes of one side are divided into different node groups, where slightly different boundary conditions will be applied in order to more accurately calculate the stiffness properties and reduce the error.

References

[1] Abaqus. *Abaqus Analysis user's manual.* Abaqus, 6.6 edition.

[2] David Adams, Layne Watson, and Zafer Gürdal. Optimization and blending of composite laminates using genetic algorithms with migration. *Mechanics of Advanced Materials and Structures*, 10(3):183–203, 2003. ISSN 1537-6494.

[3] David B. Adams, Layne T. Watson, Zafer Gürdal, and Christine M. Anderson-Cook. Genetic algorithm optimization and blending of composite laminates by locally reducing laminate thickness. *Advances in Engineering Software*, 35(1):35–43, 2004. ISSN 0965-9978. doi: https://doi.org/10.1016/j.advengsoft.2003.09.001. URL http://www.sciencedirect.com/science/article/pii/S0965997803001236.

[4] A. D. Botting, A. J. Vizzini, and S. W. Lee. Effect of ply-drop configuration on delamination strength of tapered composite structures. *AIAA Journal*, 34(8):1650–1656, 1996. ISSN 0001-1452. doi: Doi10.2514/3.13285. URL <GotoISI>://WOS:A1996VA28500016.

[5] W. C. Cui, M. R. Wisnom, and M. Jones. Effect of step spacing on delamination of tapered laminates. *Composites Science and Technology*, 52(1):39–46, 1994. ISSN 0266-3538. doi: Doi10.1016/0266-3538(94)90006-X. URL <GotoISI>://WOS:A1994PP48700005.

[6] H. T. Fan, H. Wang, and X. H. Chen. An optimization method for composite structures with ply-drops. *Composite Structures*, 136:650–661, 2016. ISSN 0263-8223. doi: 10.1016/j.compstruct.2015.11.003.

[7] Mohamed Gomaa. *Laminate blending demonstrator.* Thesis, 2019.

[8] John H. Holland. *Adaptation in natural and artificial systems : an introductory analysis with applications to biology, control, and artificial intelligence.* University of Michigan Press, Ann Arbor, 1975. ISBN 0472084607.

[9] Samuel T. IJsselmuiden, Mostafa M. Abdalla, Omprakash Seresta, and Zafer Gürdal. Multi-step blended stacking sequence design of panel assemblies with buckling constraints. *Composites Part B: Engineering*, 40(4):329–336, 2009.

ISSN 1359-8368. doi: https://doi.org/10.1016/j.compositesb.2008.12.002. URL http://www.sciencedirect.com/science/article/pii/S135983680900002Xhttps://ac.els-cdn.com/S135983680900002X/1-s2.0-S135983680900002X-main.pdf?_tid=1fbe5282-ce9d-4dac-8a4a-368024c2bba4&acdnat=1543310597_4059b52518cfb1ae2f2f6d18a7b26b64.

[10] P. Jin, X. Zhong, J. Yang, and Z. Sun. Blending design of composite panels with lamination parameters. *The Aeronautical Journal*, 120(1233):1710–1725, 2016. ISSN 0001-9240. doi: 10.1017/aer.2016.88. URL https://www.cambridge.org/core/article/blending-design-of-composite-panels-with-lamination-parameters/31132C8A9551268D29AE7B7CFA45AEC8https://www.cambridge.org/core/services/aop-cambridge-core/content/view/31132C8A9551268D29AE7B7CFA45AEC8/S0001924016000889a.pdf/div-class-title-blending-design-of-composite-panels-with-lamination-parameters-div.pdf.

[11] Zhao Jing, Xueling Fan, and Qin Sun. Global shared-layer blending method for stacking sequence optimization design and blending of composite structures. *Composites Part B: Engineering*, 69:181–190, 2015. ISSN 1359-8368. doi: https://doi.org/10.1016/j.compositesb.2014.09.039. URL http://www.sciencedirect.com/science/article/pii/S1359836814004429https://ac.els-cdn.com/S1359836814004429/1-s2.0-S1359836814004429-main.pdf?_tid=17091e11-5f4b-4d1f-a1b7-c6a30973c229&acdnat=1547146965_f0e3bcd24114af9b07d58de3f845e76a.

[12] Christos Kassapoglou. *Design and Analysis of Composite Structures : With Applications to Aerospace Structures*. Wiley, Somerset, UNITED KINGDOM, 2013. ISBN 9781118536957. URL http://ebookcentral.proquest.com/lib/delft/detail.action?docID=1160769.

[13] Birna P. Kristinsdottir, Zelda B. Zabinsky, Mark E. Tuttle, and Sudipto Neogi. Optimal design of large composite panels with varying loads. *Composite Structures*, 51(1):93–102, 2001. ISSN 0263-8223. doi: https://doi.org/10.1016/S0263-8223(00)00128-8. URL http://www.sciencedirect.com/science/article/pii/S0263822300001288https://ac.els-cdn.com/S0263822300001288/1-s2.0-S0263822300001288-main.pdf?_tid=435ee41f-4d98-4948-9129-de702deb91e1&acdnat=1543308913_56847854379d2c2ba6d2492dc48ce6e9.

[14] Rodolphe Le Riche and François-Xavier Irisarri. Multiscale composite optimization with design guidelines. In *Journée d'étude : Optimisation des composites*. URL https://hal-emse.ccsd.cnrs.fr/emse-00946617.

[15] Boyang Liu and Raphael Haftka. Composite wing structural design optimization with continuity constraints. In *42nd AIAA/ASME/ASCE/AHS/ASC Structures, Structural Dynamics, and Materials Conference*, Fluid Dynamics and Co-located Conferences, Seattle, WA, USA. American Institute of Aeronautics and Astronautics. doi: doi:10.2514/6.2001-120510.2514/6.2001-1205. URL https://doi.org/10.2514/6.2001-1205.

[16] Dianzi Liu, Vassili V Toropov, Osvaldo M Querin, and David C Barton. Bi-level optimization of blended composite panels. 2009.

[17] A. S. Llanos and A. J. Vizzini. The effect of film adhesive on the delamination strength of tapered composites. *Journal of Composite Materials*, 26(13):1968–1983, 1992. ISSN 0021-9983. doi: Doi10.1177/002199839202601306. URL <GotoISI>://WOS: A1992JP19200006.

[18] Terence Macquart, Marco T. Bordogna, Paul Lancelot, and Roeland De Breuker. Derivation and application of blending constraints in lamination parameter space for composite optimisation. *Composite Structures*, 135:224–235, 2016. ISSN 0263-8223. doi: https://doi.org/10.1016/j.compstruct.2015.09.016. URL http://www.sciencedirect. com/science/article/pii/S0263822315008521.

[19] Filippo Mattioni, Paul M. Weaver, Kevin Potter, and Michael I. Friswell. Analysis of thermally induced multistable composites. 2008.

[20] M. T. McMahon, L. T. Watson, G. A. Soremekun, Z. Gürdal, and R. T. Haftka. A fortran 90 genetic algorithm module for composite laminate structure design. *Engineering with Computers*, 14(3):260–273, 1998. ISSN 1435-5663. doi: 10.1007/bf01215979. URL https://doi.org/10.1007/BF01215979https://link.springer.com/content/ pdf/10.1007%2FBF01215979.pdf.

[21] Flemming Mortensen and Ole Thybo Thomsen. A simple approach for the analysis of embedded ply drops in composite and sandwich laminates. *Composites Science and Technology*, 59(8):1213 – 1226, 1999. ISSN 0266-3538. doi: https://doi. org/10.1016/S0266-3538(98)00160-2. URL http://www.sciencedirect.com/science/ article/pii/S0266353898001602.

[22] A. Mukherjee and B. Varughese. Design guidelines for ply drop-off in laminated composite structures. *Composites Part B-Engineering*, 32(2):153–164, 2001. ISSN 1359-8368. doi: Doi10.1016/S1359-8368(00)00038-X. URL <GotoISI>://WOS:000167418100007.

[23] Sadik L. Omairey, Peter D. Dunning, and Srinivas Sriramula. Development of an abaqus plugin tool for periodic rve homogenisation. *Engineering with Computers*, 35(2):567–577, 2019. ISSN 1435-5663. doi: 10.1007/s00366-018-0616-4. URL https://doi.org/10. 1007/s00366-018-0616-4.

[24] Omprakash Seresta, Mostafa Abdalla, and Zafer Gürdal. A genetic algorithm based blending scheme for design of multiple composite laminates. In *50th AIAA/ASME/ASCE/AHS/ASC Structures, Structural Dynamics, and Materials Conference*, Structures, Structural Dynamics, and Materials and Co-located Conferences. American Institute of Aeronautics and Astronautics. doi: doi:10.2514/6.2009-269910.2514/6. 2009-2699. URL https://doi.org/10.2514/6.2009-2699.

[25] Omprakash Seresta, Zafer Gürdal, David B. Adams, and Layne T. Watson. Optimal design of composite wing structures with blended laminates. *Composites Part B: Engineering*, 38(4):469–480, 2007. ISSN 1359-8368. doi: https://doi.org/10.1016/j. compositesb.2006.08.005. URL http://www.sciencedirect.com/science/article/ pii/S1359836806001211https://ac.els-cdn.com/S1359836806001211/1-s2. 0-S1359836806001211-main.pdf?_tid=824f7c87-8eb1-4782-b1a4-51d97224ed05& acdnat=1543935864_a53ed70387f7efde7ab4647d68f2b76d.

[26] Grant Soremekun, Zafer Gürdal, Christos Kassapoglou, and Darryl Toni. Stacking sequence blending of multiple composite laminates using genetic algorithms. *Composite Structures*, 56(1):53–62, 2002. ISSN 0263-8223. doi: https://doi.org/10.1016/S0263-8223(01)00185-4. URL http://www.sciencedirect.com/science/article/pii/S0263822301001854https://ac.els-cdn.com/S0263822301001854/1-s2.0-S0263822301001854-main.pdf?_tid=24cfb55e-b843-4d42-a75c-b5982ca71261&acdnat=1543311599_23e74ebdb7c2848784e5df984af1d3f7.

[27] Stephen W. Tsai and H. Thomas Hahn. *Introduction to composite materials.* Technomic Pub., Westport, Conn., 1980. ISBN 0877622884.

[28] Stephen W Tsai and Nicholas J Pagano. Invariant properties of composite materials. Report, AIR FORCE MATERIALS LAB WRIGHT-PATTERSON AFB OHIO, 1968.

[29] Julien Van Campen, Omprakash Seresta, Mostafa Abdalla, and Zafer Gürdal. General blending definitions for stacking sequence design of composite laminate structures. In *49th AIAA/ASME/ASCE/AHS/ASC Structures, Structural Dynamics, and Materials Conference, 16th AIAA/ASME/AHS Adaptive Structures Conference,10th AIAA Non-Deterministic Approaches Conference, 9th AIAA Gossamer Spacecraft Forum, 4th AIAA Multidisciplinary Design Optimization Specialists Conference*, Structures, Structural Dynamics, and Materials and Co-located Conferences. American Institute of Aeronautics and Astronautics. doi: doi:10.2514/6.2008-179810.2514/6.2008-1798. URL https://doi.org/10.2514/6.2008-1798https://arc.aiaa.org/doi/pdfplus/10.2514/6.2008-1798.

[30] Julien Marie Jan Ferdinand Van Campen. *Optimum lay-up design of variable stiffness composite structures.* Phd, 2011.

[31] Ellen Van den Oord. *Overcoming the curse of dimensionality in composite laminate blending.* Thesis, 2018.

[32] B. Varughese and A. Mukherjee. Analysis of tapered laminated composites with non-symmetric lay-up. *Journal of Reinforced Plastics and Composites*, 16(7):631–660, 1997. doi: 10.1177/073168449701600704. URL https://doi.org/10.1177/073168449701600704.

[33] Junbo Yang, Bifeng Song, Xiaoping Zhong, and Peng Jin. Optimal design of blended composite laminate structures using ply drop sequence. *Composite Structures*, 135:30–37, 2016. ISSN 0263-8223. doi: https://doi.org/10.1016/j.compstruct.2015.08.101. URL http://www.sciencedirect.com/science/article/pii/S0263822315007977https://ac.els-cdn.com/S0263822315007977/1-s2.0-S0263822315007977-main.pdf?_tid=b9028d12-d4e3-4068-bfd3-84f1b21a736c&acdnat=1547062726_88b91f79f912add8488bcde6b45e33de.

[34] Z. Zabinsky. Global optimization for composite structural design. In *35th Structures, Structural Dynamics, and Materials Conference*, Structures, Structural Dynamics, and Materials and Co-located Conferences. American Institute of Aeronautics and Astronautics. doi: doi:10.2514/6.1994-149410.2514/6.1994-1494. URL https://doi.org/10.2514/6.1994-1494.

[35] S. Zein and M. Bruyneel. A bilevel integer programming method for blended composite structures. *Advances in Engineering Software*, 79:1–12, 2015. ISSN 0965-9978. doi: 10.1016/j.advengsoft.2014.08.008. URL `<GotoISI>://WOS:000345345100001`.

Appendix A

Microscope pictures

Below, microscope through the thickness pictures of different sections of the blended laminate are shown. The name of the Section in each picture reveals which part of the Section is on the left of the picture and which is on the right. For example, a microscope picture named Section II-I means that on the left of the picture is Section II and on the right Section I. Each picture has an upper and lower part. All of the Sections are symmetric so upper and lower parts theoretically should be identical. However, due to the fact that the laminate was manufactured using hand layup technique, there are differences between upper and lower parts in the same ply drop section.
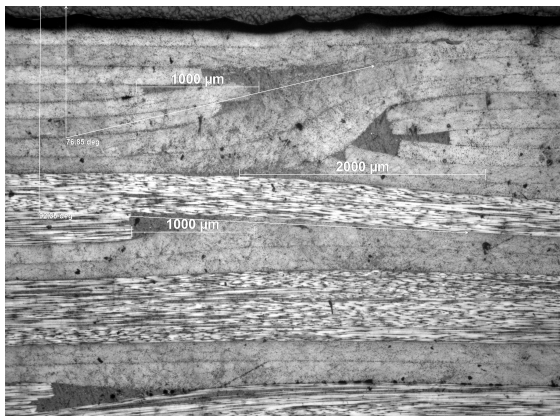
Figure Appendix A.1: Section II-I upper part, sample 1
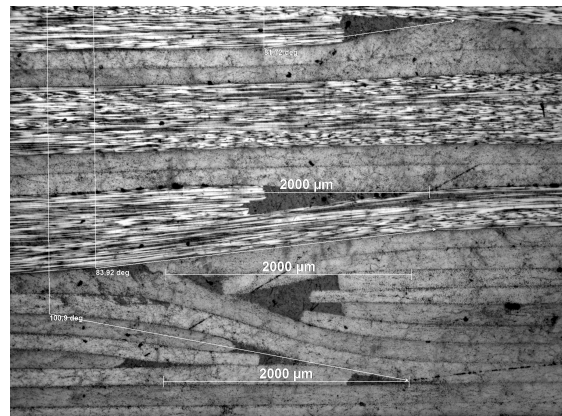
Figure Appendix A.2: Section II-I lower part, sample 1
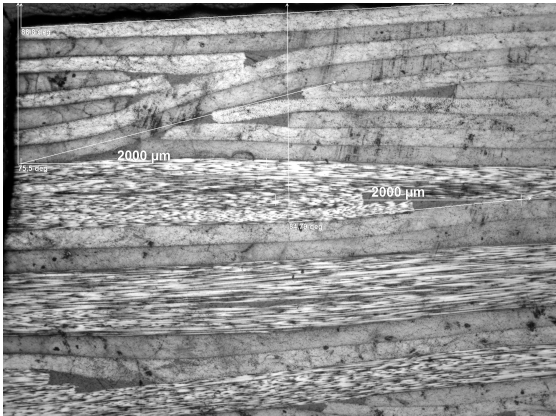
Figure Appendix A.3: Section II-I upper part, sample 2
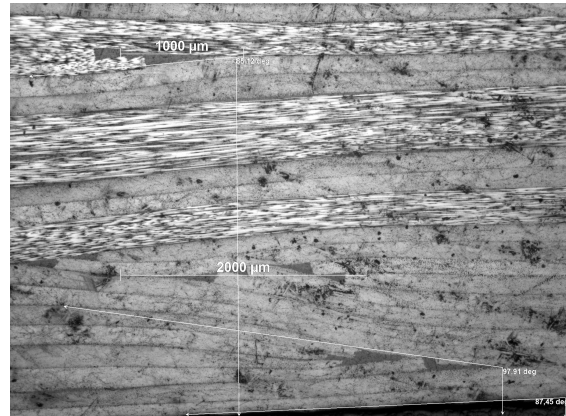
Figure Appendix A.4: Section II-I lower part, sample 2

Figure Appendix A.5: Section II-I upper part, sample 3
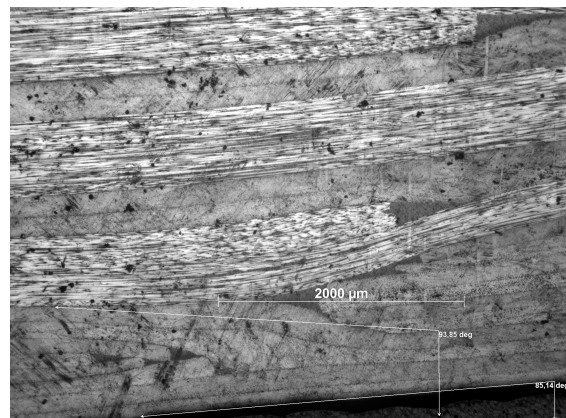
Figure Appendix A.6: Section II-I lower part, sample 3

Figure Appendix A.7: Section IV-I upper part, sample 1
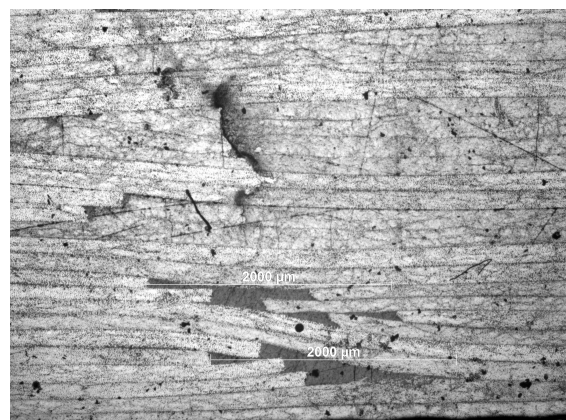
Figure Appendix A.8: Section IV-I lower part, sample 1

Figure Appendix A.9: Section IV-I upper part, sample 2
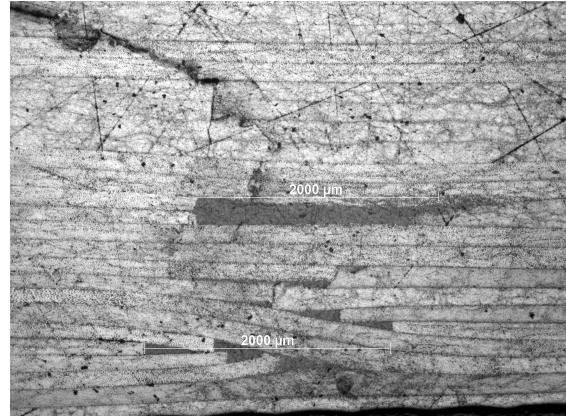
Figure Appendix A.10: Section IV-I lower part, sample 2
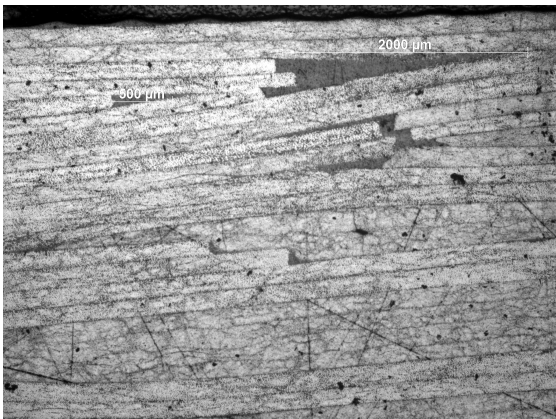
Figure Appendix A.11: Section IV-I upper part, sample 3
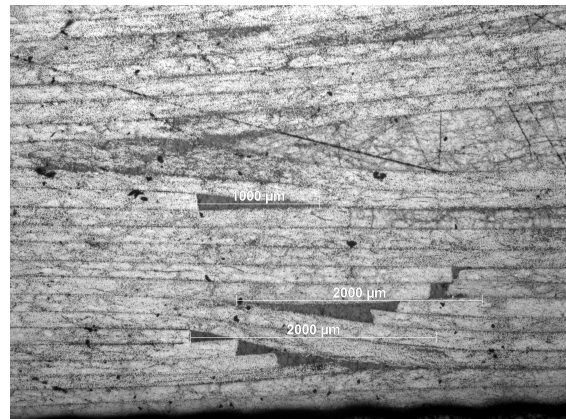
Figure Appendix A.12: Section IV-I lower part, sample 3
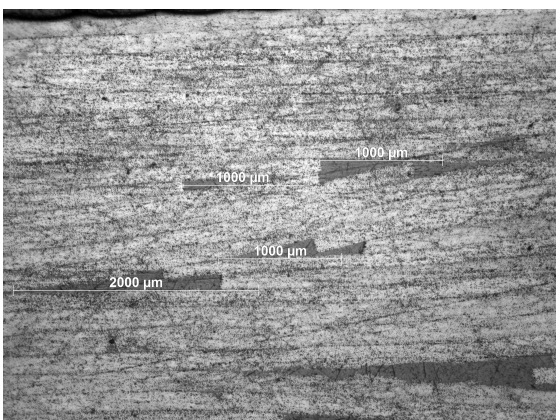
Figure Appendix A.13: Section VII-IV upper part, sample 1
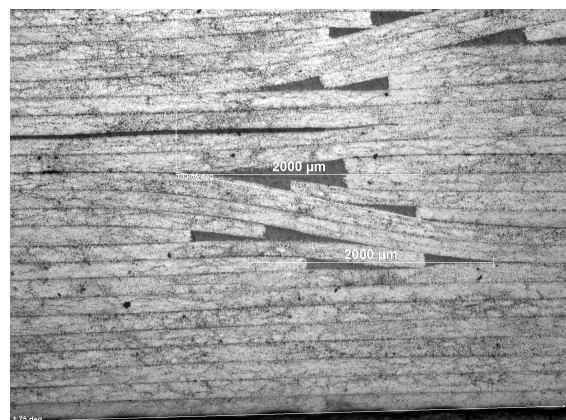
Figure Appendix A.14: Section VII-IV lower part, sample 1
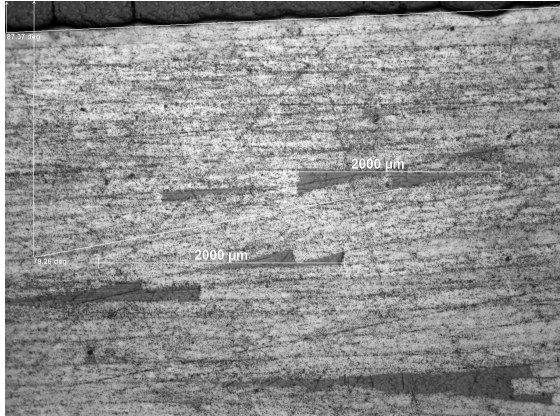
Figure Appendix A.15: Section VII-IV upper part, sample 2
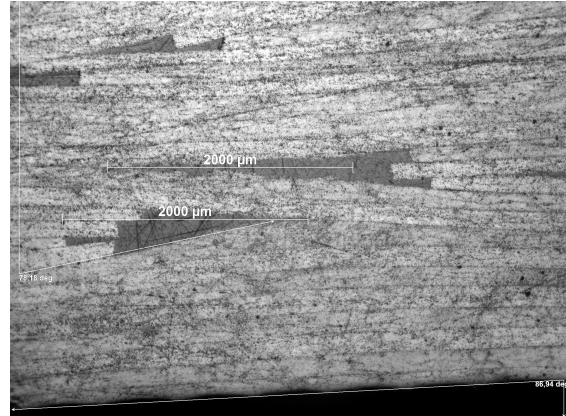
Figure Appendix A.16: Section VII-IV lower part, sample 2
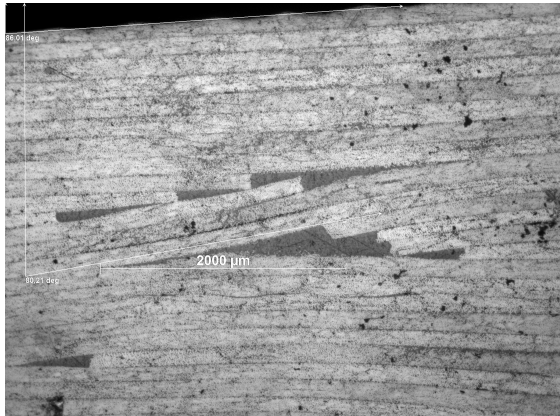
Figure Appendix A.17: Section VII-IV upper part, sample 3
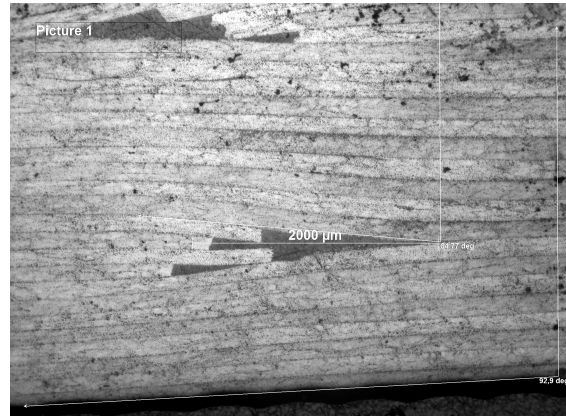
Figure Appendix A.18: Section VII-IV lower part, sample 3

Appendix B

Ply drop section models

Below, the FEM models of all ply drop sections, except ply drop sections I-II and I-II-IV-V which are presented in the main text, are presented. The figures show the different sections of the models which represent the regular plies, the ply drops and the resin pockets.
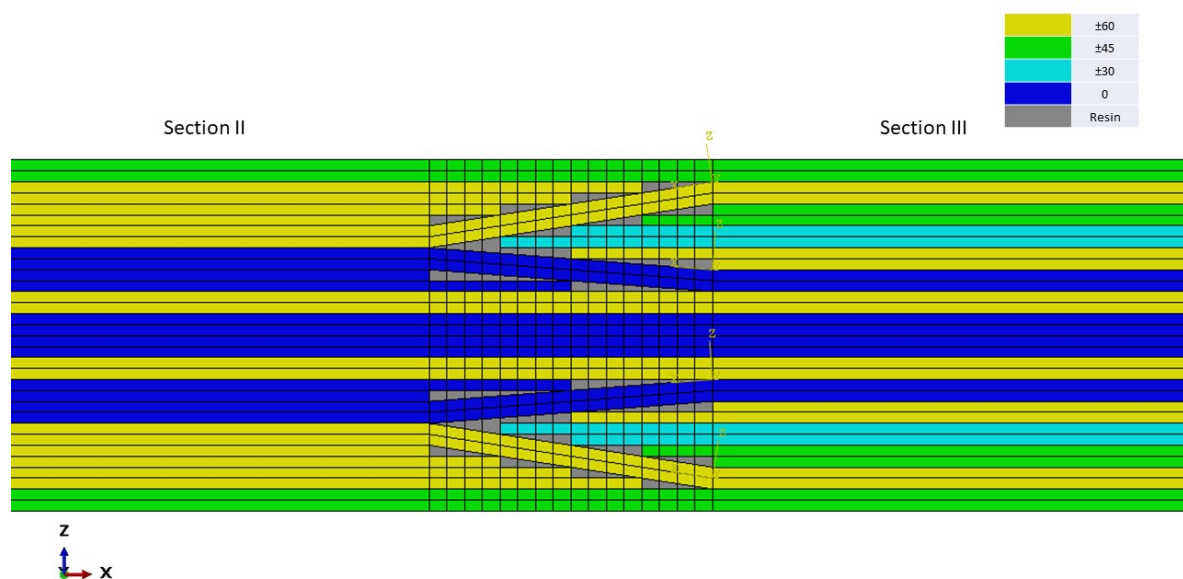
Figure Appendix B.1: FEM model of Section II-III.
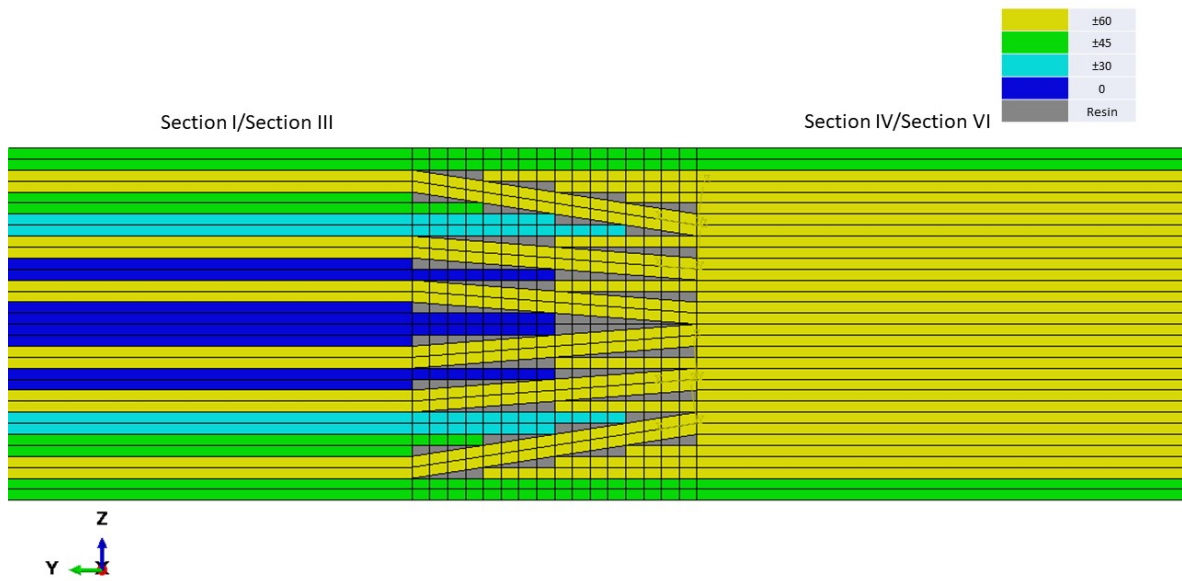
Figure Appendix B.2: FEM model of Sections I-IV and III-VI.
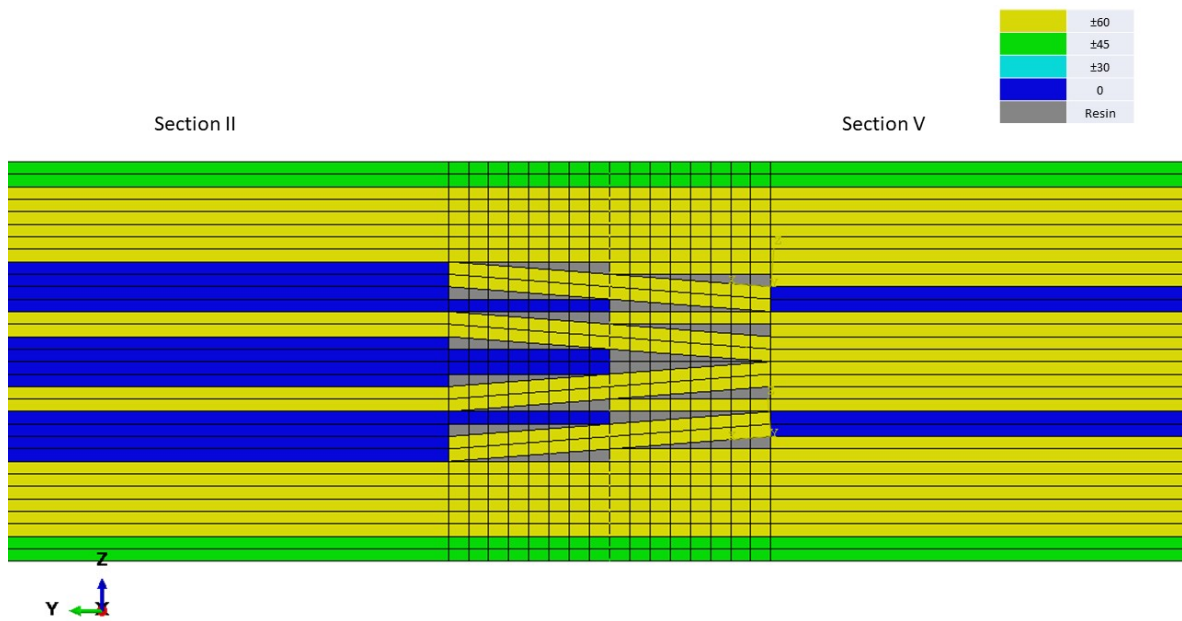
Figure Appendix B.3: FEM model of Section II-V.
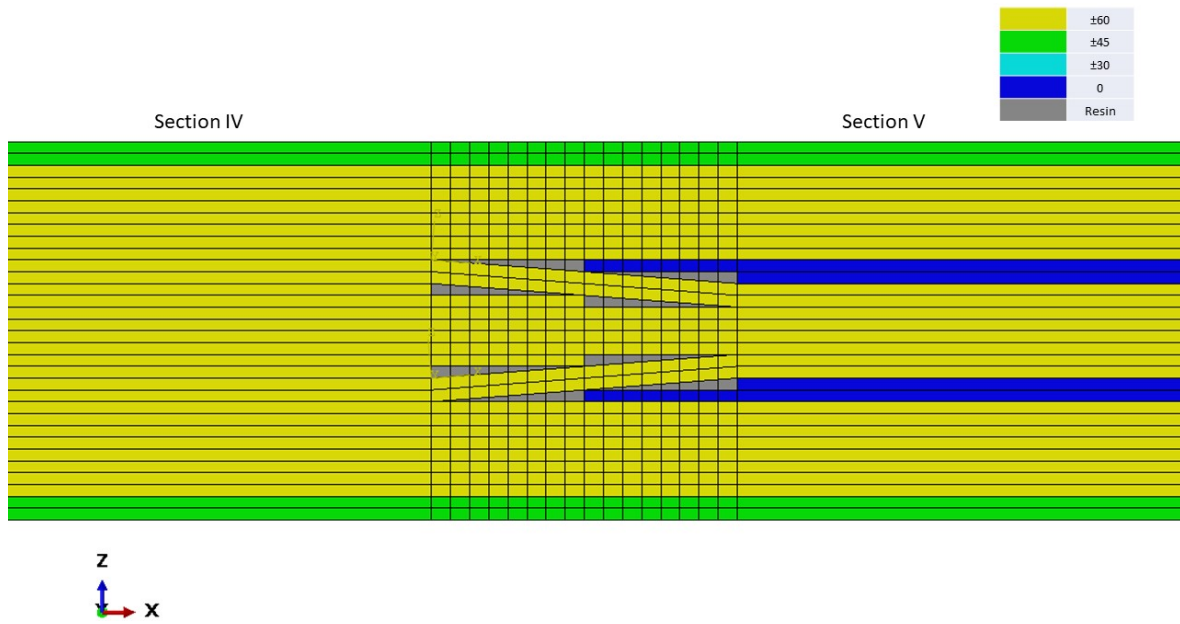
Figure Appendix B.4: FEM model of Section IV-V.
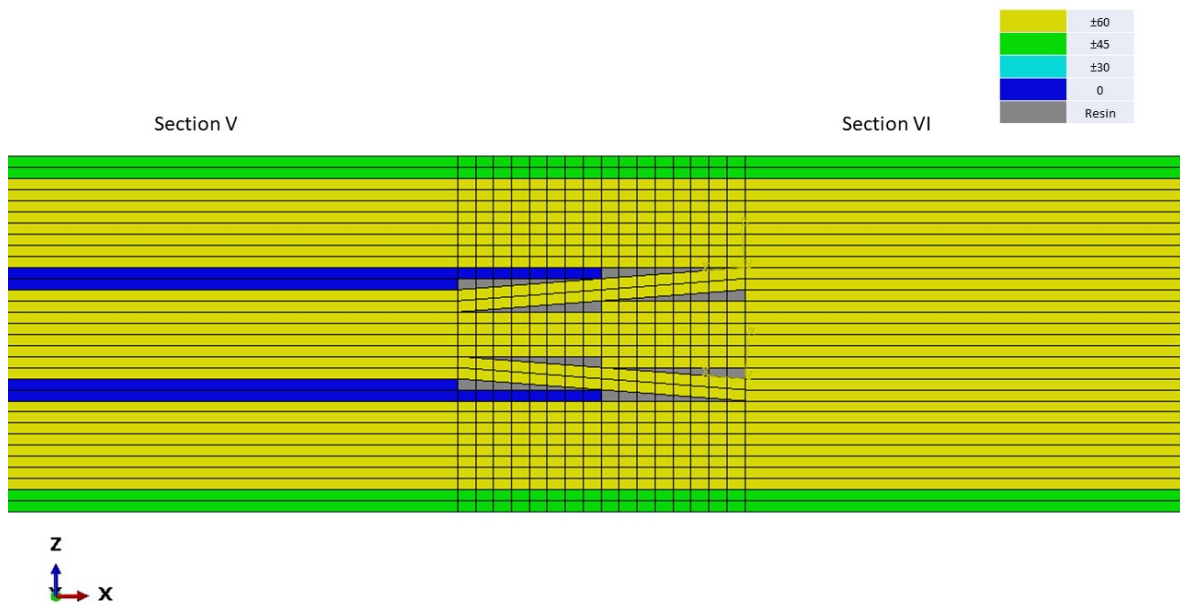
Figure Appendix B.5: FEM model of Section V-VI.
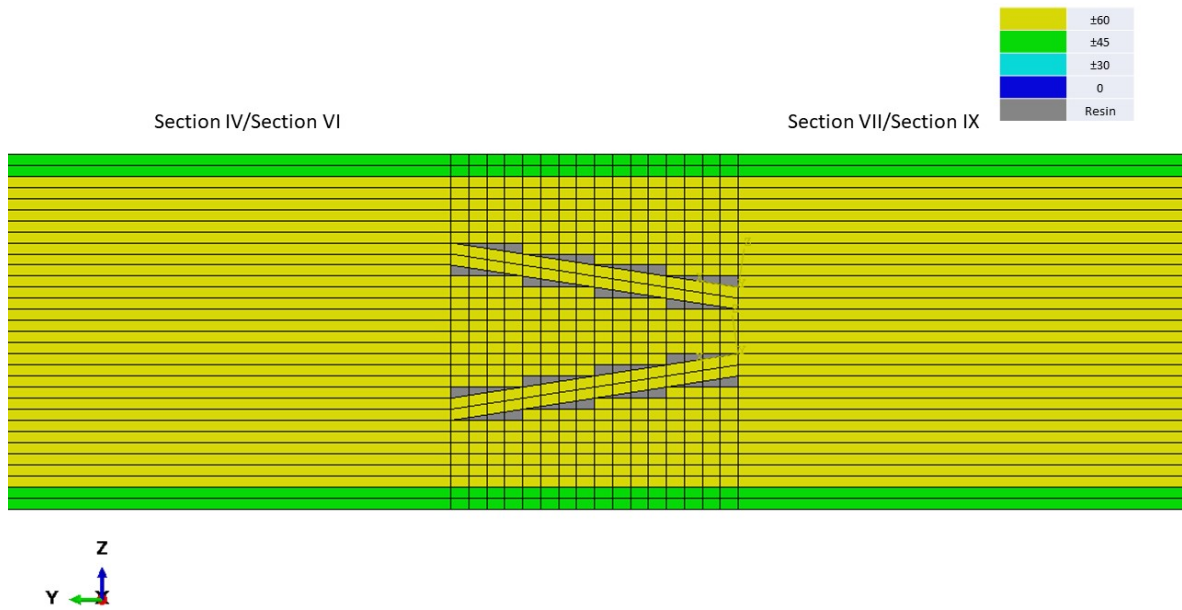
Figure Appendix B.6: FEM model of Sections IV-VII and VI-IX.
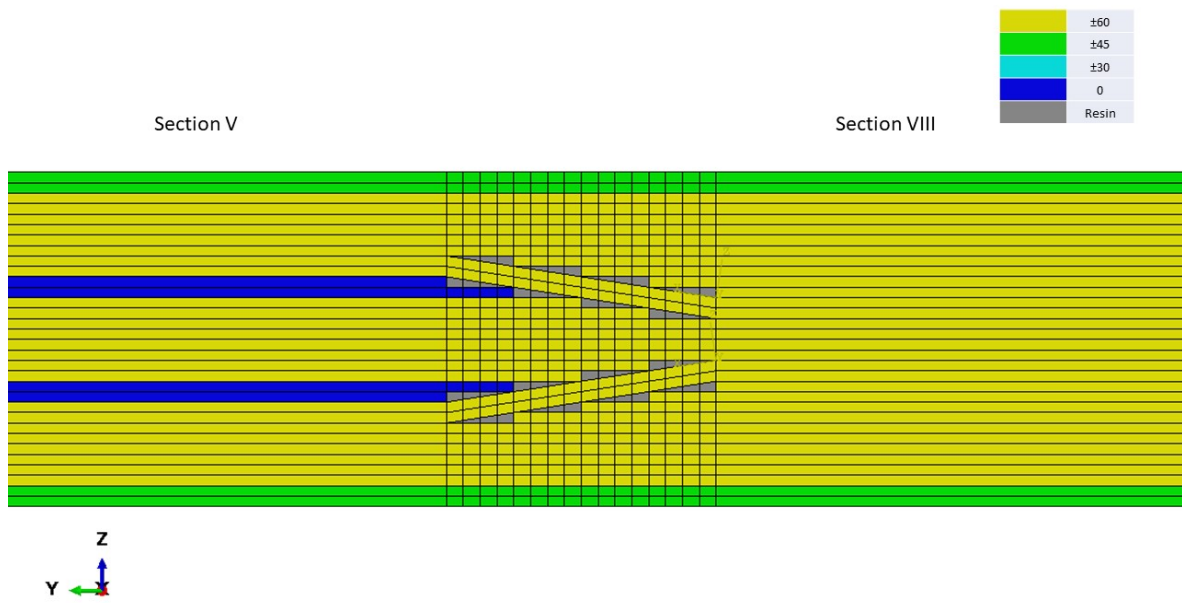
Figure Appendix B.7: FEM model of Section V-VIII.
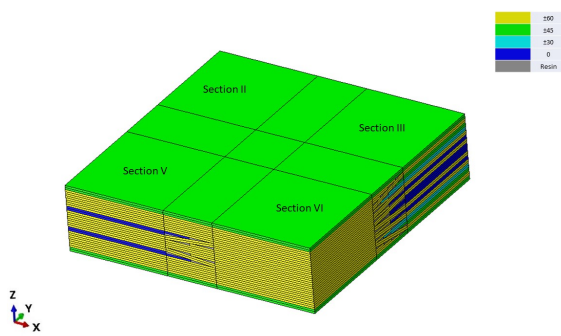
Figure Appendix B.8: FEM model of Section II-III-V-VI.
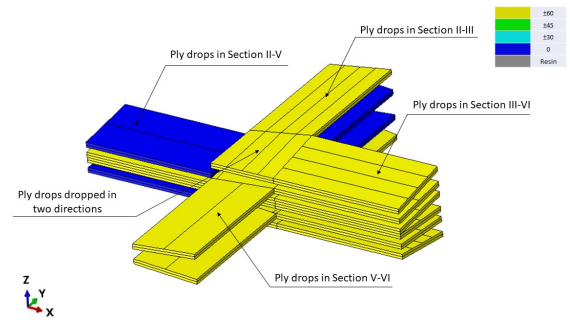
Figure Appendix B.9: FEM model of Section II-III-V-VI showing only the ply drops of the section.
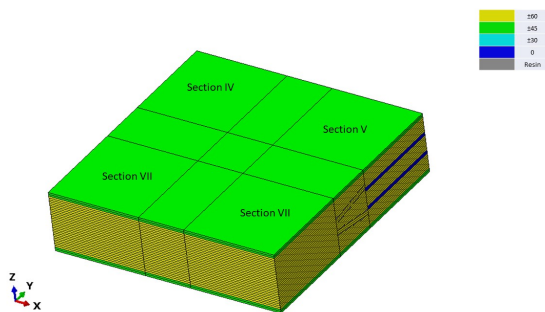
Figure Appendix B.10: FEM model of Section IV-V-VII-VIII.
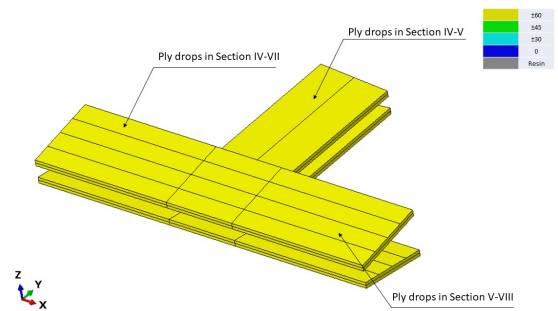
Figure Appendix B.11: FEM model of Section IV-V-VII-VIII showing only the ply drops of the section.
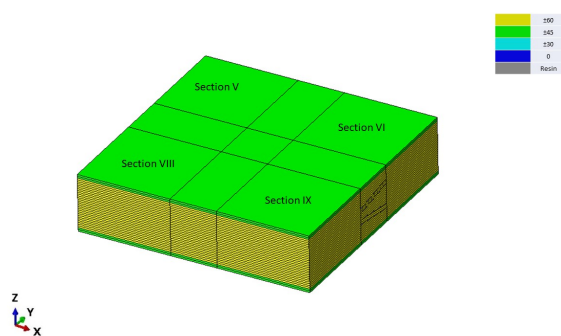
Figure Appendix B.12: FEM model of Section V-VI-VIII-IX.
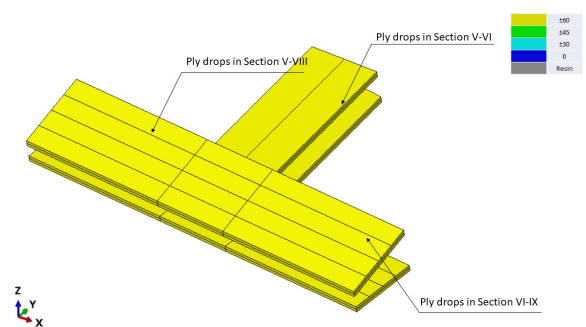
Figure Appendix B.13: FEM model of Section V-VI-VIII-IX showing only the ply drops of the section.

Global model stress results

Below, the stress results of the global FEM model of the blended laminate are shown. The results are displayed per ply for all different sections. The ply numbering works from the bottom to top. Ply 1 is at the bottom and ply 32 is at the top.
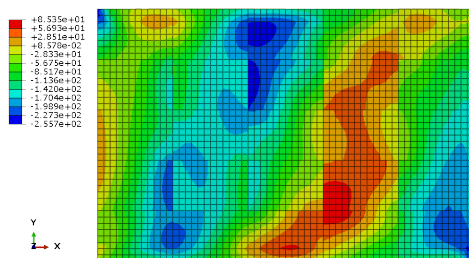
Figure Appendix C.1: Stress results at fiber direction for ply 2 of all sections of the blended laminate at 120000 N buckling load. The legend is in MPa.
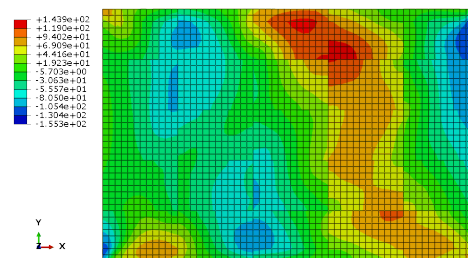
Figure Appendix C.2: Stress results at fiber direction for ply 3 of all sections of the blended laminate at 120000 N buckling load. The legend is in MPa.
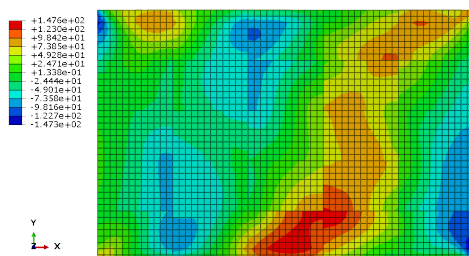
Figure Appendix C.3: Stress results at fiber direction for ply 4 of all sections of the blended laminate at 120000 N buckling load. The legend is in MPa.
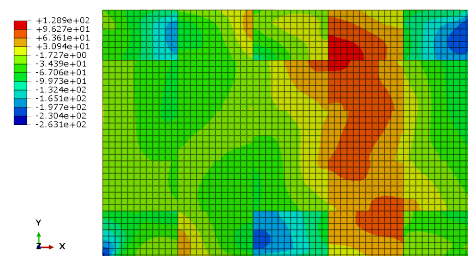
Figure Appendix C.4: Stress results at fiber direction for ply 5 of all sections of the blended laminate at 120000 N buckling load. The legend is in MPa.
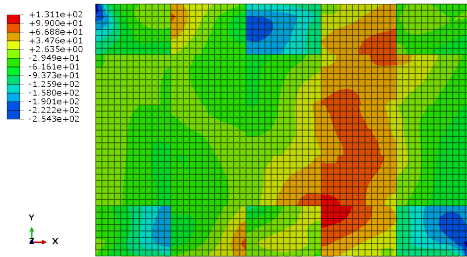
Figure Appendix C.5: Stress results at fiber direction for ply 6 of all sections of the blended laminate at 120000 N buckling load. The legend is in MPa.
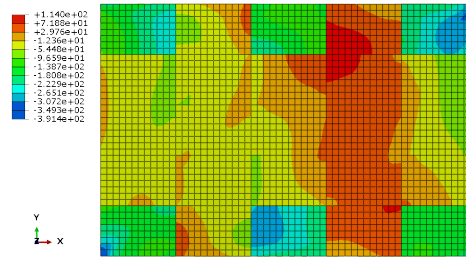
Figure Appendix C.6: Stress results at fiber direction for ply 7 of all sections of the blended laminate at 120000 N buckling load. The legend is in MPa.
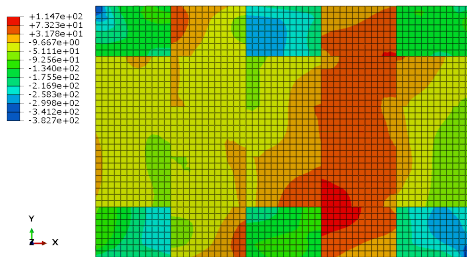
Figure Appendix C.7: Stress results at fiber direction for ply 8 of all sections of the blended laminate at 120000 N buckling load. The legend is in MPa.
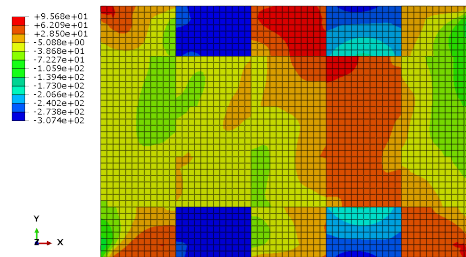
Figure Appendix C.8: Stress results at fiber direction for ply 9 of all sections of the blended laminate at 120000 N buckling load. The legend is in MPa.
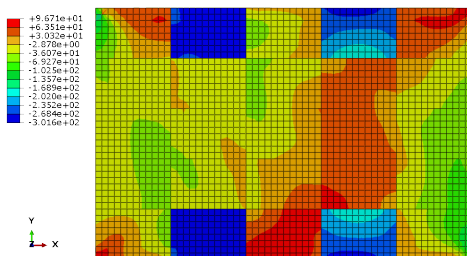
Figure Appendix C.9: Stress results at fiber direction for ply 10 of all sections of the blended laminate at 120000 N buckling load. The legend is in MPa.
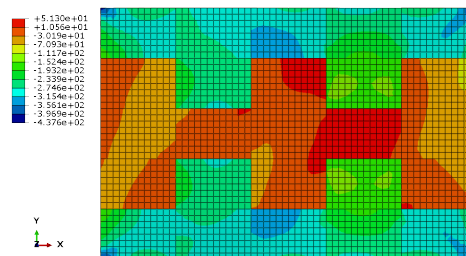
Figure Appendix C.10: Stress results at fiber direction for ply 11 of all sections of the blended laminate at 120000 N buckling load. The legend is in MPa.
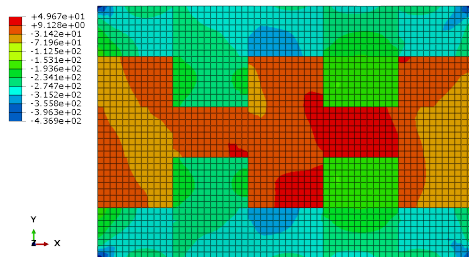
Figure Appendix C.11: Stress results at fiber direction for ply 12 of all sections of the blended laminate at 120000 N buckling load. The legend is in MPa.
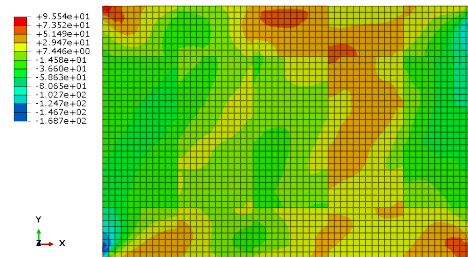
Figure Appendix C.12: Stress results at fiber direction for ply 13 of all sections of the blended laminate at 120000 N buckling load. The legend is in MPa.
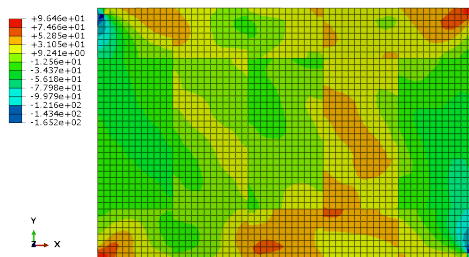
Figure Appendix C.13: Stress results at fiber direction for ply 14 of all sections of the blended laminate at 120000 N buckling load. The legend is in MPa.
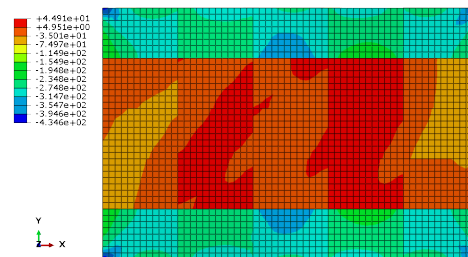
Figure Appendix C.14: Stress results at fiber direction for ply 15 of all sections of the blended laminate at 120000 N buckling load. The legend is in MPa.
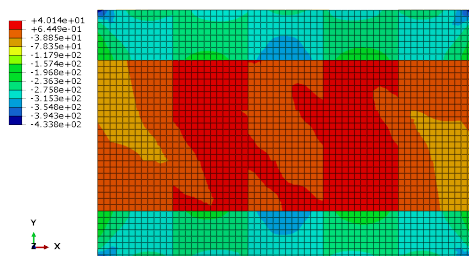
Figure Appendix C.15: Stress results at fiber direction for ply 16 of all sections of the blended laminate at 120000 N buckling load. The legend is in MPa.
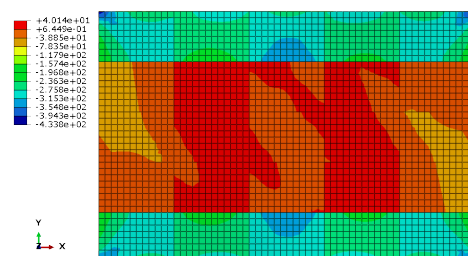
Figure Appendix C.16: Stress results at fiber direction for ply 17 of all sections of the blended laminate at 120000 N buckling load. The legend is in MPa.
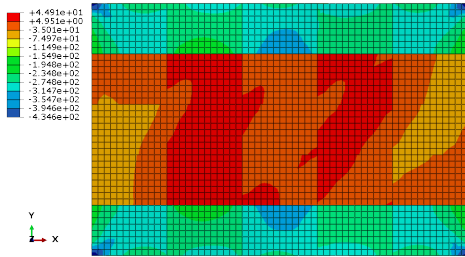
Figure Appendix C.17: Stress results at fiber direction for ply 18 of all sections of the blended laminate at 120000 N buckling load. The legend is in MPa.
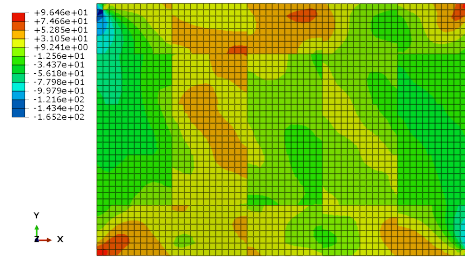
Figure Appendix C.18: Stress results at fiber direction for ply 19 of all sections of the blended laminate at 120000 N buckling load. The legend is in MPa.
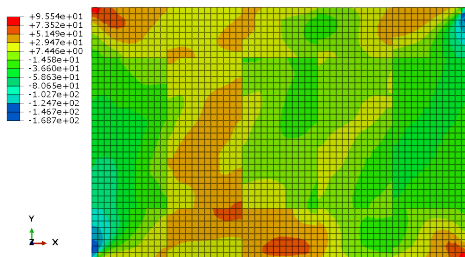
Figure Appendix C.19: Stress results at fiber direction for ply 20 of all sections of the blended laminate at 120000 N buckling load. The legend is in MPa.
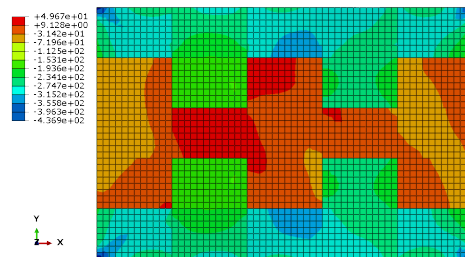
Figure Appendix C.20: Stress results at fiber direction for ply 21 of all sections of the blended laminate at 120000 N buckling load. The legend is in MPa.
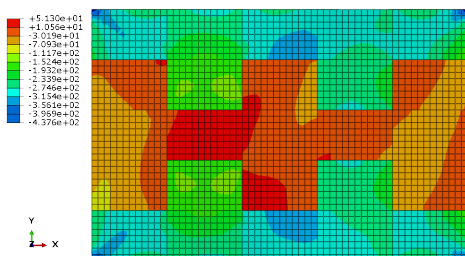
Figure Appendix C.21: Stress results at fiber direction for ply 22 of all sections of the blended laminate at 120000 N buckling load. The legend is in MPa.
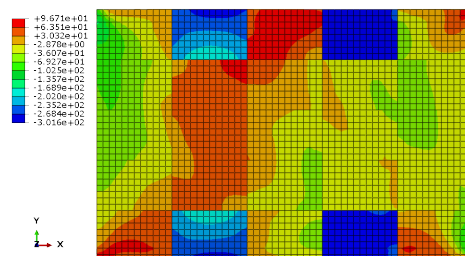
Figure Appendix C.22: Stress results at fiber direction for ply 23 of all sections of the blended laminate at 120000 N buckling load. The legend is in MPa.
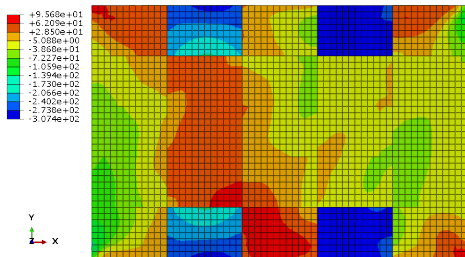
Figure Appendix C.23: Stress results at fiber direction for ply 24 of all sections of the blended laminate at 120000 N buckling load. The legend is in MPa.
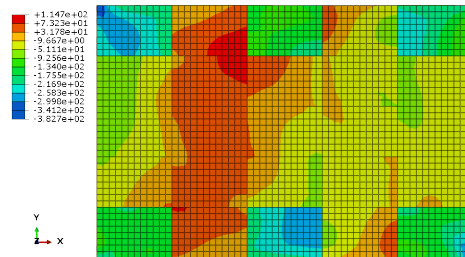
Figure Appendix C.24: Stress results at fiber direction for ply 25 of all sections of the blended laminate at 120000 N buckling load. The legend is in MPa.
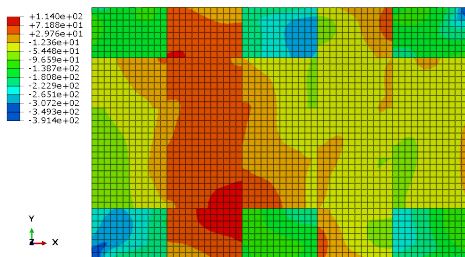
Figure Appendix C.25: Stress results at fiber direction for ply 26 of all sections of the blended laminate at 120000 N buckling load. The legend is in MPa.
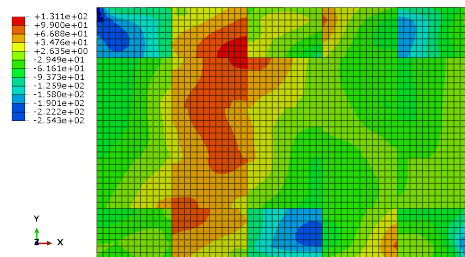
Figure Appendix C.26: Stress results at fiber direction for ply 27 of all sections of the blended laminate at 120000 N buckling load. The legend is in MPa.
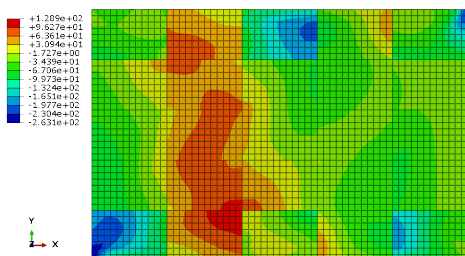
Figure Appendix C.27: Stress results at fiber direction for ply 28 of all sections of the blended laminate at 120000 N buckling load. The legend is in MPa.
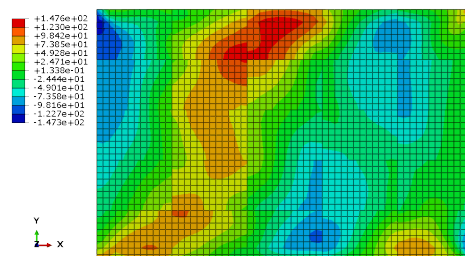
Figure Appendix C.28: Stress results at fiber direction for ply 29 of all sections of the blended laminate at 120000 N buckling load. The legend is in MPa.
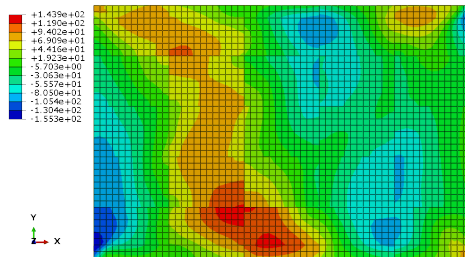
Figure Appendix C.29: Stress results at fiber direction for ply 30 of all sections of the blended laminate at 120000 N buckling load. The legend is in MPa.
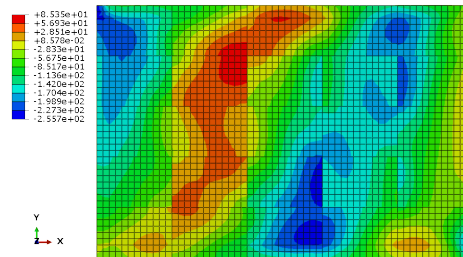
Figure Appendix C.30: Stress results at fiber direction for ply 31 of all sections of the blended laminate at 120000 N buckling load. The legend is in MPa.
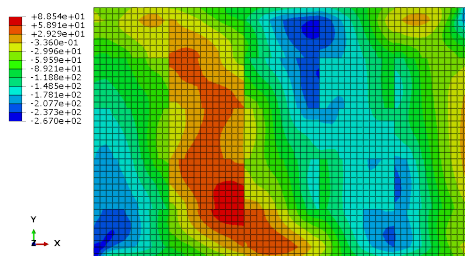
Figure Appendix C.31: Stress results at fiber direction for ply 32 of all sections of the blended laminate at 120000 N buckling load. The legend is in MPa.

Appendix D

Local models stress results

Below, the stress results of each ply drop section are shown. The max stress could be at a position that it is not shown in the figures since most of the sections have a length or width that does not allow the whole section to be shown in the picture. Nevertheless, the max stress values are stated in the legend.
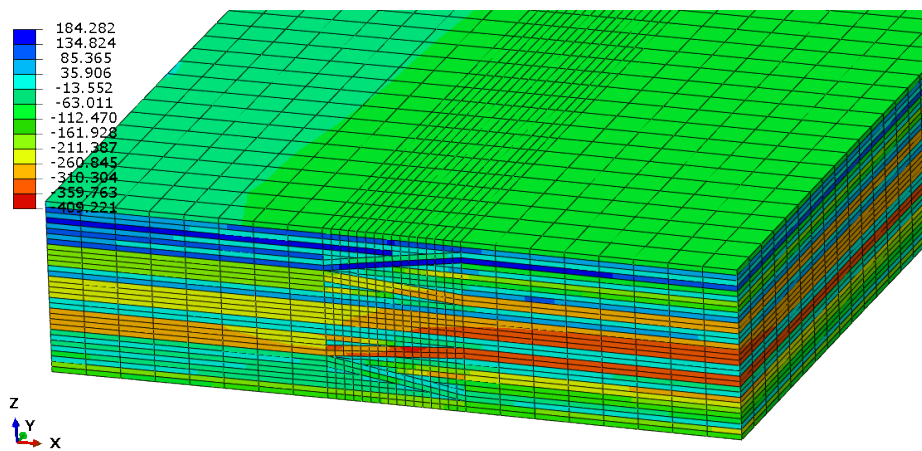
Figure Appendix D.1: Stress results of section II-III. The legend is in MPa.
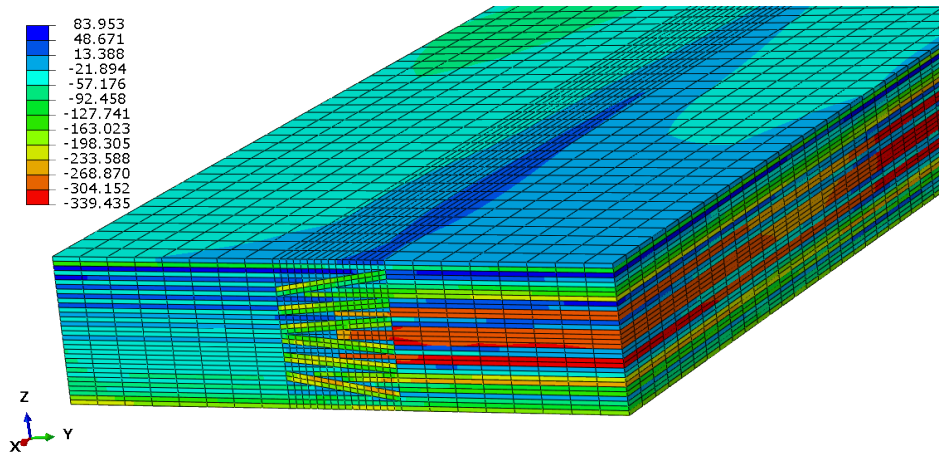
Figure Appendix D.2: Stress results of section I-IV. The legend is in MPa.
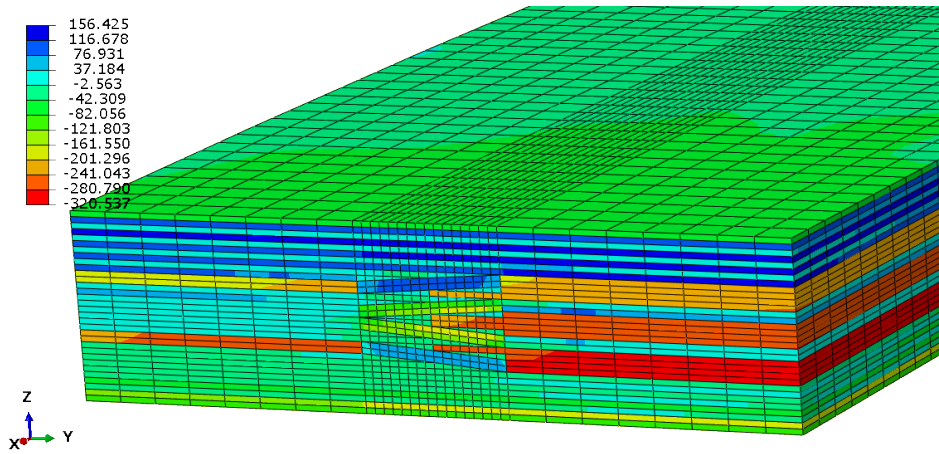
Figure Appendix D.3: Stress results of section II-V. The legend is in MPa.
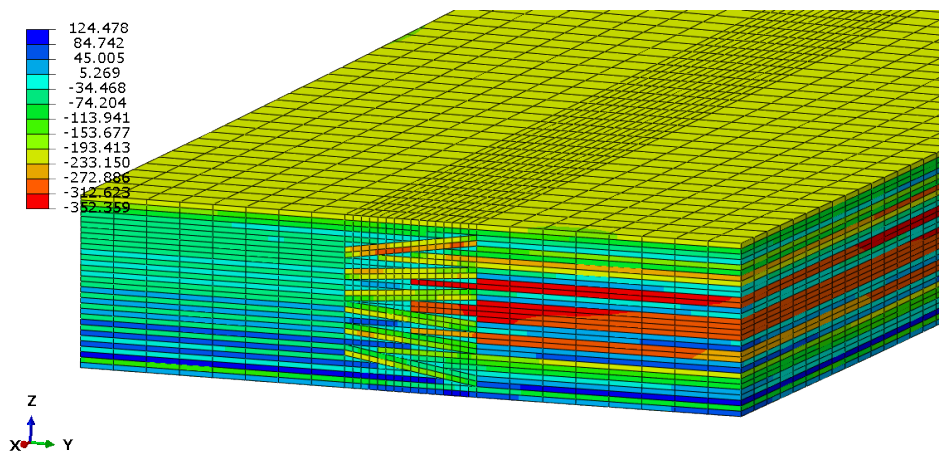
Figure Appendix D.4: Stress results of section III-VI. The legend is in MPa.
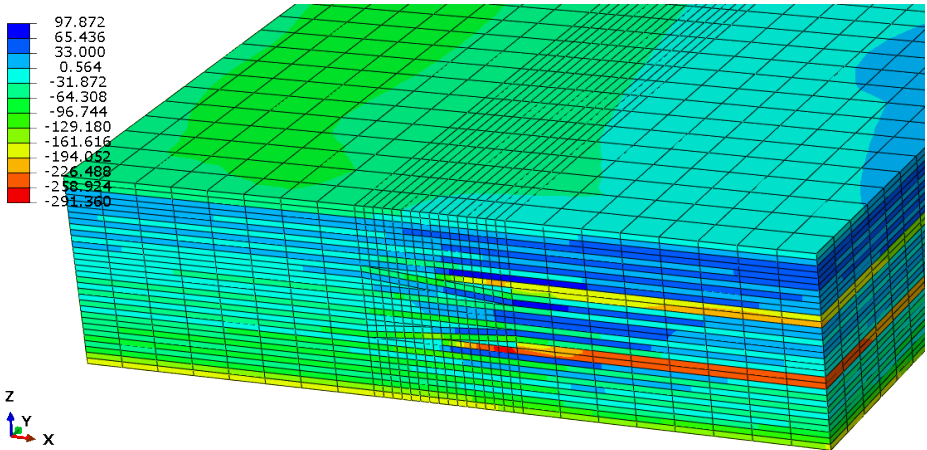
Figure Appendix D.5: Stress results of section IV-V. The legend is in MPa.
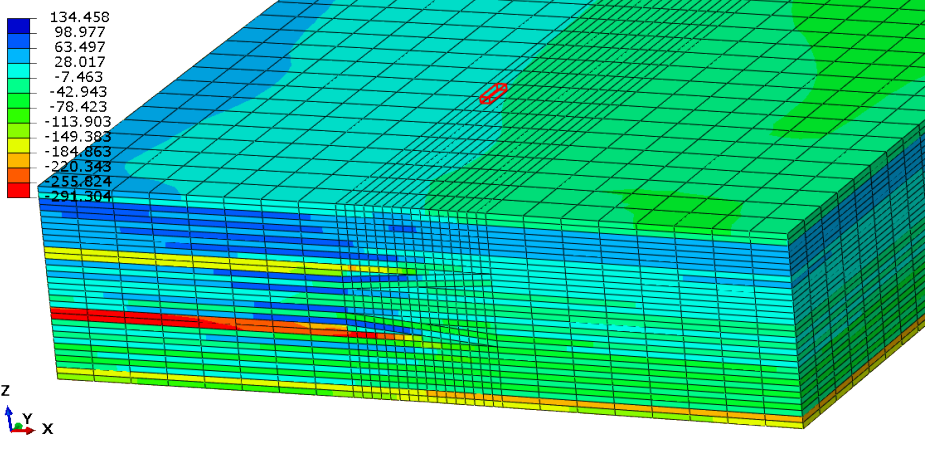
Figure Appendix D.6: Stress results of section V-VI. The legend is in MPa.
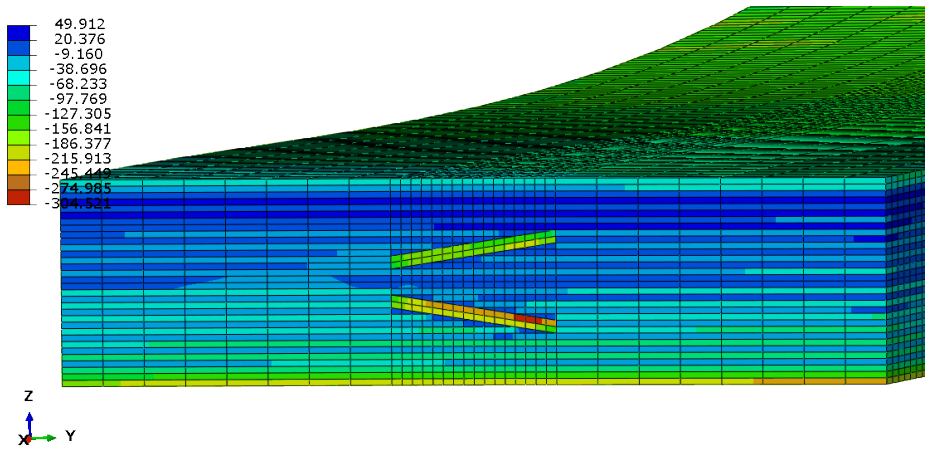
Figure Appendix D.7: Stress results of section IV-VII. The legend is in MPa.
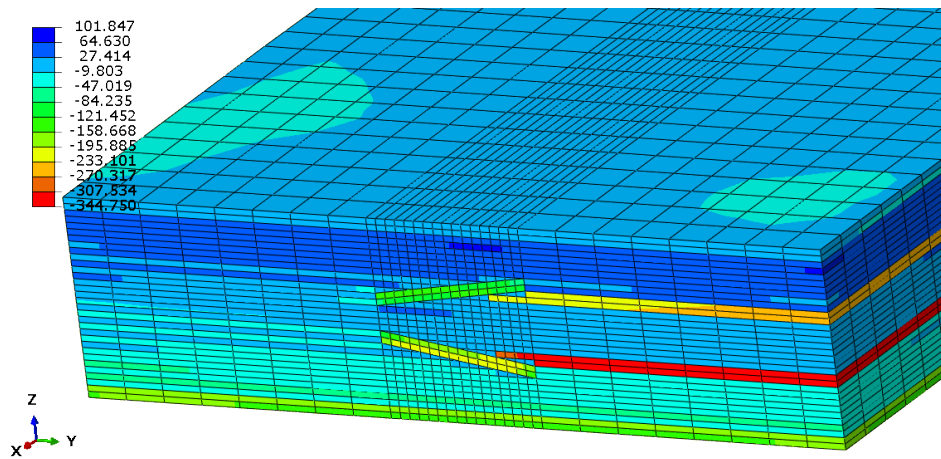
Figure Appendix D.8: Stress results of section V-VIII. The legend is in MPa.
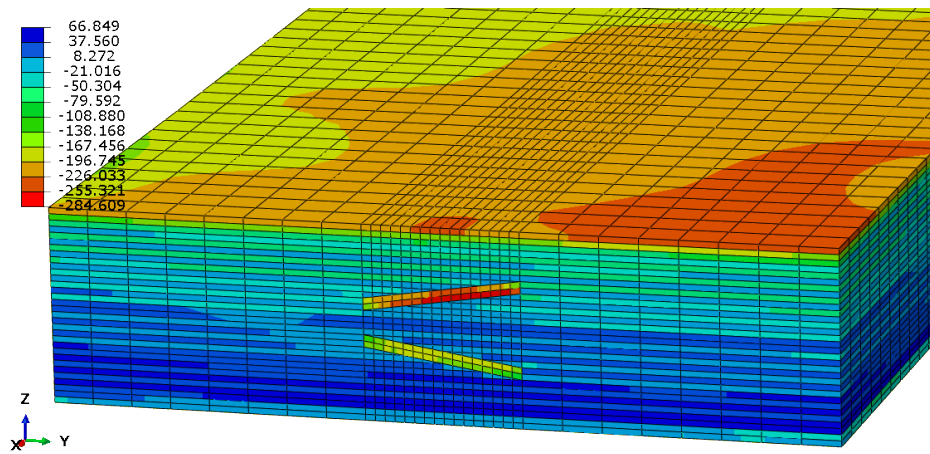
Figure Appendix D.9: Stress results of section VI-IX. The legend is in MPa.
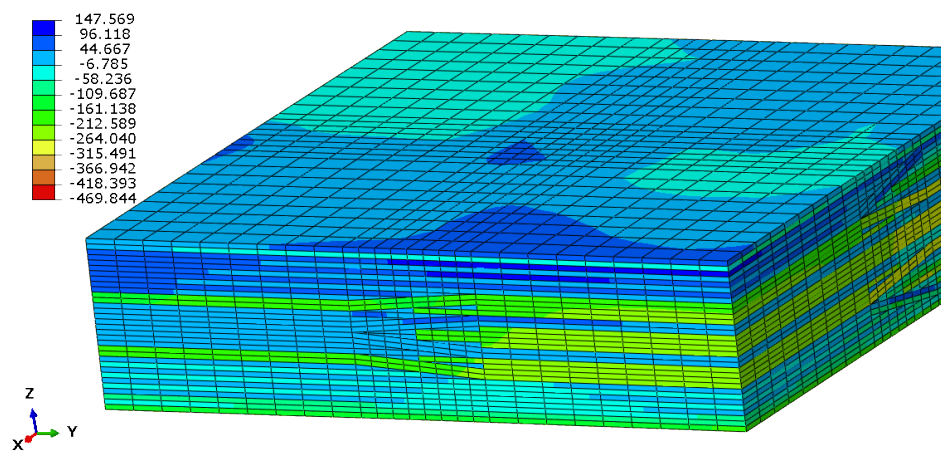
Figure Appendix D.10: Stress results of section I-II-IV-V. The legend is in MPa.
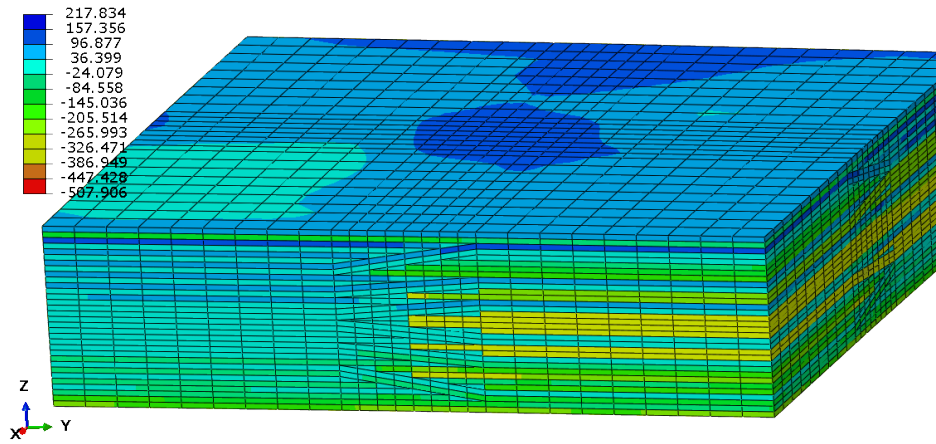
Figure Appendix D.11: Stress results of section II-III-V-VI. The legend is in MPa.
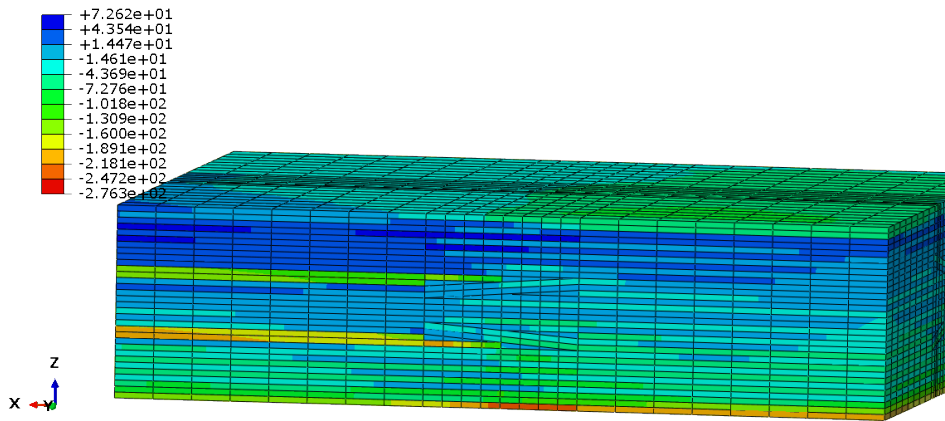
Figure Appendix D.12: Stress results of section IV-V-VII-VIII. The legend is in MPa.
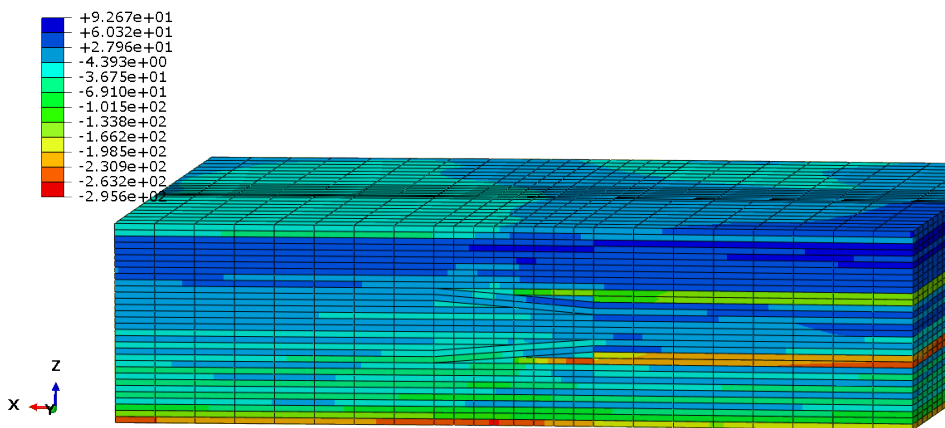
Figure Appendix D.13: Stress results of section V-VI-VIII-IX. The legend is in MPa.